Selection and high-throughput immunofluorescence detection of cell lines with a hybrid epithelial/mesenchymal phenotype : towards improved characterization of Circulating Tumor Cells

Manish Kumar Singh

Selection and high-throughput immunofluorescence detection of cell lines with a hybrid epithelial/mesenchymal phenotype: towards improved characterization of Circulating Tumor Cells

Manish Kumar Singh

A thesis presented for the degree of
Doctor of Philosophy

Jury

Dr. Catherine Alix-Panabières	IRMB et CHRU de Montpellier	Rapportrice
Dr. Marc Tramier	IGDR, Rennes	Rapporteur
Prof. Nathalie Westbrook	Inst. d'Optique Grad. School, Palaiseau	Examinatrice
Prof. Rachel Méallet-Renault	Université Paris Sud, Orsay	Examinatrice
Prof. François Treussart	ENS Cachan	Directeur de thèse
Dr François Dautry	ENS Cachan	Co-directeur de thèse

ÉCOLE NORMALE SUPÉRIEURE DE CACHAN

France

January 29, 2015

Acknowledgments

On the occasion of the finishing of the thesis, it is my desire to express my honest appreciation to all of those whose help and support made my research experience much easier.

First and foremost, I am obliged to my supervisor Prof. François Treussart, for providing me an opportunity to be the part of his research team as a PhD candidate. I am happy to say that my PhD journey has been very constructive since making that move. I really appreciate his constant motivation and productive discussions from the bottom of my heart. Without his regular support, I could not achieve so much today. I also appreciate his patience and trust in me. I am privileged and proud to be associated with his team.

I would also like to express my sincere thanks and immense gratification to Dr. François Dautry. I would like to express my appreciations and gratitude for his invaluable ideas, continuous encouragement and timely guidance to explore the new field. I also like to thank him for giving me time for unscheduled meetings. It is beyond my capacity to describe how valuable his guidance is and how much I have learned from him. I would also like to thank him for guidance, consistent support, and inspiration during of my PhD.

I would like to offer my genuine thanks to Dr. Marie Frugier Regairaz and Dr. Gérald Peyroche for their frequent consultations during my PhD. My research has been completed in their guidance. Their advices helped me greatly to improve my results.

My deepest gratefulness is also to Prof. Niko Hildebrandt for allowing me to work in his laboratory. I am also thankful to Dr. Mariana Tasso, Stina Lindén and Dr. Oya Tagit for help and sharing ideas with me. I would also like to thanks Caroline Ohana and Christine Legay for teaching me tool and techniques which are unfamiliar to me.

I am thankful to Dr. Catherine Alix-Panabières and Dr. Marc Tramier for reviewing my thesis. I am very thankful for Prof. Françoise Farace, Prof. Thomas Pons, Dr. Françoise Soussaline and Dr. Charles Homsy for constant discussion regarding the project and sharing the progress in the project.

My honest thanks to all my coworkers, lab mates, friends and well-wishers for facilitating me during the research. I would like to offer my sincere thanks to Ginette Puyhaubert and Zina Challal for her valuable help with administrative issues. I thankfully acknowledge the ANR (NanoCTCs project) for their financial supports for my thesis. I am also obligated to the ENS Cachan for providing me chance to pursue my PhD thesis at this esteemed institute.

Finally, I cannot express my appreciation to my parents for their support, love and inspiration. I am obliged to express my gratitude to my sisters for their love and support.

Thanks

Contents

1 Introduction

This thesis took place within the project **NanoCTC** funded by the French *Investments for the Future* "NanoBioTechnology" program in 2011. The project goal was to use nanotechnologies for the precise characterization of **Circulating Tumor Cells** (CTC) based on molecular and cellular investigations ultimately leading to the identification of CTC sub-populations displaying various tumorigenic and pro-metastatic potencies.

This introductory chapter describes the role of Epithelial to Mesenchymal Transition (EMT) in cancer progression. We briefly review the role of CTCs in proliferation of cancer. We then present the methods available to characterize and detect CTCs. Finally, we briefly present the basics on two technologies that we implemented in immunofluorescence experiments carried out in the context of our study: Fluorescence Resonant Energy Transfer (FRET) and fluorescent semiconductor nanocrystals (Quantum Dots).

1.1 Tumor progression

Tumors are due to an abnormal accumulation of cells and have been observed, albeit at various frequencies, in almost all multicellular organisms. By itself, an increased number of cells does not necessarily threaten the viability of its host as long as it is localized, although it can compromise some specific functions. Morbidity and mortality associated with tumors mostly result from the invasion of adjacent and distant tissues, in the latter case giving rise to metastases. It is often estimated that 80% of cancer related deaths are due to metastases.

A fundamental insight into the mechanisms which can lead to tumors has been formulated by the Nobel Prize in *Physiology or Medicine* (1966) Peyton Rous as **tumor progression**. It came from the observation that tumors can acquire their aggressiveness through a multi-step process so that, in general, tumors begin as benign hyperplasia before evolving into locally invasive and metastatic tumors. As this scheme was devised on the basis of direct observation of skin tumors, Peyton Rous could describe the changes in phenotype but could not ascertain the nature of the underlying steps. Through the development of DNA sequencing technologies, current research is providing a wealth of

data on the genetic make-up of tumors and firmly establishes a **genetic basis** of tumor progression. This does not imply that only genetic alterations are involved as some tumors, mostly pediatric tumors, can be completely or almost completely free of consequential genetic alterations. In these cases the driving force for tumor progression is assumed to be mostly epigenetic while other tumors should result from a combination of genetic and epigenetic events.

Another conclusion which can be drawn from these genetic analyses is that tumor progression will differ according to the **cell type** in which it takes place. This is in agreement with early analyses of epidemiological data which suggested that leukemia genesis requires fewer steps than solid tumors do. This is interpreted as the manifestation of the underlying biological processes which can lead to an increase in a cell population. For hematopoietic cells, which are naturally present as a suspension of individual cells in the blood, the key issues are to circumvent the regulation of cell proliferation as well as the control of their half-life since, in many cases, they are very short lived. By contrast, for the most common type of solid tumors, **carcinomas**, the initial events take place in an epithelium, a very organized type of tissue in which each cell is in strong interaction with its neighbors. Therefore an increase in proliferation can only take place if the growth-inhibitory signals from the neighboring cells as well as the mechanical constraints are overridden. Similarly, in order for an epithelial cell to egress from its tissue of origin, it has to disengage from the interactions with the other cells and acquire motility and invasiveness to move into the adjacent tissues.

1.2 Biology of carcinomas

The majority of human tumors arises within epithelial tissues and are designated as **carcinomas**. Because of its accessibility to observation and to biopsies, tumor progression has been well documented in the colon. Thus a series of premalignant states have been classified as hyperplasia, dysplasia, adenomas and carcinomas in situ, with an increasingly abnormal organization. “Truly” cancerous lesions are characterized by their ability to invade the neighboring tissue, in the case of epithelia by breaching through the basal membrane. As a final step, tumor cells can invade distal location in the organism. Although it is likely that in many cases a tumor goes through these different steps in a sequential manner, it is obviously difficult to have access to the same lesion at different times in a human patient. Thus, the reconstruction of tumor progression as a strictly ordered process is mostly an intellectual view, but it can be used as a framework to

analyze individual cases.

As alluded to above, tumor progression within an epithelium has to overcome multiple levels of regulation which are not present in the case of hematopoietic cells and probably not as much in the case of mesenchymal cells. These include the sheer mechanical constraints of an organized tissue which are transmitted to the cells via the presence of tight junction, adherens junction as well as all the signal which contribute to the organization of the epithelium for instance through the polarization of cells.

1.2.1 Mutations in tumors

The current analysis of **mutations in tumors** has confirmed that carcinomas contain more genetic events than leukemias (see Figure 1.1). Excluding the special cases of tumors associated with a mutagenic process (smoking for lung cancer, UV light for melanomas) or with a genetic instability (colon tumors with an instability of microsatellite sequences due to an inactivation of the mismatch repair pathway) carcinomas have on average about 60 mutations in the coding regions which result in a change in aminoacid on the corresponding protein. This is 4 to 5 time more that in leukemias [1]. Many genes can be altered by these mutations or by other genetic events (chromosomal translocation, deletions, and amplifications) and the catalog is still under construction (see Figure 1.2). It is however apparent that even when considering carcinomas from the same tissue of origin, a multiplicity of genetic trajectories can be observed [2].

Thus it is currently very difficult to give an informative description of the genetic events which take place during the genesis of carcinomas even if one focuses on a single tissue of origin. Alternatively, it is often proposed to assign the genes which have been altered to functional categories [3]. Although very appealing, this approach suffers from the very broad functional categories which are used (e.g. evading growth suppressors, activating evasion and metastasis ...) and our lack of a detailed understanding of regulatory pathways. With an average frequency of 46% across the 10 types of carcinomas analyzed, p53 is the most common genetic alteration. The frequent involvement of p53 had previously been noted in multiple studies and is in line with its essential role in maintaining genome integrity and controlling apoptotic response to many stresses. In this case the genetic alterations lead to a loss of function. p53 is inactivated in 94% of ovarian carcinomas making it an almost recurrent event while at the other end of the spectrum only 2% of renal clear cell carcinomas show this type of alteration. Among this set of carcinomas, adenomatous polyposis coli gene (*APC*) has the highest frequency of mutation in one type of tumor (82% in colon carcinoma), although the average frequency

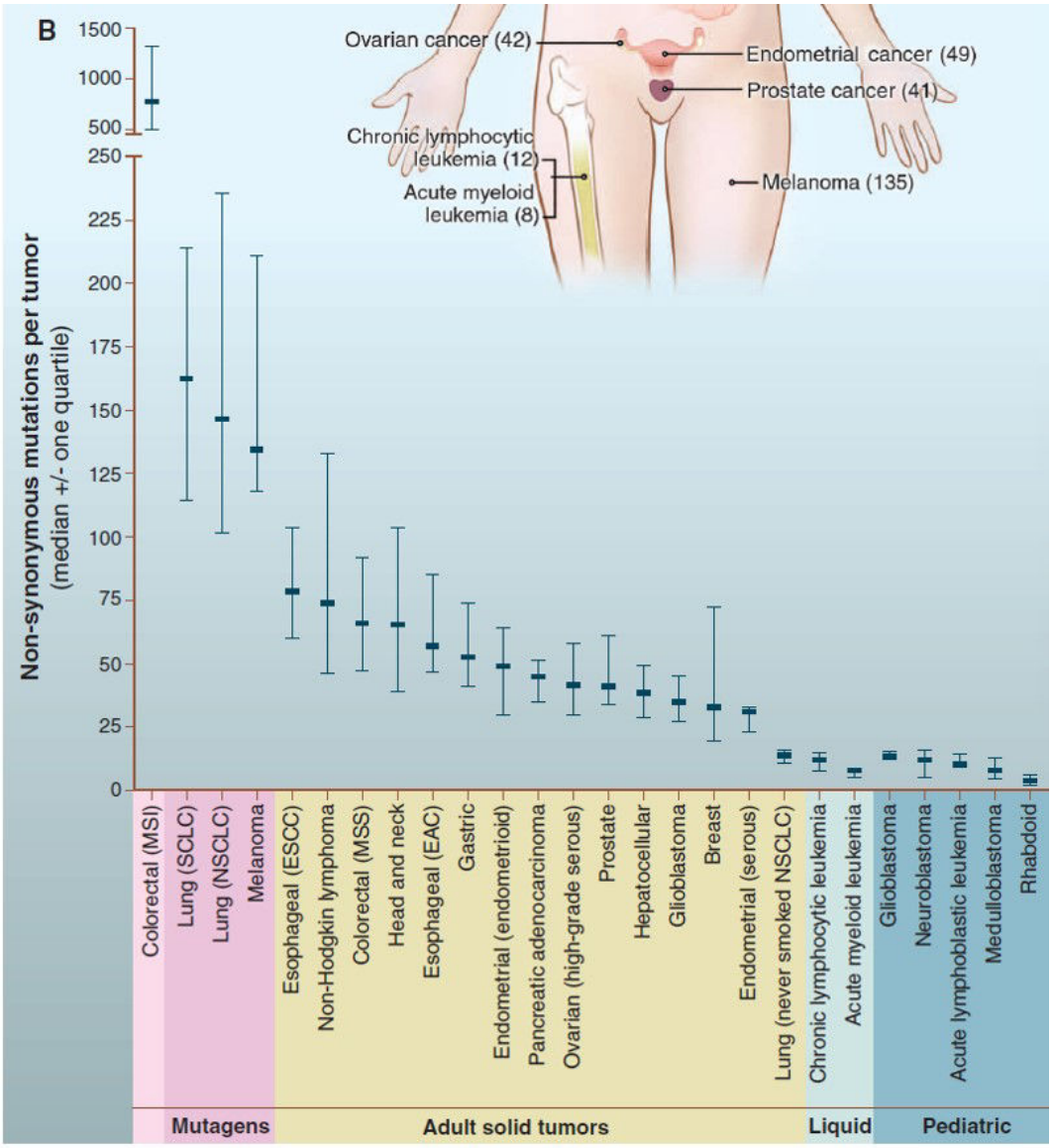

Figure 1.1 : *Analysis of the number of mutations across tumor types.* *Here only mutations detected in the coding regions of genes and which lead to change in amino acid in the protein product are taken into account. The median value and the range of the first quartile are indicated (Source: Ref. [1]).*

is quite low (7%). A similar conclusion could be reached for *KRAS* since although its average frequency of mutation in carcinomas is 7%, it is mutated in about 90% of pancreatic carcinomas. Of note in view of the markers used in my research project, E–cadherin (*CDH1*) is mutated in 2.5% of the carcinomas, the highest frequency being observed in breast carcinomas. In addition, β–catenin (*CTNNB1*) one of the partners of E–cadherin is mutated in 3% of carcinomas, the frequency reaching 28% in uterine corpus endometrial carcinomas.

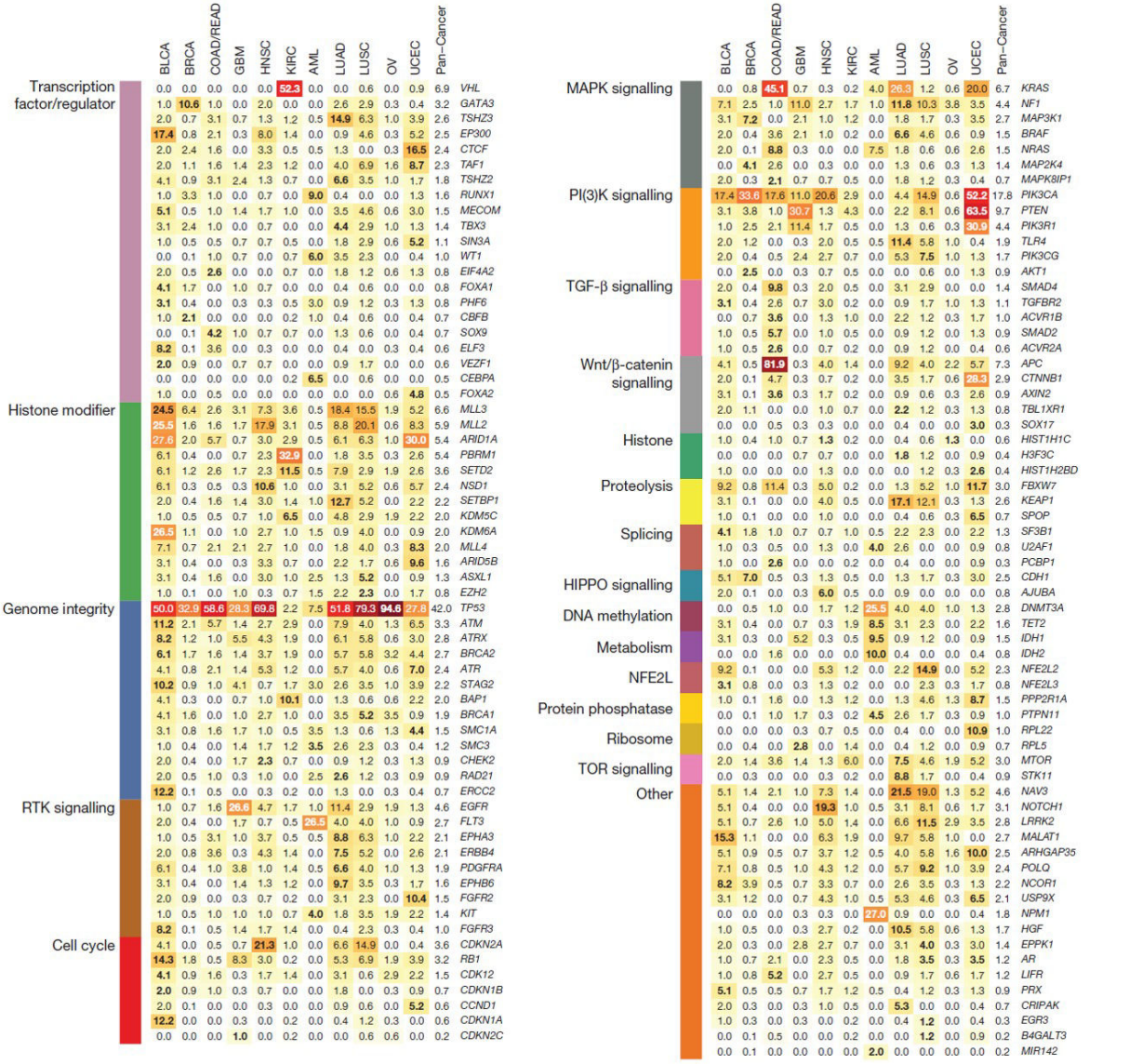

Figure 1.2 : ***A catalog of the genetic alterations observed in 12 types of cancer.*** *Genes are organized by broad functional categories and the frequencies at which they are altered in one type of tumor is indicated. BRCA: Breast adenocarcinoma; LUAD: Lung adenocarcinoma; LUSC: Lung squamous cell carcinoma; UCEC: Uterine corpus endometrial carcinoma; GBM: Glioblatoma multiforme; HNSC: Head and neck squamous cell carcinoma; COAD/READ: Colon and rectal carcinoma; BLCA: Bladder carcinoma; KIRC: Kidney clear cell carcinoma; OV: Ovarian serous carcinoma: AML: Acute myeloid leukemia (Source: Ref. [2])*

1.2.2 Involvement of cadherins in carcinoma progression

Cadherins belongs to a family of trans-membrane glycoproteins that are responsible for calcium-dependent homophilic interactions between cells. There are many cadherin

genes in mammals which can be organized by the similarity between the protein products. Type I cadherins comprise the most extensively studied cadherins including E– and N–cadherins. They have five extracellular domains which are variations of an ancestral domain, the extracellular cadherin domain (EC). E–cadherin is expressed by epithelial cells and plays a major role in the transmission of the forces between cells. Importantly, the cytoplasmic domain of E–cadherin interacts with the actin cytoskeleton through a molecular complex which contains β-catenin (Figure 1.3). The homophilic interaction is mediated by a dimerization of the first extracellular domain (EC1) of two cadherins present on opposite cellular membranes. The clustering of cadherins within the cellular membranes leads to the formation of adherens junctions transforming the weak binding affinity between a pair of molecules into a mechanically significant one between two cells. This is achieved by weak interaction between dimers as illustrate on Figure 1.3. Beyond this critical role in the mechanical organization of epithelium, E–cadherin is also involved in the transduction of signals to the cell nucleus, since it sequesters β–catenin to the cell membrane. In the absence of E–cadherin, β–catenin can translocate to the nucleus, interact with transcription factors and induce the expression genes involved in cell proliferation [4]. Thus E–cadherin is a tumor suppressor as has been documented in several models of tumorigenesis, including breast and colon cancer [5, 6]. However, some publications reported an inverse relationship between expression of E–cadherin and the occurrence of metastases in some models [6]. In conclusion, E–cadherin is a central player of epithelium architecture (and therefore of cell immobilization within the tissue) as well as a regulator a cell proliferation [7, 8].

1.2.3 Metastases

The leading cause of cancer mortality is the formation of metastases, i.e. secondary tumors at distant sites within the body [10]. In many cases the origin of these secondary tumors can be unambiguously tracked back to the primary tumor, indicating that somehow cells have egressed from the tumor and moved inside the body before giving rise to new tumors in other organs (or at a distant site within the same organ). Both the lymphatic and the blood vessels can be used to gain access to new sites. Thus it is necessary for the tumor cells to gain access to the circulation by intravasation and subsequently to leave the circulation by extravasation. Afterwards, the tumor cell should start growing in this new environment in order to generate a secondary tumor. Consequently, the metastatic process involves a number of steps requiring that tumor cells are motile, invasive and able to grow in an environment different from that of their origin

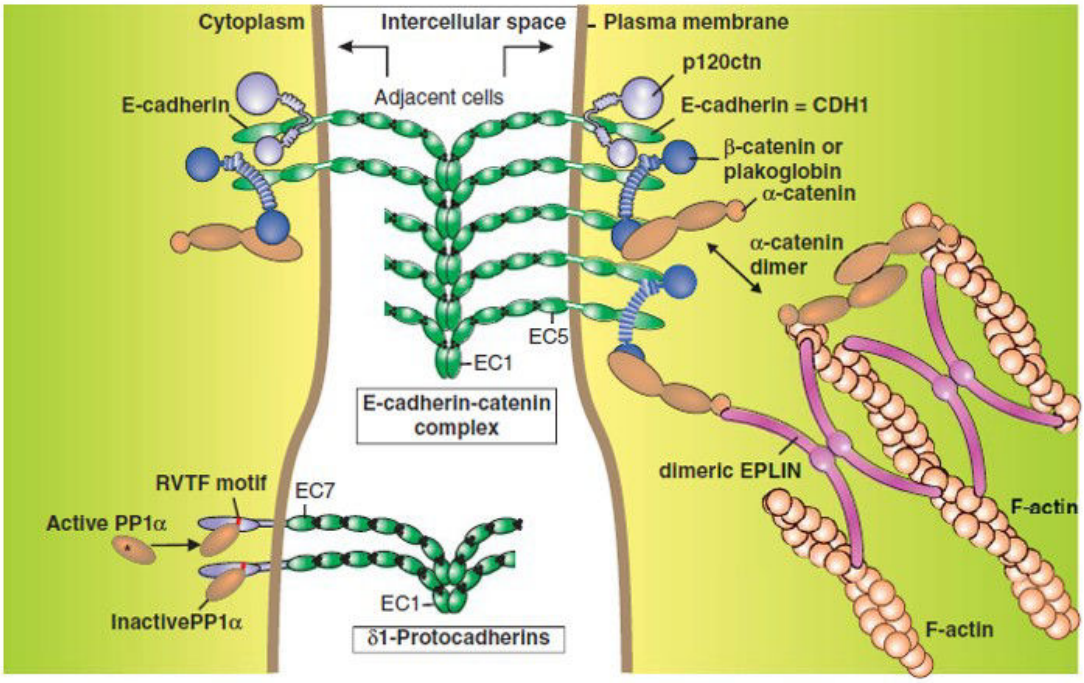

Figure 1.3 : ***Schematic representation of the E–cadherin organization at the adherens junction.*** *Source: Ref. [9].*

(see Figure 1.4). Each of these steps constitutes a barrier that only a small number of cancer cells manage to overcome. Thus the metastatic process is believed to be highly inefficient, but it is difficult to put numbers on the yield of each step.

The primary tumor cells must first invade the extracellular matrix and the various layers of stromal cells in the surrounding tissue. The extracellular matrix degradation is mainly carried out by enzymes called matrix metalloproteinase, whose activity is abnormally elevated in tumor cells [11]. The interaction of tumor cells with stromal cells (fibroblasts, adipocytes, macrophages and other immune cells) promotes proliferation and migration through the signal transduction initiated by adhesion molecules such as integrin [12, 13].

Tumor cells must cross the blood vessel wall formed of endothelial cells and then pericytes. This step, called intravasation, may be facilitated by the secretion of vascular endothelial growth factor (VEGF) by the cancer cells themselves. This factor stimulates the formation of new blood vessels within the tumor micro environment via a process called neovascularization. Low cohesion between adjacent endothelial cells lining the blood vessel and the absence of pericyte coverage in these new vessels facilitate the intravasation of cancer cells [15].

Once the endothelial barrier has been crossed, cells enter into the circulation and

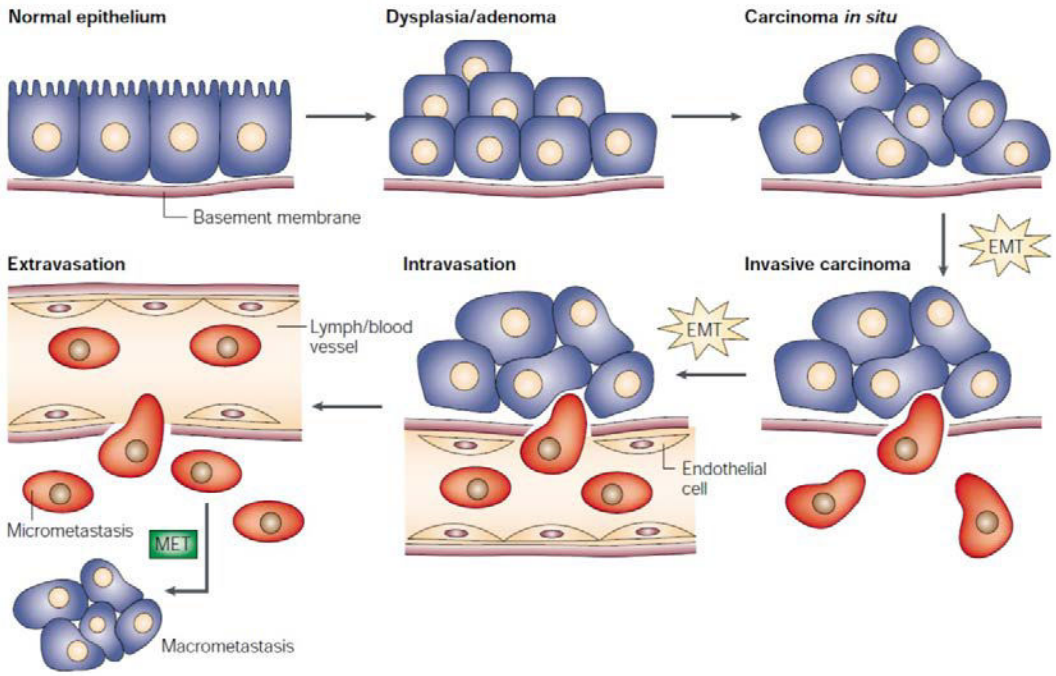

Figure 1.4 : ***Different steps involved in metastasis formation including the epithelial-mesenchymal transition of carcinoma cells.*** *Source: Ref. [14]*

constitute **circulating tumor cells**. CTC must survive a variety of stresses before crossing again the endothelial barrier in order to reach distant organs. For instance, epithelial cell normally adhere to the extracellular matrix via integrin and this is essential for cell survival. In the absence of such an anchor, epithelial cells undergo anoikis, a form of cell death triggered by loss of anchorage to the substrate [16]. Therefore, CTC must develop a mechanism of resistance against anoikis. Once into the parenchyma of distant organs, CTC can initiate the growth of a secondary tumor. However, in most cases the dispersed tumor cells enter a state of dormancy in the form of micro-metastases. These cells are resistant to traditional chemotherapy that targets rapidly dividing cells and are responsible for the development of late metastases (months or years after the primary tumor) [17].

1.2.4 Epithelial–Mesenchymal Transition

The large number of genetic alterations present in adult solid tumors could allow epithelial cells to acquire the functional modifications required to become invasive and to metastasize. However, some biologists like Robert Weinberg at MIT (Cambridge, USA), have been arguing for a long time that it was unlikely that independent mutations could generate a coherent phenotype able to perform complex tasks like intravasation.

While at this point it is impossible to give a documented answer to this question, the similarity between the metastatic process and some normal biological programs such as wound repair and cell migration during the embryonic development has suggested another way to approach these issues. Indeed, during embryonic development there are several waves of cell migration which allow epithelial cells to migrate from one tissue into another one. This process has been named **Epithelial–Mesenchymal transition** (EMT) since the first step is a change in cellular phenotype which in essence transforms epithelial cells into mesenchymal cells. This transformation can be observed at the cell membrane (through changes in adhesion molecules), in the cytoskeleton or in the regulatory networks which are active in the cells. As mesenchymal cells have only weak interactions with their environment and are intrinsically motile, this transition provides a framework to explain how initially epithelial cells can egress from their tissue of origin. Importantly, the reverse transition (Mesenchymal–Epithelial transition) can also take place allowing the cell to acquire its initial epithelial phenotype again. Figure 1.5 illustrates the changes in morphology and phenotype which take place during EMT [14, 18].

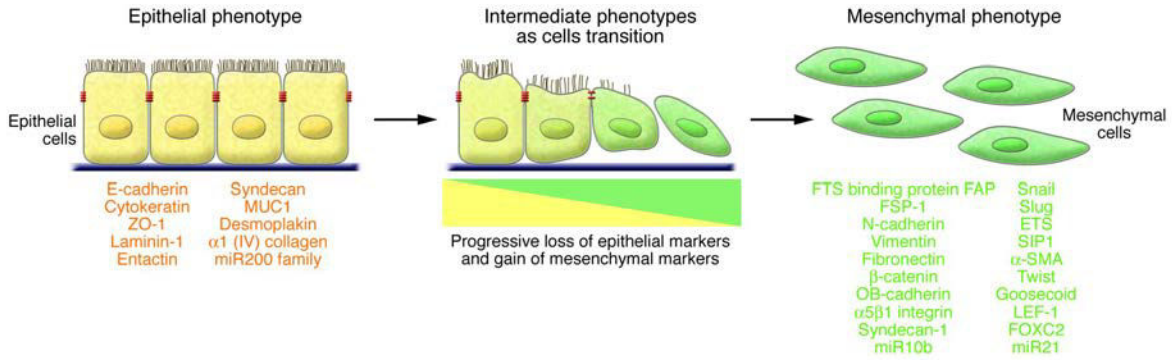

Figure 1.5 : ***EMT involves a transition in morphological and phenotypic characteristic of cells.*** *Proteins (like E–cadherin, cytokeratin . . .) shown in orange are typical proteins expressed in epithelial cells, but due to the EMT these proteins deregulate and gain mesenchymal phenotype shown in green (such as, N–cadherin, vimentin, fibronectin . . .). Source: Ref. [18].*

Epithelial cells are in close contact with each other and attached on the basal membrane which confirm their apical-basal polarity necessary for their function. Due to the presence of intercellular junctions, the organization of the actin cytoskeleton and the presence of a basal membrane in contact with the cells, epithelial cells can migrate within the epithelium by sliding along the basal membrane but cannot detached from it. By contrast, mesenchymal cells have only weak interactions with each other and have a directional polarity for promoting their migration. In culture, they present a fibroblastic

phenotype and do not form cell clusters like epithelial cells. The EMT is therefore made of a series of **morphogenetic events** during which the apical-basal polarity is lost, the intercellular junctions are altered, the cytoskeleton and the extracellular matrix are changed and the transcription of genes result in inducing migratory characteristics [18]. Intercellular cohesion is decreased due to the reduction of the expression of E–cadherin and zonula occludens-l, which are proteins forming the adherens and tight junctions respectively. The reorganization of the cytoskeleton is demonstrated by the reduction or loss of expression in keratins and the increase in expression of vimentin and actin in the periphery of the cell. The expression of the transcription factor Snail and Slug induce EMT in part by repressing E–cadherin. [14, 18, 19]

1.2.5 The Cadherin switch

The EMT induces many changes in cell organization which are in part due to changes in gene expression. E–cadherin and N–cadherin have been extensively used as markers of EMT since one of the salient features is the replacement at the cell membrane of E–cadherin (normally expressed on epithelial cells) by N–cadherin (normally expressed on mesenchymal cells). Although these two proteins have similar amino acid sequences and structures, they confer very different properties to the cells, since N–cadherin generates only weak homophilic interactions between cells. This difference in the strength of interactions is emblematic of the key features of epithelial and mesenchymal cells, the first ones being stably entrapped in an epithelium while the second ones are motile and invasive, not only because of the modifications of the cytoskeleton or the expression of proteases but also because of their ability to make transient contact with their neighbors thus allowing cell reptation.

A **cadherin switch** in which N–cadherin replaces E–cadherin has been also observed to take place in solid tumors which are not really derived from epithelial cells. This is typically the case for melanomas since the melanocytes are derived from the neural crest and not from an epithelium. Importantly, melanocytes have to leave the neural crest and to migrate into the epidermis during development by a process which can be assimilated to an EMT/MET cycle. It is frequently argued that the propensity of melanomas to metastasize is the indication that somehow the melanocytes have kept an ability to undergo an EMT/MET.

1.2.6 Relevance of the EMT/MET cycle for metastasis

The analogy between an EMT followed by a MET and the metastatic process is compelling. Since a potential involvement of an EMT-like process was stressed by Jean-Paul Thiery in 2002 [14], many studies both experimental and clinical have been devoted to test the pertinence of the analogy. The number of publication dealing with EMT and cancer has thus grown from 21 in 2002 to over 1200 in 2014. Many instances of correlation between the expression of markers of EMT and invasiveness have been reported. For instance, N–cadherin expression is associated with a migratory phenotype of breast adenocarcinoma [20, 21], pancreatic [22, 23] and prostate [24] cells. However, at the same time, the prognostic value of EMT markers has been limited to small scale studies suggesting that the classification of tumor cells as epithelial or mesenchymal is of limited value.

J.-P. Thiery and collaborators have recently performed an extensive study of the predictive value of EMT markers across carcinomas [25]. The originality of this study is to use a "universal" Epithelial-Mesenchymal index (E/M index) for all tumors, independently of the tissue of origin, based on a weighted analysis of transcriptome data. This allowed exploiting the large number of transcriptome analyses performed on different tumor types. A first conclusion is that tumors can be assigned to the full E/M index scale and that there is no immediate link with aggressiveness. Indeed, the main predictor of the E/M ranking is the tissue of origin and the clinical subtype (Figure 1.6). Therefore, in contrast with the apparent universality of the EMT/MET analogy, the steady state expression of epithelial and mesenchymal markers is associated with the type of carcinoma. In addition, the E/M index is similar between clinical samples and cell lines of the type of tumor, indicating that the stromal environment is not required for maintaining the E/M status. This was somehow unexpected since the stroma and the immune system are known sources of factors which can induce an EMT. Finally, a bad prognostic can be associated with either an Epi or a Mes phenotype, depending upon the tissue. The large dispersion observed between studies can in part be assigned to the different repartition of clinical subtypes in these cohorts.

Although very rich in information, there are several potential limitations to this type of study, like the presence of non-tumor cells in the analyzed samples (both stromal and immune cells are mesenchymal in nature) and the heterogeneity of tumors. Another source of difficulty comes from the snapshot nature of the determined index. EMT/MET are by nature dynamical processes which cannot be considered as steady state profiling of tumors. These points are discussed in the next section.

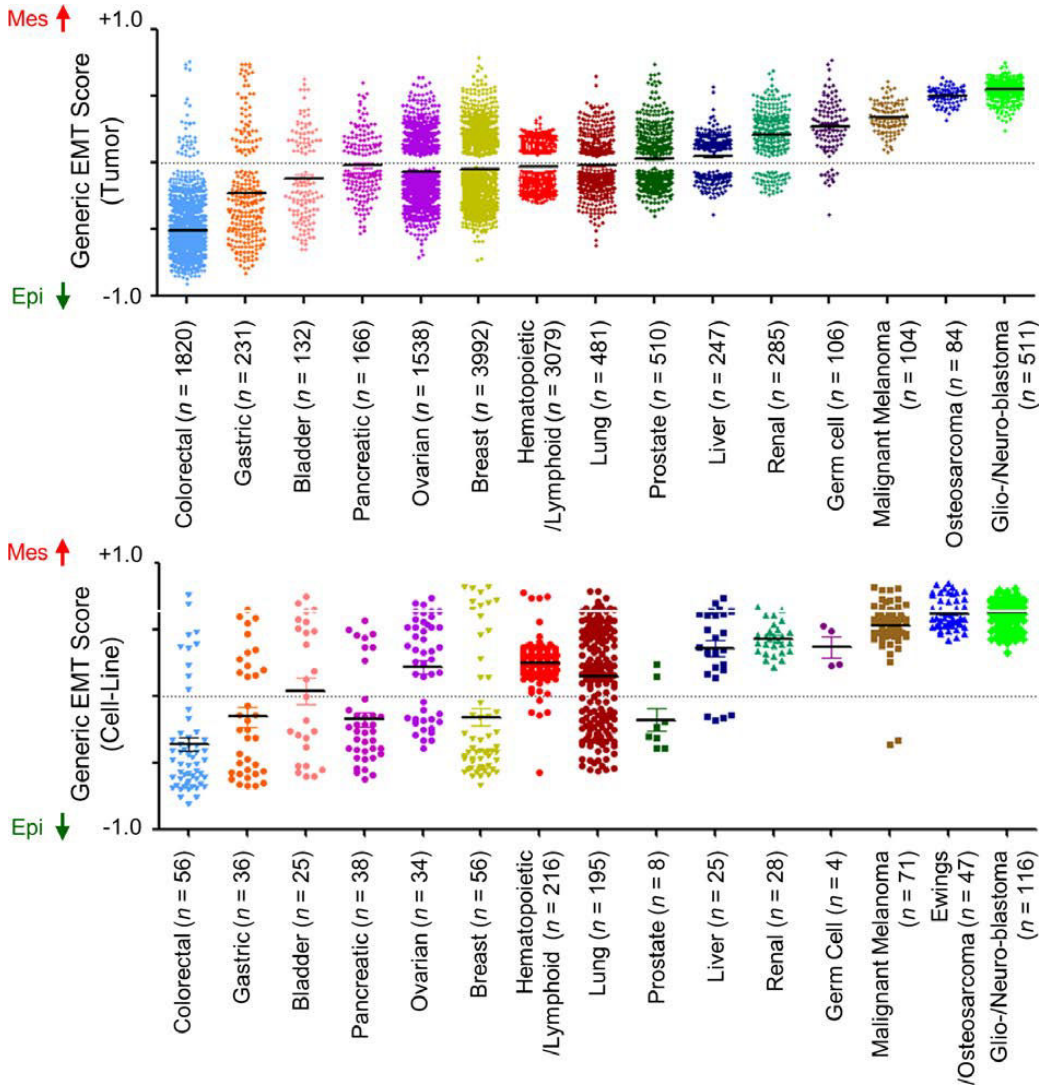

Figure 1.6 : ***Classification of solid tumors according to a epithelial–mesenchymal index (*Generic EMT score*).*** *The upper panel describes the results for tumor samples and the lower one the results for cell lines. Source: Ref. [25].*

1.3 Tumor heterogeneity

It is a standard observation by pathologists that tumor are heterogeneous. This could have several meanings. First, tumors can contain a significant amount of stromal cells which can interfere with their characterization, for instance when sequencing the genomic DNA or analyzing the transcriptome. In addition, they can be infiltrated by immune cells which can similarly contribute to the apparent genotype/phenotype. Although these "normal cells" are as much as possible excluded from the subsequent analyses they are not always passive bystanders and can also be involved in tumor progression. Indeed,

both fibroblasts and immune cells can secrete growth factors which can stimulate tumor cell proliferation or alter their phenotype. Nonetheless, most of the current efforts in cancer biology are focused on the tumor cells themselves.

1.3.1 Genetic heterogeneity

The classical scheme of tumor progression is based on a Darwinian selection process. The occurrence of a new mutation alters the fitness of the tumor cell (here meaning its ability to accumulate by proliferation and to resist to cell death) and the new population will either overgrow the others or be eliminated depending upon the beneficial or detrimental impact. Implicitly, it has been assumed for a long time that the selection process was complete and therefore that within a tumor all the cells shared the same genetic events. This vision was based on the idea that mutations were infrequent and since tumor progression is usually a slow process extending over several years, the selection could be completely carried out. With the advent of sequencing it has become possible to directly test this notion even if at the present time sequencing of individual cells is still challenging. One of the first in depth study of intratumor heterogeneity has been performed by sequencing the coding regions within the genomic DNA extracted from several fragments of a pancreatic tumor as well as from metastases from the same patient [26].

This study revealed that the spectrum of mutations differed between these samples. However, they shared a common pool of mutations and it was possible to reconstruct the history of the tumor and its metastases which, in this case, originated from the fully developed tumor. Since then a number of sequencing project have been carried out and have confirmed that tumors are often very heterogeneous in their genetic makeup [27]. It is therefore likely that not all the cells present in the tumor contribute equally to its evolution and in particular that metastases are due to specific subpopulations. It is even possible that the driving genetic events in the metastases differ from those of the primary tumor and thus that these different tumors warrant different therapies [28].

1.3.2 Epigenetic heterogeneity and plasticity of the phenotype

In addition to the genetic heterogeneity there is also the possibility that tumor cells differ at the epigenetic level. In its simplest form, this could be interpreted as meaning that within the tumor some cells spontaneously differentiate while others are more like **“stem cells”**, i.e. able to self-review and to give differentiated progenies. In agreement

with this idea, cells can be sorted on the basis of their expression of markers of pluripotency or differentiation. This has been first achieved in leukemia and since then applied to almost all types of tumors [29, 30].

Beyond the ability to identify subpopulations this allowed exploring whether all the cells within the tumor are equally tumorigenic. However, this can only be performed in animal models and consequently, when applied to human tumors, the residual immune system of even the most immunocompromised models is always an issue in view of the strong rejection of xenografts. Nonetheless, these studies have indicated that the more undifferentiated cells are usually the one with the highest tumorigenicity. While a hierarchy of stem cells, precursors and differentiated cells has been well characterized in the hematopoietic system, the situation is much less clear for other tissues but it is likely that a similar organization is pertinent for other tissues. The characterization of the different levels of "adult stem cells" is actively pursued [31].

As their normal counterparts, cancer stem cells can self-renew and differentiate into one or several cell types. They also might be naturally resistant to several chemotherapeutic agents and they can be selected *in vivo* by a not completely efficient therapy [32]. However, beyond their ability to induce tumors when transplanted in low numbers and to regenerate the initial tumor heterogeneity the exact nature of cancer stem cells and the extent to which they are similar to normal stem cells (for instance by being mostly quiescent) is still a matter of debate. It is tempting to assume that a major route to tumor progression is to be initiated within an adult stem cell. However alternative explanations are possible since some of the genetic events occurring favor the reprogramming of differentiated cells into stem cells [33].

The characterization of cancer stem cells has led to an unexpected observation: in contrast to the normal differentiation process which is believed to be irreversible (once cells are differentiated, they cannot spontaneously move back to their previous undifferentiated state), cancer cells can evolve both in a forward direction (differentiate) and in a "backward" direction (dedifferentiate). This has been illustrated by cell sorting experiments in which cells are purified according to markers of their differentiation state. If the purified populations are grown separately, they give rise in many cases to the initial mixture of differentiated and undifferentiated cells [34]. This can also be observed in breast cancer cell lines which can be sorted in three distinct populations stem-like, basal-like and luminal-like. Each of these three populations can give rise to a mixture of the three which is similar to the initial unsorted population [35]. Of note, these experiments were performed with cell lines which can be cloned (grown from a single isolated cell)

and therefore are expected to be genetically homogenous.

These observations have led to the concept of **phenotypic plasticity** of tumor cells which might have important practical implications. For instance, if we believe that cancer stem cells are the one that will resist to chemotherapy and later on will give rise to a relapse, it would be advisable to tailor the treatment towards the stem cells and to ignore the more abundant compartment of "differentiated" tumor cells. However, even if we had the proper therapeutic agents, it is likely that in response to a depletion of cancer stem cells, the more differentiated ones would replenish the stem cell compartment so that in a world of phenotypic plasticity there is no clear cut distinction between the compartments.

1.4 Circulating tumor Cells

As mentioned in the previous section, circulating tumor cells (CTCs) represent an obligatory intermediate between the primary tumor and the micrometastases. CTCs have been observed as early as in the 19th century by the Australian physician Thomas Ashworth [36]. However, the field of CTC research has really emerged in the last decade, with the development of efficient CTC detection technologies.

1.4.1 Clinical significance of CTCs

CTCs are rare in comparison with nucleated blood cells, typically a few cells per mL of blood which contains approximately 10^7 white cells. Nonetheless, the presence of even few CTCs in the peripheral blood of cancer patients is an indicator of a bad prognosis in a variety of solid tumors. In a pioneering study by M. Cristofanilli and colleagues, the authors established that patients with more that five CTCs per 7.5 mL of blood have a smaller progression-free survival and smaller overall survival durations in metastatic breast cancer [37]. These data have been validated by several independent studies and similar results have been obtained in patients with other cancers, including prostate, colorectal and lung cancers [38–41].

The number of CTCs can also be used to monitor the patient response to an ongoing conventional or targeted anticancer therapy. Different studies have reported a decrease in the number of CTCs in response to therapy and have shown that this decrease was associated with a better prognosis. The utility of CTC counts as a pharmacodynamic marker is currently evaluated in a prospective clinical trial [38, 42]

Finally, a few studies suggest that CTCs might be used as"sentinel" for the presence of cancer [43, 44].

1.4.2 Biology of CTCs

For each gram of tumor, three millions of cells are released in the blood circulatory system every day [45]. Out of these cells, only 1% survive and an even smaller fraction (0.1%) has the potential to give rise to metastases. There are two compartments where these cells can be traced: (i) the blood circulatory system (CTCs) and (ii) the bone marrow and regarded as disseminated tumor cells (DTCs).

The ability of circulating tumor cells to leave the primary tumor site, survive in the circulation and at some point reach and colonize a distant organ is necessarily associated with specific biological properties.

Survival of CTCs in the blood circulation

Isolated epithelial cells normally undergo an apoptotic process called anoikis, which is triggered by the loss of cell anchorage to the extra-cellular matrix. A major mechanism of resistance of CTCs to anoikis is probably related to their ability to form clusters, which are frequently detected in patients and are called circulating tumor microemboli (CTM) [42]. CTM are defined as clusters of at least three CTCs, which can also be associated with other cell types such as fibroblasts, hematopoietic or endothelial cells. Interestingly, apoptosis has been detected less frequently within CTM than in single CTC in patients with small-cell lung cancer [41]. In addition, the proliferative index of CTCs was reduced in CTM (based on a Ki-67 staining), suggesting a dormant state of clustered cells and a potentially higher resistance to chemotherapy [41]. A low Ki-67 staining has also been reported in CTCs from breast cancer patients [46]. Additional factors probably contribute to the resistance to anoikis and other cell death mechanisms in CTCs. One such factor could be the hyperactivation of the WNT signaling pathway [47].

Epithelial-Mesenchymal Transition in CTCs

As already discussed, the EMT probably plays a major role in the metastatic potential of a primary tumor. Thus, EMT markers have been analyzed in CTCs from patients in a number of studies [42]. A high heterogeneity in the expression of epithelial and mesenchymal markers has been observed in CTCs, both within and between patients, in several cancers including lung, breast, prostate, and head and neck cancers.

An elegant study performed by M. Yu and colleagues demonstrated that different types of CTCs can be observed in breast cancer patients, some expressing a purely epithelial or mesenchymal phenotype, whereas others co-expressed epithelial and mesenchymal markers ("hybrid phenotype"). Most interestingly, different subtypes of CTCs were

sometimes observed in the same patient and their relative proportions were then found to vary during disease progression and treatment [48].

The concomitant expression of epithelial and mesenchymal markers in the same CTC could reflect a partial EMT and allow the CTC to easily accomplish an EMT/MET cycle. On the other hand, epithelial and mesenchymal CTCs could also cooperate to form metastases. Such cooperation has been demonstrated by co-injection of different cell types in mice [42].

1.5 Methods of CTCs enrichment and detection

CTCs occur at very small concentrations in the blood, fluctuating between 1–7 cells per 10 mL in most cancer patients, which poses a difficult task for any diagnostic system.

The most regularly established methods for CTC enrichment and detection methods are based on size, density, immune-magnetic separation and microfluidics as summarized in figure 1.7.

1.5.1 CTC enrichment and detection based on epithelial marker EpCAM

In this method, CTCs are captured by magnetic beads coated with anti-EpCAM. This system was first used by Allard et al., who analyzed 900 blood samples from patients with different metastatic tumors [51]. The system is intended for the enumeration of circulating tumor cells of epithelial origin ($CD45^-$, $EpCAM^+$, and cytokeratins 8^+, 18^+, and 19^+) in whole blood. Cell nuclei were stained with DAPI. The number of cells with $CK^+/DAPI^+/CD45^-$ assessed using a four dyes by a semi-automatic fluorescence microscopy CellTracks Analyzer II (Janssen Diagnostics, USA) [52, 53].

This technique commercialized under the name CellSearch® (Janssen Diagnostics, USA) is the only one approved at the moment by the FDA (Food and Drug Administration, USA) for the detection of CTC in clinics. The CellSearch system allows reproducible determination of the number of CTCs in the blood sample. The advantage of this method is the fact that the isolated cells retain their structure and can be further analyzed. Furthermore, this method has been successfully assessed in many large clinical trials. By studying the same samples in different research centers ensures high reproducibility of the results. Despite its many advantages CellSearch only allows the identification of CTCs expressing EpCAM protein which may be reduced during the process of EMT.

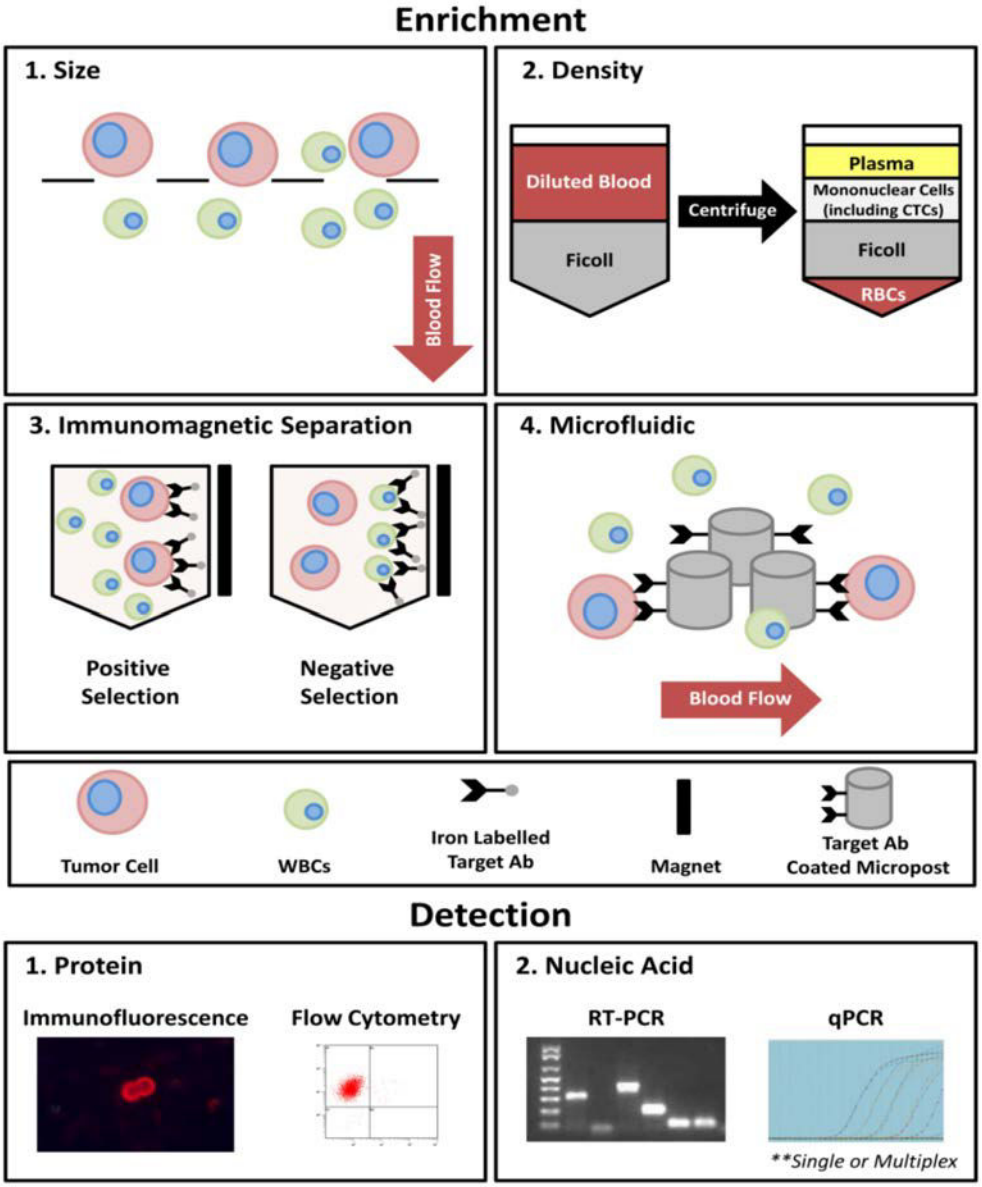

Figure 1.7 : ***Frequently used methods for CTC enrichment and detection.*** *Top panel: enrichement techniques 1. Size-based techniques use (ISET); 2. density based enrichment (OnCoquick); 3. magnetic beads enrichment (CellSearch); 4. microfluidic enrichment (CTC-chip). Bottom panel: two major techniques used for detection and characteristic rely on protein detection with antibodies (1.) illustrated by cytometry and mRNA detection (2.) illustrated by RT-PCR. Source: Ref. [49]*

The advantage of the CellSearch system is that it allows the recovery of cells for further analysis. On other hand, the system measures only EpCAM and cytokeratins (8, 18, and 19) expressions, and it is therefore impossible to detect CTCs which do not express these markers or express them with some heterogeneity like for EpCAM in mammary carcinomas [54]. Cytokeratin are frequently used to isolate epithelial cells in

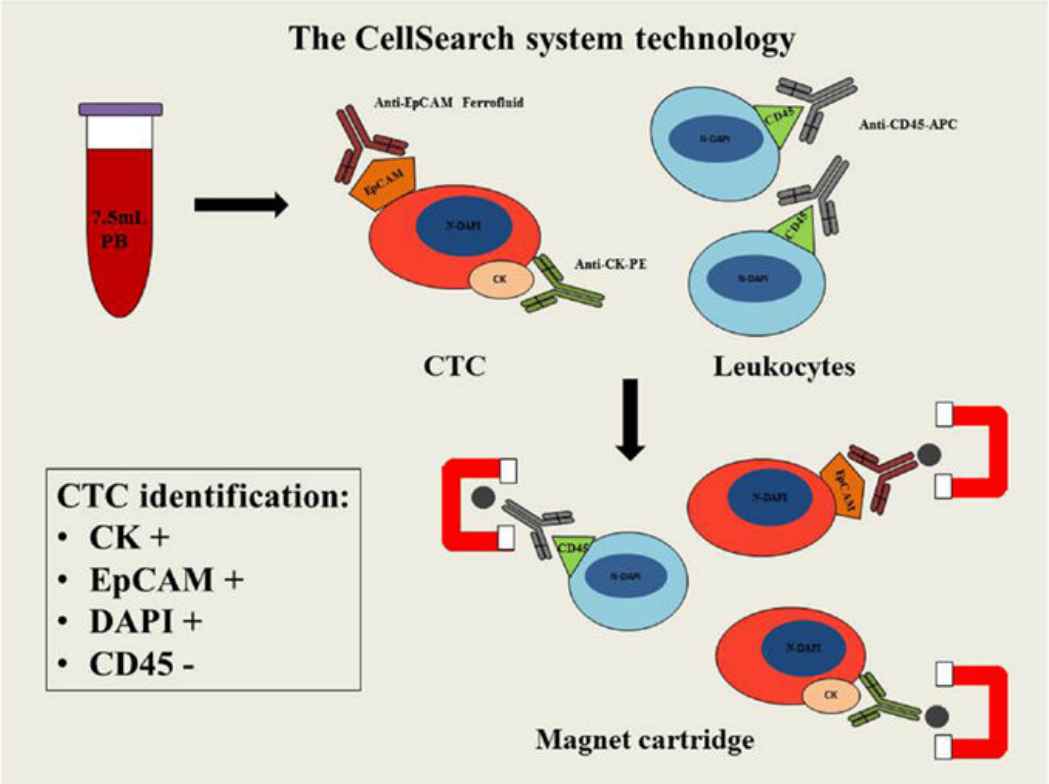

Figure 1.8 : *Schematic diagram of CellSearch system technology.* *CTCs are identified by EpCAM (positive), cytokeratin (positive), and DAPI (positive) and CD45 (negative) among blood cells. Source: [50]*

an heterogeneous population but they are not specific to a type of tissue, so that there is a non-negligible probability that they come from a contamination during patient blood sampling. Hence, there is a need of additional markers to improve the CTC detection specificity.

The latest capture method based on EpCAM expression is the microfluidic platform CTC-chip developed at the Massachusetts General Hospital Center for Engineering in Medicine (panel 4 of figure 1.7). In this method, the blood flows through a plate to target CTCs with anti-EpCAM-coated micro posts under precisely controlled laminar flow conditions and without requisite pre-labelling or samples processing. Captured cells are then labeled and analyzed by fluorescent microscopy [55]. A similar fully automated method for rare cell sorting was recently developed by Jean-Louis Viovy (Institut Curie, Paris). It uses anti-EpCAM-coated magnetic microspheres self-assembled into columns, thus making a compact filter where cells are captured [56]. This system is capable of capturing a large number of CTCs with low contamination.

1.5.2 Isolation methods based on cell size

The method of isolation of epithelial tumor cells on the basis of their size (panel 1 of Figure 1.7) like the one commercialized under the name ISET® (isolation by size of epithelial tumor cells, RareCells, Paris) allows the isolation of cell with sizes larger than 8 μm. Isolated tumor cells were immunostained for surface markers and the analyzed and validated individually. Cells are considered as tumor cells [57] if: (i) they are CD45 negative ($CD45^-$); (ii) they have a large ($\geq$12 μm), hyperchromatic, irregular-shaped nuclei ; (iii) the nuclear to cytoplasmic ratio is larger than 50%.

The ISET system is not antigen dependent, which is why it can detect more cells than the CellSearch. On other hand, it required a manual validation which impacts the reproducibility. Moreover, the studies conducted so far did not support the hypothesis that all CTCs are greater than 8 μm [58].

1.5.3 Alternative enrichment and detection strategies

Due to the low sensitivity and specificity of the previously described techniques, some manufacturer have developed tests combining multiple criteria. For example the AdnaTest (AdnaGen AG, Germany) is a technology combining cell immunomagnetic capture (relying on EpCAM) and RT-PCR (Reverse Transcription Polymerase Chain Reaction). The captured cells are lysed in order to isolate mRNA then analyzed by quantitative RT-PCR to quantify HER2 (human epidermal growth factor), MUC1 (surface glycoprotein) and GA733-2. The limitation of this method is that the expression of MUC1 is also present on activated T- lymphocytes [59].

In the above mentioned methods for CTCs enrichment and detection do not differentiate between apoptotic and viable CTCs. The EPISPOT assay developped at the Laboratory of Rare Human Circulating Cells (Institute of Research in Biotherapy, Montpellier, France) is capable of detecting viable CTCs and not apoptotic ones. This technique identifies CTCs based on secreted proteins from different cancer cells put in culture for 48 hours; for example CK-19, MUC1 in the case of breast cancer, PSA for prostate cancer and thyroglobulin for thyroid cancer [60,61]. The information obtained from this approach are very significant because only viable cell would be able to cause metastases. A limitation is the difficulty to obtain a large number of cells in culture, and an insufficient reproducibility of the results.

1.5.4 Detection of nucleic acids

Nucleic acid based techniques recognize particular DNA or mRNA markers such as PSA, HER-2, CEA in the specimen to indirectly identify the presence of CTCs [62–64]. Some studies have isolated nucleic acids directly from plasma [65, 66], while others have first purified the nucleated cells from blood and then extracted nucleic acids. CTCs detection using mRNA is more effective as compare to DNA because often DNA molecules are released by necrotic or apoptotic CTCs and can contribute in false-positive detection. This method offered potentially a high sensitivity, being capable of detecting one CTC in 5 mL of blood. However it suffers from many false-positive and negative which make it unsuitable for diagnosis.

As mentioned above, nucleic acid can also be detected directly in the plasma. Circulating free DNA can be identified in healthy person and in considerably greater concentrations in patients with cancer [67]. In 1940, Mandel and Mëtais reported the presence of free nucleic acids in plasma [68]. The presence of high content of free DNA was also observed in patients with pancreatic cancer. The plasma DNA content is also reduced after chemotherapy [69]. More recent works confirmed the presence of free circulating DNA and RNA in patient blood [66, 70] and also established a relationship between the concentration of free DNA in plasma and the type of cancer [71–73]. It is believed that the presence of DNA/RNA in plasma arise from lysis of tumor cells. The presence of free DNA/RNA can therefore be a useful tool for non-invasive, rapid, sensitive and accurate method for diagnosis of various types of cancer.

Although the analysis of nucleic acid is often proposed as an alternative to CTCs characterization, the two approaches are not equivalent. Circulating nucleic acid detection does not provide cell specific data which can be misleading in some situation. Indeed in response to treatment, sensitive cells will be killed and their nucleic acids will be released, while the resistant cells will be unaffected. Thus circulating nucleic acids and CTCs may provide opposite views of tumor cell sub-population.

1.5.5 Need for better CTC detection techniques

The identification of CTCs is necessary to further characterize them at the molecular level and thus to better understand their biological properties. A molecular analysis could be particularly useful in the clinical practice to select a personalized anticancer therapy, especially one that could eradicate potential metastasis precursor cells. An important issue of current CTCs detection techniques is the low number of CTCs collected. In addition, the CellSearch System only detects the CTCs expressing the epithelial marker

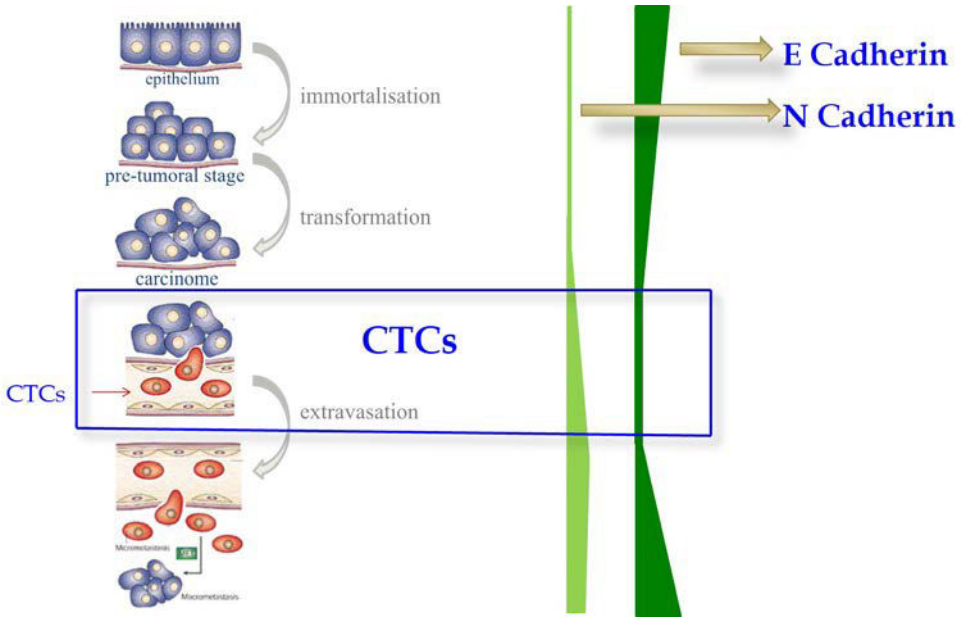

Figure 1.9 : ***Relation between different stages of tumor progression and the level of E-/N- cadherin expression.***

EpCAM and thus cannot identify CTCs harboring a low expression of epithelial markers (which might be the most invasive). Moreover, various studies have shown the presence of mesenchymal phenotype on CTCs [74, 75].

In this thesis we focused on the detection of cells expressing hybrid phenotype, based on the co-expression of E– and N–cadherins (Figure 1.9)

1.6 Advanced fluorescent techniques used to characterize cancer cells

To detect and quantify E– and N–cadherins in cells we used **flow cytometry** and **immunofluorescence** imaging combined with advanced fluorescence techniques: (i) time-resolved **Fluorescence Resonant Energy Transfer (FRET)**, (ii) high-throughput automatized image acquisition and processing, and (iii) immunolabeling using **fluorescent nanocrystals (quantum dots, QDots)**.

Flow cytometry and immunofluorescence are two robust and well established tools have their own advantages and disadvantages, but together they complete each other. Flow cytometry offers fast analysis of different characteristics of single cells. The data obtained is both qualitative and quantitative along with high dynamic range. Flow cytometry is used for immunophenotyping of a range of samples. Flow cytometer are

capable to characterize 100,000s of cell in few minute individually. It provide physical information like, size, granularity, along with multiple phenotypic characteristic. This system is important for this study because of its sensitivity, high dynamic range and quantitative ability.

In order to study the localization of proteins in cells we used widefield **epifluorescence** and fluorescence **confocal** microscopy. Epifluorescence was implemented in a high throughput acquisition system. It provides a large number of images, but due to a large depth of field in this mode, we capture the whole cell fluorescence along the direction of light propagation. On the contrary confocal microscopy uses spatial filtering allowing to collect fluorescence of less than 1 μm thick sections of the cell. Figure 1.10 shows the difference between the two different techniques for the same sample in imaging E–cadherin: confocal microscopy indicate that E–cadherin is localized at the cell membrane, while epifluorescence is less discriminant.

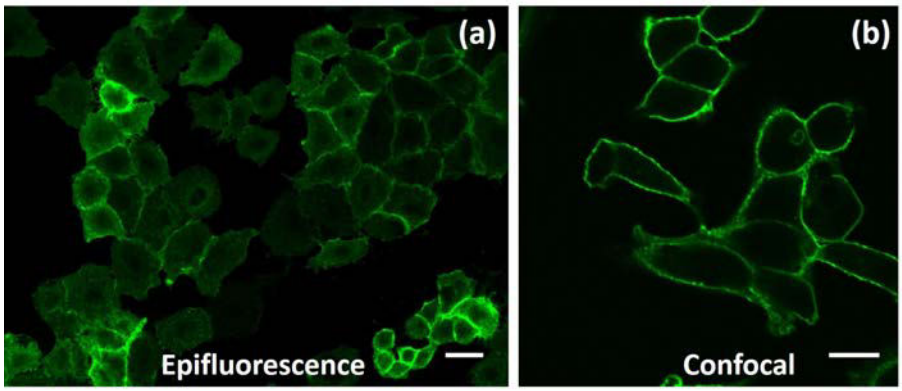

Figure 1.10 : ***Comparison between image of FITC dye-labeled E–cadherin in a culture od MCF7 human breast cancer cells, acquired by epifluorescence (a) and by confocal (b) systems.*** *Scale bars: 20 μm.*

To go further in the analysis of E– and N– protein localization and organization we used Förster resonance energy transfer (FRET), which is a technique capable of detecting two fluorophore-labeled proteins located at distance smaller than 10 nm.

1.6.1 Principle of FRET detection

The FRET is non-radiative transfer of energy between nearby fluorophores. It is a dipole-(induced)dipole coupling mechanism [76]. The distance between the donor and the acceptor molecule is typically in the range of 1-10 nm. When a donor is excited, it jumped into a higher energy state (S_0 to S_1, as shown in Figure 1.11) from which it

first relaxes non-radiatively in picosecond timescale to the first excited state and from there it can return to S_0 ground state either by emitting a fluorescence photon or by the non-radiative process involved in FRET, when an acceptor is within the dipole-dipole interaction range and if its absorption spectrum overlaps with the emission spectrum of the donor (see Figure 1.11(b)). In the later case (efficient FRET) the donor fluorescence will be quenched and at the same time the acceptor gets excited by the energy transfer and then emits fluorescence [77–80].

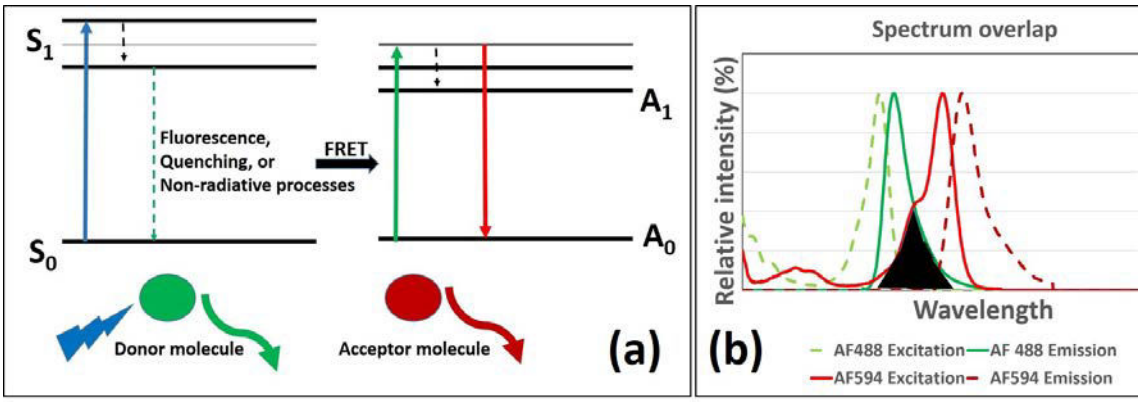

Figure 1.11 : *(a) Jablonski diagram illustrating the FRET process, (b)Spectral Overlap (black area) between AF 488 (in green) and AF 594 (in red) allowing the FRET between these two dyes to take place.*

Certain condition must be satisfied for FRET to occur:

1. There should be a spectral overlap between excitation of an acceptor and emission of the donor (as displayed on Fig.1.11(b)), given by the integral $J \equiv \frac{\int_0^\infty F_D(\lambda)\epsilon_A(\lambda)\lambda^4\, d\lambda}{\int_0^\infty F_D(\lambda) d\lambda}$, where $F_D(\lambda)$ is fluorescence intensity of donor, $\epsilon_A(\lambda)$ is the extinction coefficient of the acceptor, with ϵ_A given in unit of $\text{cm}^{-1}.\text{mol}^{-1}$, λ is taken in unit of cm, so that J is in unit $\text{cm}^6\text{mol}^{-1}$.

2. No FRET occurs when the donor and acceptor dipoles are orthogonal. The relative orientation being characterized by a factor κ^2 varying between 0 (when perpendicular) to 4 (when parallel) [81].

Förster [82] demonstrated that FRET efficiency E depends on the inverse sixth power of distance between donor and acceptor (R):

$$E = \frac{R_0^6}{R_0^6 + r^6},$$

where R_0 (Förster radius) is the distance at which 50% of energy is transferred to an acceptor fluorochrome. R_0 can be related to acceptor and donnor parameters, and its value (in **cm**) can be inferred from the following relation:

$$R_0^6 = 8.79 \times 10^{-25} n^{-4} \kappa^2 J \eta_Q \quad (\text{cm}^6)$$

where η_Q is the donor quantum yield in the absence of acceptor, n is the refractive index of the medium. Typical values of R_0 are in the 2-10 nm range for organic dyes. During this thesis, we used FRET as a tool to investigate the co-expression of E– and N–cadherin at the cell membrane.

The most frequent method for detecting and quantitating bio-molecules relies on organic dyes. Fluorescent dyes are well established probes for bio-sensing applications that include, cellular imaging, protein detection, immunoassays, nucleic acid detection .... However, these organic dyes often suffers from chemical degradation, photobleaching, pH dependencies, limited stability in aqueous medium, and short fluorescence lifetime. Semiconductor nanocrystals (QDots) have been developed to overcome some of these limitations, and we used custom-made QDots coupled to antibody to improve immunofluorescence imaging of E– and N–cadherin in cultured cancer cells.

1.6.2 Fluorescent semiconductor nanocrystals: Quantum dots

QDot is made of a nanocrystalline core composed of two to three semiconductor elements from columns I to VI of the periodic table, with the most well known one being CdSe (columns II-VI). They are synthesized in solution by heating precursors, organic surfactants and solvents. This nanostructure is a 1D quantum well with quantified energy levels. An exciton (i.e. an electron-hole pair) can be created by photoexcitation[1], which decay through photoluminescence (electron-hole pair recombination) at a wavelength depending on the ground-to-excited state energy difference. This energy difference is governed by the nanoparticle size (see Figure 1.12(a)), allowing for the production of QDots of desired emission wavelength.

The bare core is extremely reactive and can result in an unstable structure leading to emission anomalies like blinking and to photochemical degradation. To overcome these drawbacks, a shell (of ZnS, in the case of CdSe) is grown on the core [83, 84].

For QDots biofunctionalization, an additional coating of polymer is used to make it susceptible to bio-molecules. A typical diagram of QDots is presented in figure 1.12(b).

[1]The photoexcitation energy is larger than the bandgap in order to promote an electron from the valence to the conduction band. This is usually done with UV or deep blue illumination.

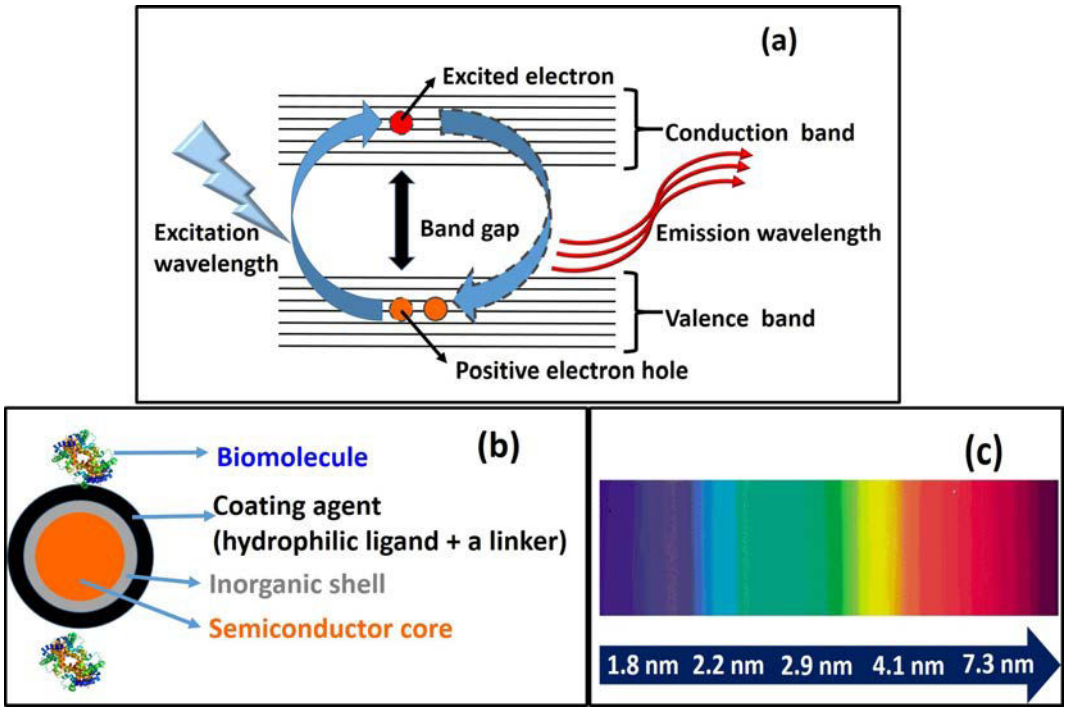

Figure 1.12 : ***Quantum dots.*** *(a) Photoexcitation and emission of a QDot. (b) Multilayer structure of a QDots used in bioimaging. (c) Core size (bottom arrow) vs emission spectrum.*

QDots have numerous of advantages over conventional fluorophore:

- Their emission spectrum can be tuned, because it depends on the size of the crystal.
- They have a broad absorption spectrum and their narrow (width $\simeq$10 nm) emission facilitates dense multiplexed imaging.
- Moreover, QDots are brighter than conventional fluorophores and are more resistant to photobleaching.
- The photoluminescent lifetime of QDots are nearly 20–50 ns, which makes imaging of live cells possible without the background autofluorescence of the cell (radiative lifetime $\approx$ 1 ns), using time-gated detection [85].

Altogether these properties make it ideal candidate for imaging [86]. The significance of QDots for our researches is vital because QDots can be very robust tool for fluorescence multiplexing imaging, and high-throughput screening.

1.7 Manuscript outlines

This thesis deals with a part of NanoCTCs project. The aim of NanoCTC project is to develop a set of technological tools that allows characterization of CTCs based on molecular and cellular profiling that eventually leading to the identification of CTCs subpopulation. This project intent to use photoluminescent nanoparticles (i.e. QDots and terbium) for imaging and FRET. But the major objectives of this thesis are;

- We first identified a cell line which co-expresses E– and N–cadherin, which could be used as a model of CTC at an intermediate stage of EMT.
- We then proposed a new fluorescence-based tools to improve the identification of these model cells in the situation of clinical detection of CTC.
- We explored the possibility of using FRET technique to characterized co-expressing cells. We used Terbium complex as donor and dye as an acceptor to label E–cadherin and N–cadherin respectively to see the energy exchange between them.
- We then bio-functionalized semiconductor nanoparticles (QDots) to E–cadherin and N–cadherin

The NanoCTC project in which the thesis work was realized, involved six partners and most of the work was done in collaborations with some of them.

In **chapter 2**, we present the results of the selection of cancer cell lines that co-express epithelial and mesenchymal markers, using fluorescent dye-based immunophenotyping methods, i.e. immunofluorescence and flow cytometry. We described the population expressed in hybrid phenotype cell line. We demonstrated the pattern of localization of heterodimer proteins on co-expressing cells.

In **chapter 3**, we establish a protocol to identify by high-throughput automatic immunofluorescence imaging two populations of cells having different epithelial/mesenchymal phenotypes, in co-cultures of them at different proportions. This chapter describes the tool that could quantify phenotype of CTCs among other type of cells. We presented an example where same system successfully identified A549 cells (prototype of CTCs) among blood cells at a concentration of 3000 cells in 1 mL of blood or 3000 cell per 10 million leukocyte.

Chapter 4 deals with investigation of the time-gated FRET between terbium complex as a donors attached to E–cadherin membrane protein and fluorochrome as an acceptors attached to N–cadherin membrane protein. Their co-expression at the mem-

brane is measured directly by exciting the terbium donors and detecting emission of the fluorochrome acceptors.

Chapter 5 presents the results of immunofluorescence labeling of E–cadherin in MCF7 cell line using quantum dot. The various conjugation methods used for biofunctionalization of QDs are presented along with the corresponding results.

Finally, we provide a conclusion and some prospects.

1.8 Publications

Published *Terbium-Based Time-Gated Förster Resonance Energy Transfer Imaging for Evaluating Protein-Protein Interactions on Cell Membranes*, Stina Lindèn, Manish Kumar Singh, Marie Regairaz, François Dautry, François Treussart, and Niko Hildebrandt.
Published in *Dalton Transactions (2015) doi: 10.1039/C4DT02884H).*

In preparation Biofunational quantum dots as specific cell markers for diagnostics and cell identification, *M. Tasso, M. K. Singh, A. Fragola, V. Loriette, E. Giovanelli, N. Lequeux, F. Treussart, F. Dautry, T. Pons.*

2 Selection of a cell line serving as a model of CTC

Summary

As discussed in the introduction Chapter 1, most of the currently used approaches to study CTCs introduce biases. This is particularly important in the current phase of investigation during which we would like to identify if some sub-populations of CTCs are particularly informative in terms of diagnostic, prognostic and response to therapy. The epithelial / mesenchymal characteristics of tumor cells are of key interest in view of the proposed role of the Epithelial Mesenchymal transition in the metastatic process but are the prime targets of selections biases since CTCs are often selected on the basis of an epithelial marker. Here we attempt to develop techniques which could allow the detection of CTCs with a hybrid phenotype (expressing epithelial and mesenchymal markers) potentially in the absence of any selection. One hallmark of the hybrid phenotype is the co-expression of E– and N–cadherin. The proposed approach is to use a

FRET between appropriately labeled antibodies targeting E– and N–cadherin. Because of the short range of FRET, co-expression of E– and N–cadherin by the same cell is obviously a prerequirement but this might not be sufficient if the two molecules are not in close proximity on a molecular scale i.e. in the 10 nm range. In order to test whether co-expression of E– and N– cadherin could lead to a FRET based detection it was therefore necessary to identify cells which could be considered a reasonable model of tumors cells with a hybrid phenotype.

Although cells with a hybrid phenotype have been occasionally observed in many laboratories, they have not been extensively studied until recently when it became apparent that, in tumor cells, EMT is not an all or none phenomenon. Accordingly, transcriptome studies indicate that many but not all of the standard tumor cell lines can co-express E– and N–cadherin [25]. For instance, A549 a cell line established form a lung adenocarcinoma expresses both mRNA. Previous work in the laboratory had indicated that some melanomas cell lines can co-express E– and N–cadherins and these were used during the initial optimization of the protocols.

2.1 Setting up conditions for immunofluorescence and flow cytometry cell phenotype analysis

Name	**Human/Animal**	**Organ**
MCF7 (NCI 60 panel)	human	breast adenocarcinoma
Hs 578T (NCI 60 panel)	human	breast, carcinoma
A549 (NCI 60 panel)	human	lung carcinoma
T1	human	primary tumor(lymphoblast)
G1	human	ganglionic metastasis
I2	human	primary tumor
M1	human	ganglionic metastasis
I5	human	melanoma primary tumor
M2	human	ganglionic metastasis tumor
M4T	human	melanoma primary tumor
M4T2	human	melanoma cutaneous metastasis
Colo	human	colon, metastasis tumor
NIH 3T3	mouse	mouse embryo (fibroblast cells)

Table 2.1 : *Cell lines investigated for identification of hybrid epithelial & mesemchymal phenotype.*

2.1.1 Cell lines tested for different phenotypes and techniques

We considered various cell lines from primary and secondary tumor of different cancers. Some of the cell lines from the National Cancer Institute, USA (NCI-60 panel) were also analyzed (see Table 2.1). These cell lines were tested for the expression of E–cadherin and N–cadherin by immunofluorescence and flow cytometry.

Immunofluorescence (IF) refers to a microscopy technique to analyze the localization of antigens – usually proteins in cells or tissue sections through the binding of antibody. The antibody can either bear a fluorophore chemically conjugated to it (**direct immunofluorescence**) or it can be recognized by a secondary antibody conjugated with the fluorophore (**indirect immunofluorescence**). In the later case, we have two control experiments: (i) we remove the primary antibody and only use the secondary antibody with its conjugated fluorophore, (ii) we omit both primary and secondary antibodies to obtain the autofluorescence intensity level. This approach is highly informative because of the detailed information on the localization of the signal which can be further enriched by using several fluorophores in the same experiment. It should be noted however that the dynamic range of single detection is often limited although of high sensitivity CCD cameras has dramatically improved it.

Flow cytometry (FC) is a robust technique for analysis of multiple parameter of individual cell within heterogeneous population. It also provides information about cell size and complexity. In flow cytometry, the cell target labeling with fluorophore is done in similar manners as in immunofluorescence: it also involve the use of fluorescent dyes conjugated to antibodies. This technique allows both qualitative and quantitative along with high dynamic range. Flow cytometry is capable to analyze 100,000s of cells, individually in a short duration of time. Some flow cytometry systems are equipped with sorting technique that allows users to quantify cells from heterogeneous population. However because cytometry allows a rapid analysis and does not require the cells to be immobile, cytometry can be performed more easily on live cells.

Western blot is a reliable method to detect the level of protein expression in a complex mixture extracted from cells. This method separates proteins based on size during electrophoresis process, smaller the size of protein faster it migrates. Then, it detects protein expression using antibodies. Western blot separates the proteins in different band and each protein has unique molecular weight. The specificity can be determine by using molecular weight makers, which also confirms the specificity of antibody to target proteins. In this study, we used western blot to measure the expression of proteins in tumor cells and also to confirm the specificity of the antibodies.

The **optimization of IF and FC protocols** is required to avoid the molecular target denaturation and to minimize non-specific binding. It consists in testing different primary and secondary antibodies, buffers, dissociation media, fixatives, and mounting media... The details of the protocols are given in section B. Here we present the main results of all these tests we obtained in initial phase of this study while working on establishing the protocol for IF and FC. This tests were preformed on different cell lines from various primary and metastatic tumor. Finally, we selected 3 cell lines with different phenotype.

2.1.2 Cell fixation

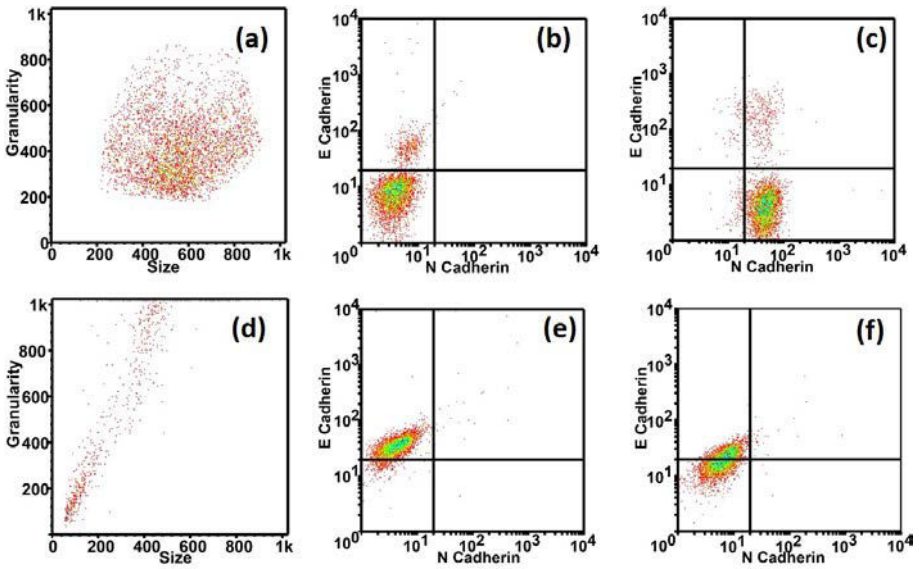

Figure 2.1 : ***Flow cytometry immunophenotyping: comparison between living and fixed M1 cells.*** *Top row (a-c) correspond to living cell and bottom row (d-f) to fixed cells with ethanol fixative. (a) and (d) are the dot plot between size and granularity and (b), (c), (e) and (f) are dot plot between E– and N–cadherin. (b) and (e) are control experiments where cells were exposed to APC Mouse IgG1, κ Isotype Ctrl and Antibody PE Mouse IgG1, κ Isotype Ctrl; (c) and (f) show the specific labeling of E–/ N–cadherin using APC anti-human CD324 (E-Cadherin) antibody and PE anti-human CD325 (N-Cadherin) antibody.*

Cadherins are transmembrane proteins that mediate cell–cell adhesion and ensure the maintenance of normal tissue architecture [20]. Their fixation is a critical step, because it can damage the 3-dimentional architecture of the sample [87]. The two main types of fixation are **precipitation** and **cross-linking**. **Precipitation** is done usually with an organic solvent such as acetone, ethanol, or methanol. These types of fixative are

good for wide field microscopy because they are able to increase the level of antigenicity. However, it also result in dehydrating the sample a lot, almost up to 70 % which eventually result in changing the architecture of the sample. Moreover, precipitation fixatives strip lipids from cells resulting in their deformation [88]. Figure 2.1 show the impact of ethanol fixative on the cell shape and on the detection of N–cadherin, in a flow cytometry experiment. Living cells (Figure 2.1(a-c) shows wide diversities of cell sizes and granularity, and display N–cadherin expression, while cells fixed with ethanol (Figure 2.1(d-f) have a completely different morphology and do not show N–cadherin signal. Moreover, ethanol-fixed cells display an increase in non-specific binding for E–cadherin targeting. These results indicate that ethanol, and by extension other precipitation fixatives, are not adapted to cadherin protein detection.

Cross-linking should be preferred. It is accomplished with aldehydes such as paraformaldehyde or glutaraldehyde. This fixative maintain the cell architecture by forming bridges between proteins group and cell membrane.

2.1.3 Cell confluence

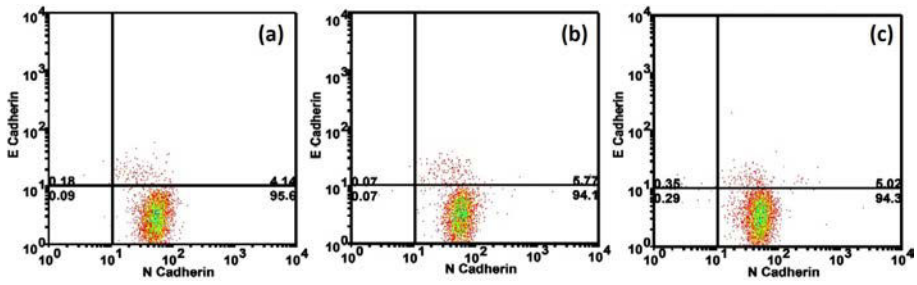

Figure 2.2 : ***Effect of cell confluence in E– and N–cadherin expression, using flow cytometry.*** *Sample were treated with APC anti-human CD324 (E–cadherin) antibody and PE anti-human CD325 (N–cadherin) antibody for specific labeling. (a), (b), and (c) are at 10 %, 30 % and 70 % confluence respectively. All the sample shows similar profile and almost 95 % (4^{th} quadrant) of the cell population express N–cadherin in all the different confluency conditions.*

Because cadherins are primarily involved in cell-cell interactions, it is unclear to which extent their expression at the cell membrane is affected by their engagement in adherens junction. As a first indication of the role of cellular interaction, We tested the effect of cell culture confluency on the E–/N–cadherin expression. Three different flask were prepared at different seeding density of I2 cells and final confluency of these flask were 10%, 30% and 70%. E–/N–cadherin expression was tested by flow cytometry. The results displayed in Figure 2.2, indicate that the level of confluency does not impact the

expressions of both cadherins. Moreover, almost 95% of I2 cells were detected positive for N–cadherin expression (an indication of the background signal autofluorescence plus nonspecific binding of the secondary antibody is provided by Figure 2.2(b). In summary, even at low density, cells express detectable levels of cadherins at their membrane.

2.1.4 Dissociation medium in flow cytometry experiments

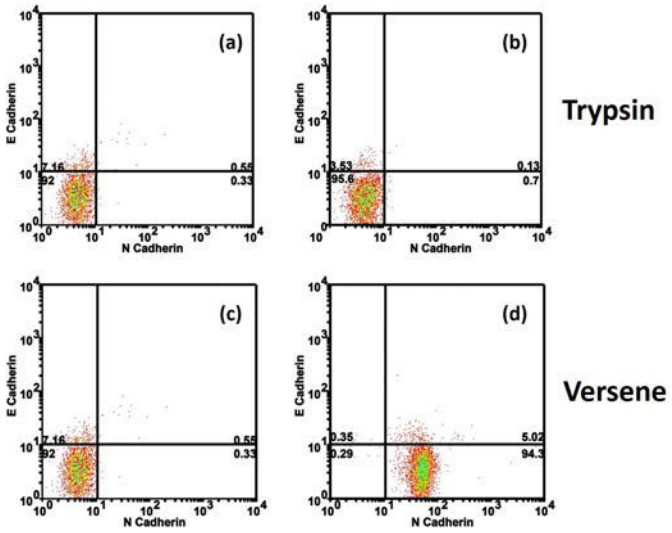

Figure 2.3 : ***Flow cytometry experiment, to detect cadherins in I2 cells: comparison between Versene (EDTA-based) and trypsin dissociations.*** *Top row samples (a)-(b) were dissociated using Trypsin and bottom row samples (c)-(d) were dissociated using Versene. (a) and (c) were treated with APC Mouse IgG1, Isotype Ctrl and PE Mouse IgG1, Isotype Ctrl antibodies and (b) and (d) were treated with anti E–cadherin APC Mouse IgG1 and anti N–cadherin PE Mouse IgG1 antibodies.*

Cytometry uses a unicellular suspension of cells to measure their fluorescence while a constant flow of buffer carries them though the laser beams of the cytometer. Appropriately, it was initially developed for hematopoietic cells which grow in suspension. When used for cells which adhere to a substratum when growing in culture, it is therefore necessary to first detach the cells from the culture dish as well as form each other. Because cadherins are expressed at the cell membrane and have been identified by their sensitivity to calcium, the classical approaches to detach cells (proteases or calcium chelation) could lead to a loss of detection. We therefore tested different cell dissociation media for their effect on cadherin detection by flow cytometry. Trypsin, EDTA (also known under the trade name of Versene) or a combination of these are frequently used. Figure 2.3 shows E–/N–cadherin expression in I2 cells when either trypsin or Versene (from Gibco®; it is a EDTA solution for use as a gentle non-enzymatic cell dissociation reagent) are used. It

clearly indicates that N–cadherin is undetectable after treatment by trypsin but not by Versene. We therefore used Versene in all further flow cytometry experiments.

2.1.5 Antibody selection

The crucial feature of a primary antibody is specificity for the antigen. Immunocytochemistry experiments were optimized to get specific labeling with the lowest non-specific background, which requires the optimization of various parameters: antigen-antibody concentration, incubation time and appropriate blocking buffer. The same optimization is required for secondary antibodies labeled with fluorophore.

Reactivity	**Host**	**Ref.#**	**Conjugation**	**supplier**
E-cadherin	Rabbit	sc-7870	Unconjugated	Santa Cruz Biotechnology
N-cadherin	Rabbit	sc-7939	Unconjugated	Santa Cruz Biotechnology
Anti-rabbit	Donkey	A-21207	Alexa Fluor 594	Life Technologies
Anti-rabbit	Donkey	ab7007	PE	abcam
Anti-rabbit	Donkey	A-31572	Alexa Fluor 555	Life Technologies
E-cadherin	Goat	AF648	Unconjugated	R&D systems
E-cadherin Biotinylated	Goat	BAF648	Unconjugated	R&D systems
Anti-goat	Donkey	sc-2024	FITC	Santa Cruz Biotechnology
Anti-goat	Donkey	A-21081	Alexa Fluor 350	Life Technologies
N-cadherin	Mouse	ab19348	Unconjugated	abcam
N-cadherin Biotinylated	Mouse	ab93524	Unconjugated	abcam
N-cadherin	Mouse	ab98952	Unconjugated	abcam
Anti-mouse	Goat	4408	Alexa Fluor 488	Cell signaling technology
Anti-mouse	Donkey	A-21202	Alexa Fluor 488	Life Technologies
Anti-mouse	Donkey	A-21203	Alexa Fluor 488	Life Technologies
Anti-mouse	Donkey	sc-2099	FITC	Santa Cruz Biotechnology
E-cadherin	Mouse	324108	APC	BioLegend
E-cadherin Isotype Ctrl	Mouse	400122	APC	BioLegend
N-cadherin	Mouse	350805	PE	BioLegend
N-cadherin Isotype Ctrl	Mouse	400114	PE	BioLegend

Table 2.2 : *List of antibodies used for detection of E-/N–cadherin.*

To determine the expression levels of E– and N–cadherin at the cell membrane, we tested a large number of antibodies in different conditions (antibody concentration, temperature...) so that we achieve the strongest fluorescence emission while minimizing non-specific binding and intra-cellular labeling (Table 2.1.5). Of note, cadherins like most membrane proteins are actively internalized and the immunodetection of cadherins in the cytoplasm is not necessarily an indication of nonspecific binding. However, inter-

nalization takes place via endocytosis and most of the cytoplasmic signal can be expected to be associated with vesicles.

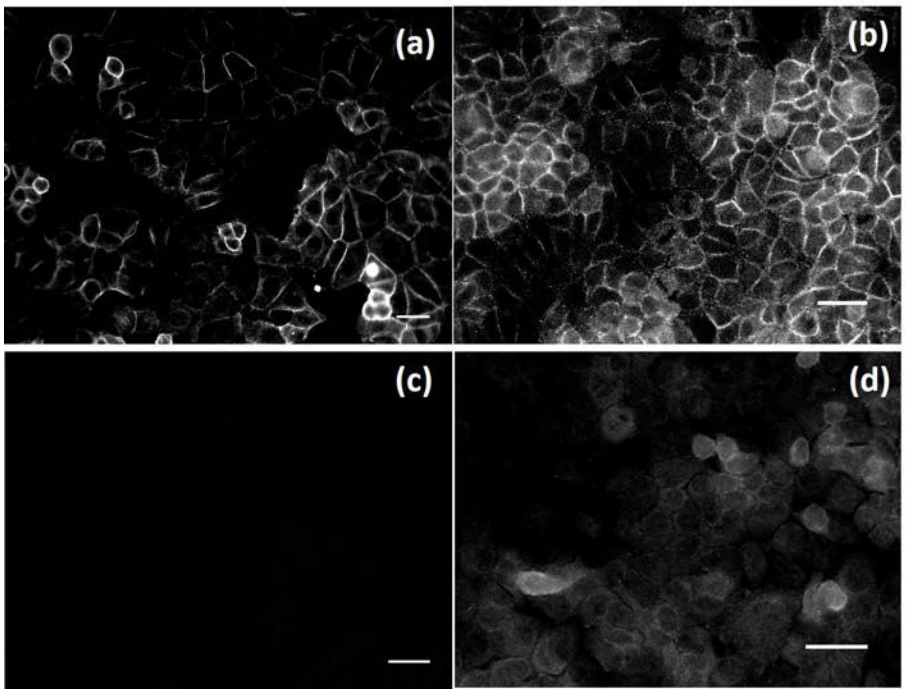

Figure 2.4 : ***Immunofluorescence E–cadherin labeling of MCF7 cells: membrane vs. intracellular labeling (a)(b) and non-specific binding (c)(d).*** *(a) Fixed cells labeled with anti-E–cadherin goat polyclonal and FITC-conjugated secondary antibody. (b) Fixed cells labeled with anti-E–cadherin rabbit polyclonal and anti-rabbit AF555 dye-conjugated secondary antibody. (c) cells treated with anti-goat FITC alone, with no sign of non-specific binding. (d) cells treated with anti-mouse AF594 dye-conjugated antibody showing a high level of non-specific binding. Scale bars: 20 µm.*

Figure 2.4 displays an example of such optimizations. Figure 2.4(a) shows that anti-E–cadherin goat polyclonal (primary)/anti-goat FITC-conjugated (secondary) system provides a membrane labeling only, while rabbit polyclonal/anti-rabbit AF555-dye conjugated also leads to intracellular labeling which could be due to non-specific labeling. Figure 2.4(c) and (d) show *control experiments* where only the secondary antibody is used. In Figure 2.4(c) anti-goat FITC-conjugated antibody was used and show no sign of non-specific binding while Figure 2.4(d) where anti-rabbit AF555 dye-conjugated antibody was used, shows high non-specific background.

Figure 2.5 shows the results of E–/N– cadherin expression in different tumor cells obtained by western blot method. Both antibodies detect proteins of expected size of E–cadherin and N–cadherin. However, It is also apparent that the N–cadherin antibody detect many other bands some of which might be unrelated to N–cadherin.

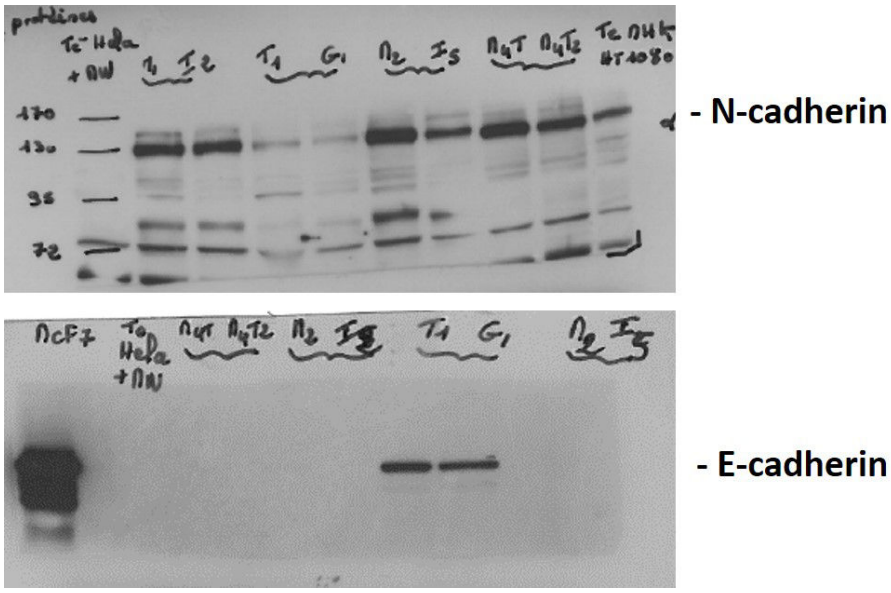

Figure 2.5 : ***Western blot analysis of E–/N– cadherin expression in different cell lines.***

Conclusion: the tests revealed that **anti E–cadherin goat polyclonal** and **anti N–cadherin mouse monoclonal** antibodies are the optimal primary antibodies.

2.2 Selection of cell lines expressing E– or/and N–cadherin

Using the optimized immunofluorescence and flow cytometry protocols, we have selected three cell lines for further use: MCF7 (an estrogen dependent breast carcinoma cell line) expressing strongly E–cadherin only , M4T (a cell line established form a melanoma metastasis) with high expression of N–cadherin only, and A549 (a lung adenocarcinoma cell line) co-expressing E–cadherin and N–cadherin.

MCF7: It has been reported that MCF7 cell express high level of E–cadherin [89]. We confirmed this statement as shown on Figure 2.6. The fluoroscence in Fig. 2.6(a) indicates the detection of E–cadherin at the cell membrane, while the complete absence of fluoroscence in image Fig. 2.6(b) indicates the low level of nonspecific binding of the secondary antibody. By confocal microscopy which allows to exclude light coming from out of focus areas like the upper membrane of the cells, it is clear that E– cadherin accumulates at the cell membrane whether or not they are engaged in cellular junctions. However, the signal can be higher at cell junctions in agreement with a stabilization of cadherins in adherens junctions.

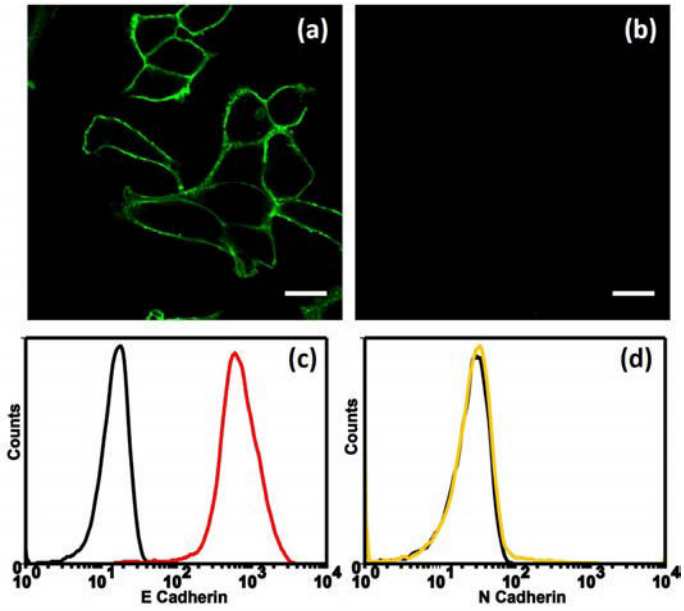

Figure 2.6 : *Detection of E–Cadherin on MCF7 cell line.* *(a) Confocal raster scan of MCF7 cells labeled by immunofluorescence (anti-E–cadherin goat polyclonal primary antibody and anti-goat FITC secondary antibody) to detect E–cadherin membrane protein. (b) Control: confocal image of MCF7 cell in the absence of primary antibody. (c)(d) Flow cytometry measurement of (c) E–cadherin and (d) N–cadherin proteins membrane expression for MCF7 cells. For E–cadherin labeling, MCF7 cells were targeted with APC anti-human CD324 (E–cadherin) antibody (red line). Control sample was treated with APC Mouse IgG1, κ Isotype Ctrl (black regular line). For N–cadherin labeling, MCF7 were treated with PE anti-human CD325 (N–cadherin) antibody (yellow line). Control sample was treated with PE Mouse IgG1, κ Isotype Ctrl (black regular line). These results show that MCF7 cells express E–cadherin but not N–cadherin. Scale bars: 20 μm.*

M4T: it expresses N–cadherin and the single is mostly at the cell membrane although a cytoplasmic single can be observed. Similarly to E–cadherin, but to a greater extent, the accumulation of N–cadherin is more pronounced at cell-cell junctions (see Figure 2.7). Complementary experiments did not reveal E–cadherin expression in M4T cells. This results was crossed checked by western blot (see figure 2.5), which confirms the expression of N–cadherin and absence of E–cadherin.

A549: it expresses both E–cadherin and N–cadherin (see Figure 2.8). Similar results were reported in Ref. [90]. Moreover, the flow cytometry N–cadherin vs E–cadherin dot plot of A549 cells (Figure 2.9) shows the presence of two phenotypes: one (40% of total population) positive for E–cadherin, but negative of N–cadherin (E^+/N^-), and the other (58%) positive for both E– and N–cadherin (E^+/N^+).

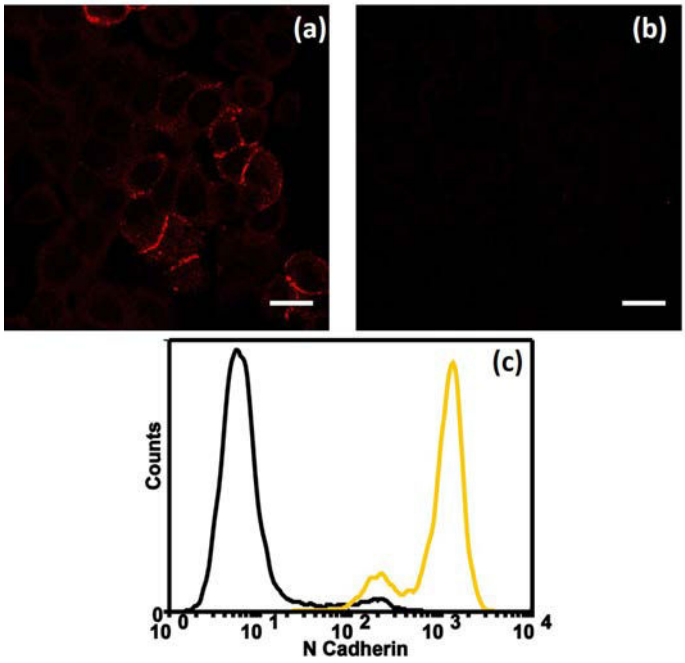

Figure 2.7 : ***Detection of N–Cadherin in M4T cell line.*** *(a) Confocal raster scan of immunofluorescently labeled M4T cell using anti N–cadherin mouse monoclonal antibody and AF594 anti-mouse antibody. (b) Control: confocal raster scan of immunolabeled M4T cell in the absence of primary antibody anti N–cadherin mouse monoclonal. (c) Flow cytometry histogram in which yellow curve corresponds to cell labeling with primary antibody anti N–cadherin biotinylated mouse monoclonal and secondary antibody streptavidin–PE, while regular black histogram represents control sample which is treated with only secondary antibody. Scale bars: 20 µm.*

Sorting (E^+/N^+) A549 cells. The (E^+/N^+) population of A549 cells is interesting for this study where E– and N– cadherins are co-expression is needed. We therefore sorted the two populations (E^+/N^+) and (E^+/N^-) and kept them in culture for 4 weeks to check their stability. At each passage or splitting of cells we tested them for the expressions of E– and N–cadherins. The results are presented in Figure 2.10. All samples were labeled with APC-conjugated anti-human CD324 (E–cadherin) antibody and PE-conjugated anti-human CD325 (N–cadherin) antibody. This result show a high stability of cadherin expression levels in both cell sub-populations over the period of 4 weeks. This is particularly clear for the E^+/N^+ cells; while in the E^+/N^- population, from the first passage on, a minority of E^+/N^+ cells can be detected. This behavior could reflect either an asymmetric plasticity of the cells or the presence in the sorted E^+/N^- cells of a few E^+/N^+ which would have been inefficiently labelled for N-cadherin. Since the presence of two populations can be observed in many cultures of A549 it is likely that there is an equilibrium between these two populations even though this wasn't visible under our

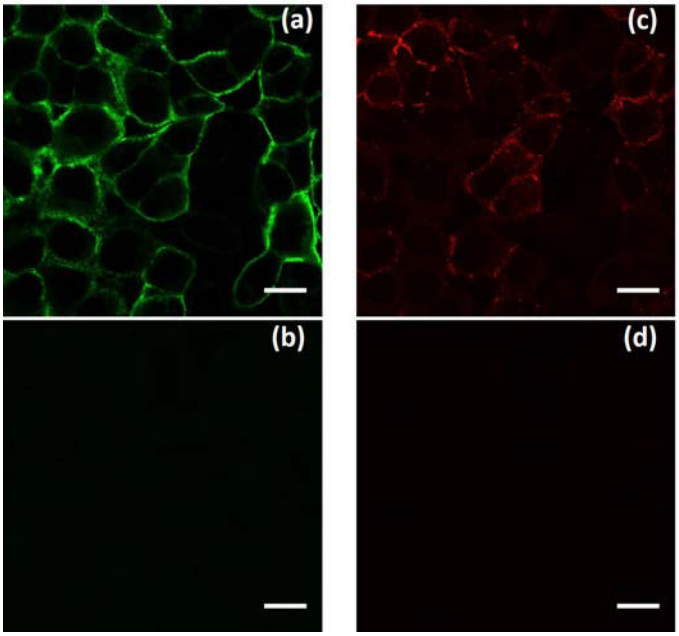

Figure 2.8 : *immunofluorescence detection of E–/N–cadherin in A549 cell line.* *(a) exposed to anti E–cadherin goat polyclonal primary antibody and anti-goat FITC secondary antibody. The fluorescence indicates the existence of E–cadherin in this cell line at the cell membrane. (b) Cells were only treated with anti-goat FITC secondary antibody. The absence of fluorescence indicates no non-specific binding. (c) Cells exposed to anti N–cadherin mouse monoclonal primary antibody and anti-mouse AF594 secondary antibody. The fluorescence indicates the existence of N–cadherin on this cell line at the membrane. (e) Cells treated only with anti-mouse AF594 secondary antibody, the absence of fluorescence indicate no non-specific binding.Scale bars: 20 µm.*

culture conditions.

We further consider A549 (E^+/N^+) sub-population as the model cell line to develop the FRET-based detection of E– and N–cadherin pairs.

2.3 Localization of E–/N–cadherin

Cadherins are usually defined as mediating homophilic interactions [91–93]. It is therefore unclear how E– and N– cadherins are organized in the membrane of cells which co-express them. One extreme situation would be that E– and N–cadherin accumulate in distinct domains and form two types of junctions E/E and N/N. At the opposite, it has been described that in endoderm derived tissues such as the liver epithelial cells can express both E– and N–cadherin and form heterotypic junctions in both normal and tumor cells [94].

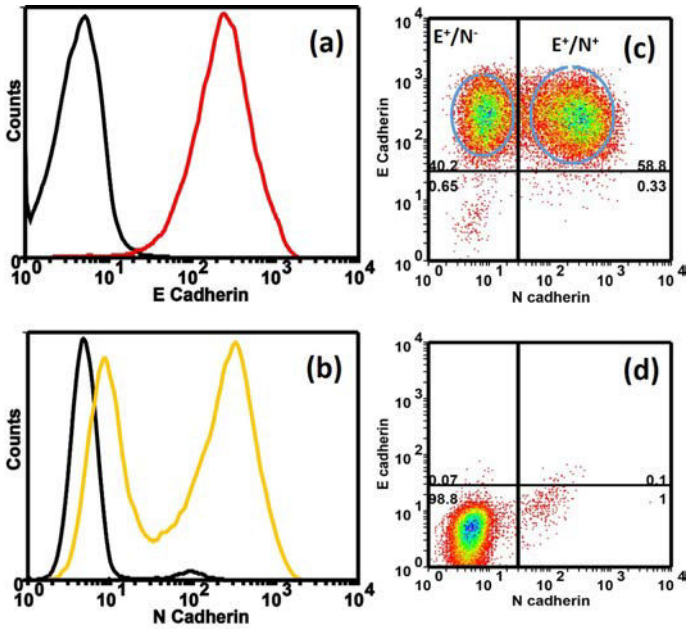

Figure 2.9 : ***Detection of E–/N–Cadherin in A549 cell line by flow cytometry.*** *(a)Histogram shows the detection of E–cadherin in red color and black line represent the control sample measurement.(b)Histogram shows the detection of N–cadherin in yellow color and black line represent the control sample measurement. (c) Dot plot shows A549 cells labeled simultaneously with APC anti-human CD324 (E–cadherin) antibody and PE anti-human CD325 (N–cadherin) antibody. (d) Control samples treated with APC Mouse IgG1, κ Isotype Ctrl antibody and PE Mouse IgG1, κ Isotype Ctrl antibody.*

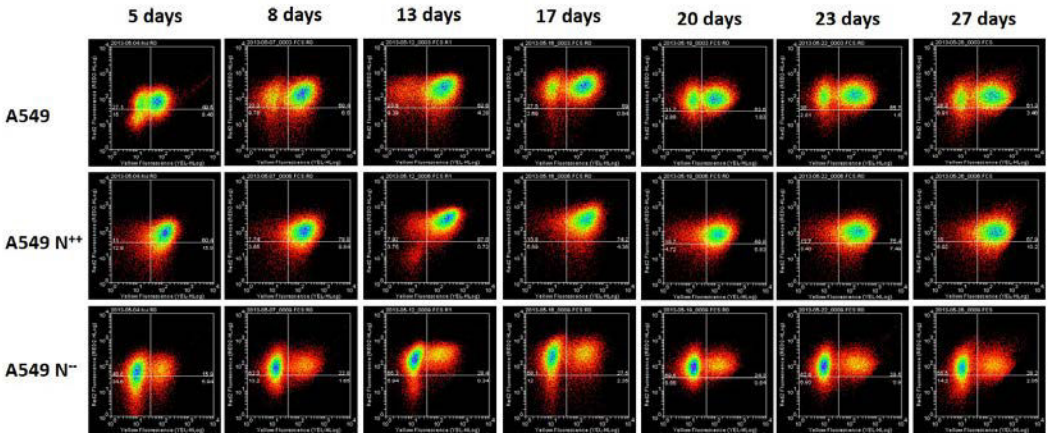

Figure 2.10 : ***E–/N–cadherin expression stability after cell sorting of A549 cell sub-populations****. The X-axis represents the expression level of N–cadherin and the Y-axis represents the expression level of E–cadherin. Top row (A549) presents results from original A549 cell line. Its shows two major populations, in first and second quadrants. Middle row shows the stability over time of the* (E^{+}/N^{+}) *sub-population. The bottom row shows the stability of stability of the* (E^{+}/N^{-}) *sub-population.*

We studied the localization of E– and N–cadherin expression in A549 cells. Figures 2.11(a) to (c) show that A549 cells express both proteins at similar intensity levels and at the same location (red and green mixing leading to a yellow color in that case) only in central part of cell aggregates. In the periphery of the aggregates, where the cell density is more heterogeneous, either E– or N–cadherin expression dominates. These results are in agreement with the one reported in [94]. In comparison, Fig. 2.11(d) displaying immunolabeling of MCF7 cells shows only E–cadherin expression (as expected) with similar level of membrane expression in the central part and periphery of the cell.

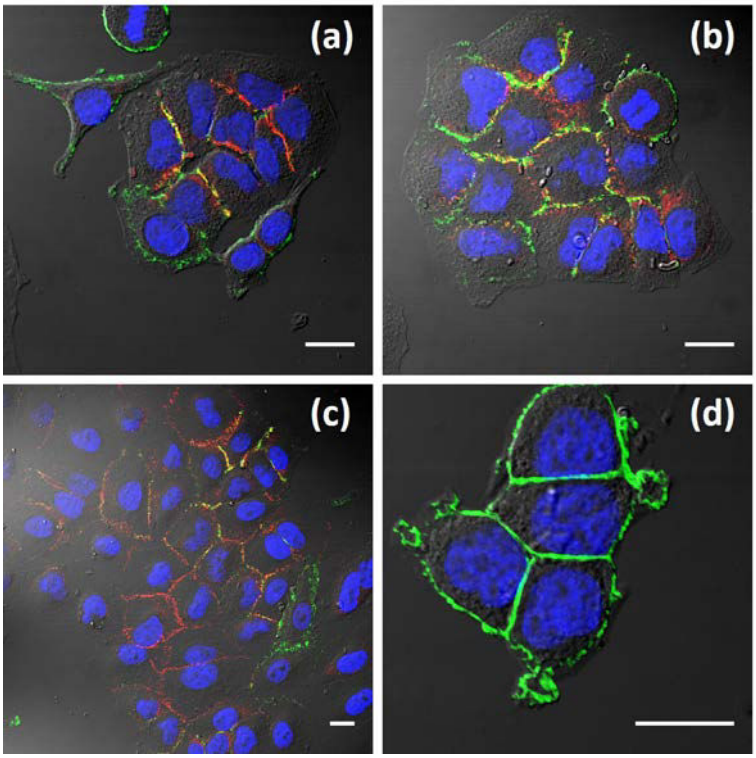

Figure 2.11 : ***Identification of E– and N–cadherin containing adherens junction in various cell lines by immunofluorescence****. Cells were treated with anti E–cadherin goat/anti-goat FITC-conjugated antibody and anti N–cadherin mouse/anti-mouse AF594 dye-conjugated antibody. FITC appears in green, while AF594 is in red. The blue color corresponds to the labeling of the nucleus with DAPI dye. Individual figures are merges of the three colors and the transmission phase contrast image. (a) to (c) A549 cells and (d) MCF7 cells. Scale bars: 20 µm.*

2.4 Phenotypic plasticity

As presented in the introduction, current data suggest that the level of steady state expression of epithelial and mesenchymal markers by tumor cells has a low prognostic

value. Since EMT is a reversible process, it has been proposed that a measure of the phenotypic plasticity (i.e. the ability of cell to change an epithelial to a mesenchymal phenotype, or the reverse) would be a better indicator of the metastatic potential. One key factor controlling the epithelial mesenchymal transition is TGF-β (Tumor Growth Factor-β). However the response to TGF-β requires several days either when inducing EMT by adding TGF-β or MET by removing TFG-β. When investigating CTC a much shorter test would be desirable.

In the LBPA laboratory at ENS Cachan, a group had been investigating the activity of PKD1, which is a serine threonine kinase involved in the regulation of many signaling pathways and implicated in tumor progression [95]. Notably, PKD1 has been shown to regulate EMT and metastasis [96].

Consequently we explored whether an inhibition of PKD1 would induce a change in phenotype in tumor cell lines which could be used as an indicator of their phenotypic plasticity. We used a commercially available inhibitor Gö 6976 which is active at concentration around 1 μM. However this inhibitor is also active on the classical PKC isoforms. An analysis of the implication of PKD1 can therefore only be establish by comparing the activity of Gö 6976 with that of Gö 6983 which is active at a concentration of 1 μM on PKC α, β, and γ and not on PKD1 [97]. Gö 6976 and Gö 6983 inhibitors were purchased from Calbiochem (San Diego, CA, USA).

Four human tumor cell lines M2, T1, G1 and MCF7 were used for this study. The cells in culture were exposed to Gö 6976 and Gö 6983 for 3, 24 and 76 hours before the analysis. Immunofluorescence and flow cytometry were used to characterize the phenotype of the cells, using the same protocols as in appendix B .

2.4.1 PKD1 inhibition induces changes in morphology

Figure 2.12 and 2.13 shows the transmission images of M2 and G1 tumor cell lines respectively. We observe that upon the addition of Gö 6976 the cells become bigger and tend to form clusters (even after only 3 hours of incubation) compared to controls consisting of untreated cells and cells treated with PKC inhibitors (Gö 6983) alone. These results suggest that PKD1 plays a role in cell-cell adhesion.

2.4.2 Cadherin expression

Since it has been observed that PKD1 can regulate EMT, we investigated whether the changes in morphology induce by Gö 6976 were associated with change in the expression

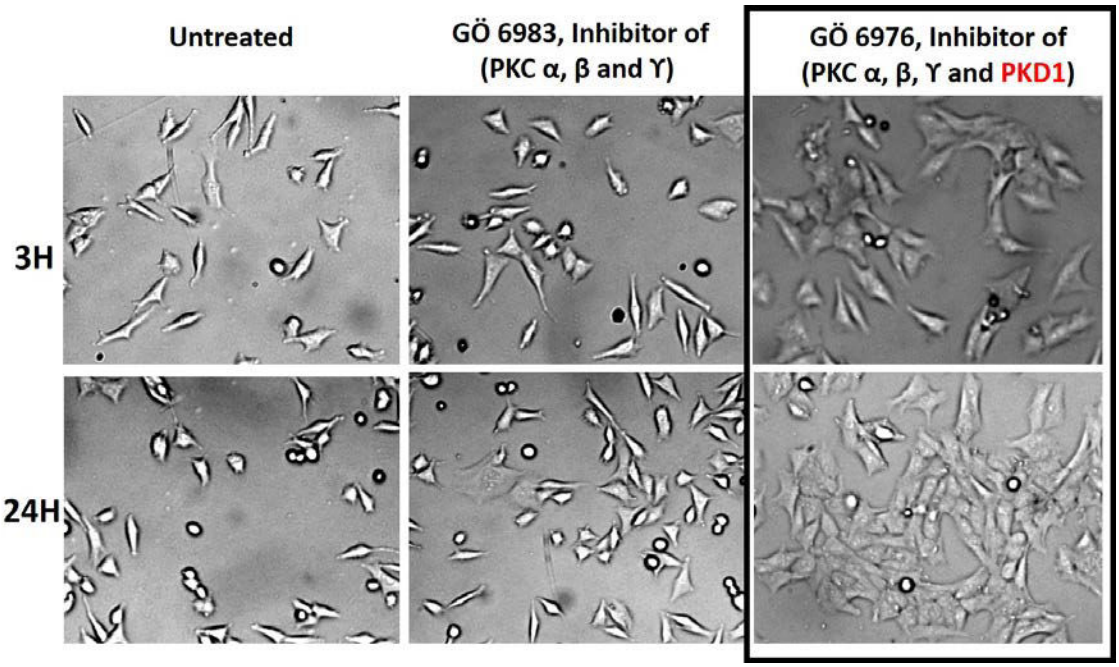

Figure 2.12 : *Morphological changes in M2 cell line on treatment with inhibitor.* *Cells that are exposed to selective inhibitor (Gö 6976) shows major change in cell morphology as compared to untreated cells or cells treated with non-selective inhibitor (Gö 6983). Other observation is clustering of cells on treatment with selective inhibitor.*

of E–/N– cadherin. We used immunofluorescence and flow cytometry methods to analyze the transition in E–/N– cadherin expression after 3, 24 and 72 hours of treatment by selective inhibitor(Gö 6976), non-selective inhibitor (Gö 6983) and without any treatment.

M2 cell line

In M2 cell line, cells were only positive for N–cadherin after 24 hours of treatment by inhibitors and no significant expression of E–cadherin were observed. An increase in E–cadherin was visible after 72 hours (see figure 2.14(a)) in all the samples. The sample treated by Gö 6976 show slightly higher expression of E cadherin (around 28% of cell population) as compared to untreated sample (18%) and Gö 6983 inhibitor (17%) but this is unlikely to explain a difference in morphology. On other hand, Immunofluorescence results (see figure 2.14(b)), show no sign of increase in expression of E cadherin.

G1 cell line

By flow cytometry figure 2.15(a) no change in expression of E–and N–cadherin was observed at both time points. Similar results were observed by immunofluorescence

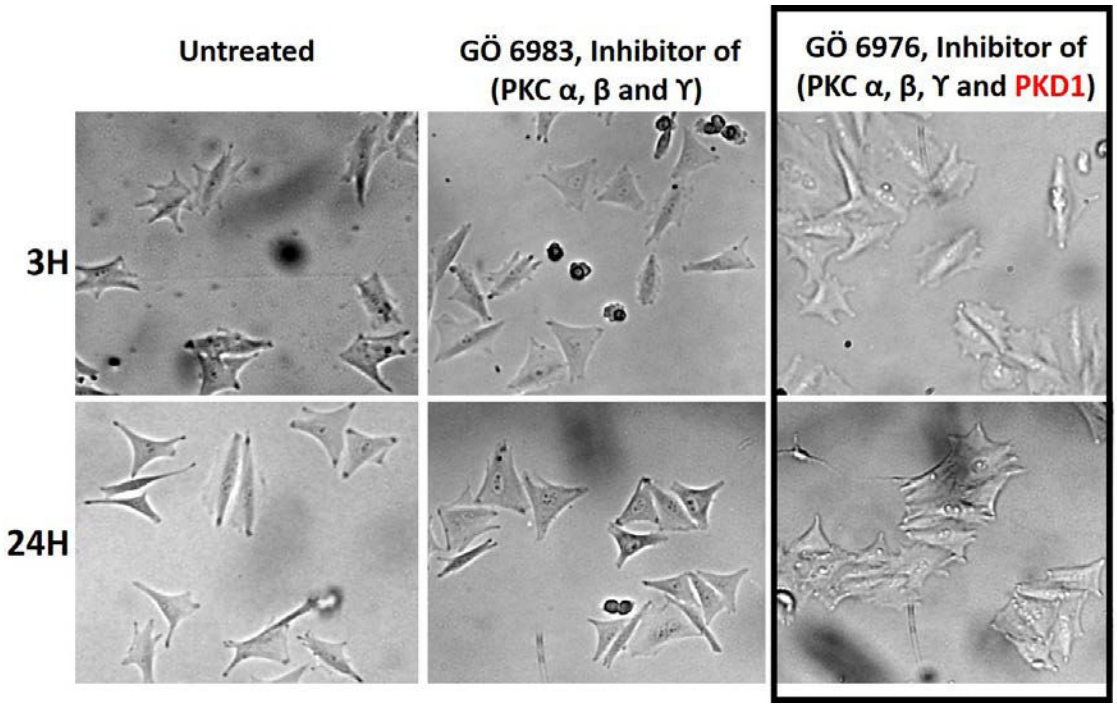

Figure 2.13 : ***Morphological changes in G1 cell line on treatment with inhibitor.***. *G1 cell line shows clustering of cells on treatment with selective inhibitor Gö 6976.*

experiments (see figure 2.15(b)).

2.4.3 Perspectives on PKD1 inhibition

We have observed change in morphology in several cell lines, which can be detected only after few hours of treatment by the selective inhibitor (Gö 6976). These changes were associated with increase in clustering of cells, suggesting a possible modification of the epithelial / mesenchymal state of the cells. However, our preliminary analysis indicates no major change in the expression of the cadherins. Thus, at this stage we cannot correlate the changes in morphology with an EMT/MET plasticity. Further studies would be necessary in order to assess the true nature of the observed changes and to determine whether or not they are informative about the metastatic potential of tumor cells.

2.4.4 Conclusion

In this chapter we identified a robust cell line to use it as a prototype of hybrid phenotype, i.e. A549 (E^+/N^+) sub-population. We developed an immunofluorescence protocol resulting in specific labeling of E–/N–cadherins with minimum background. We

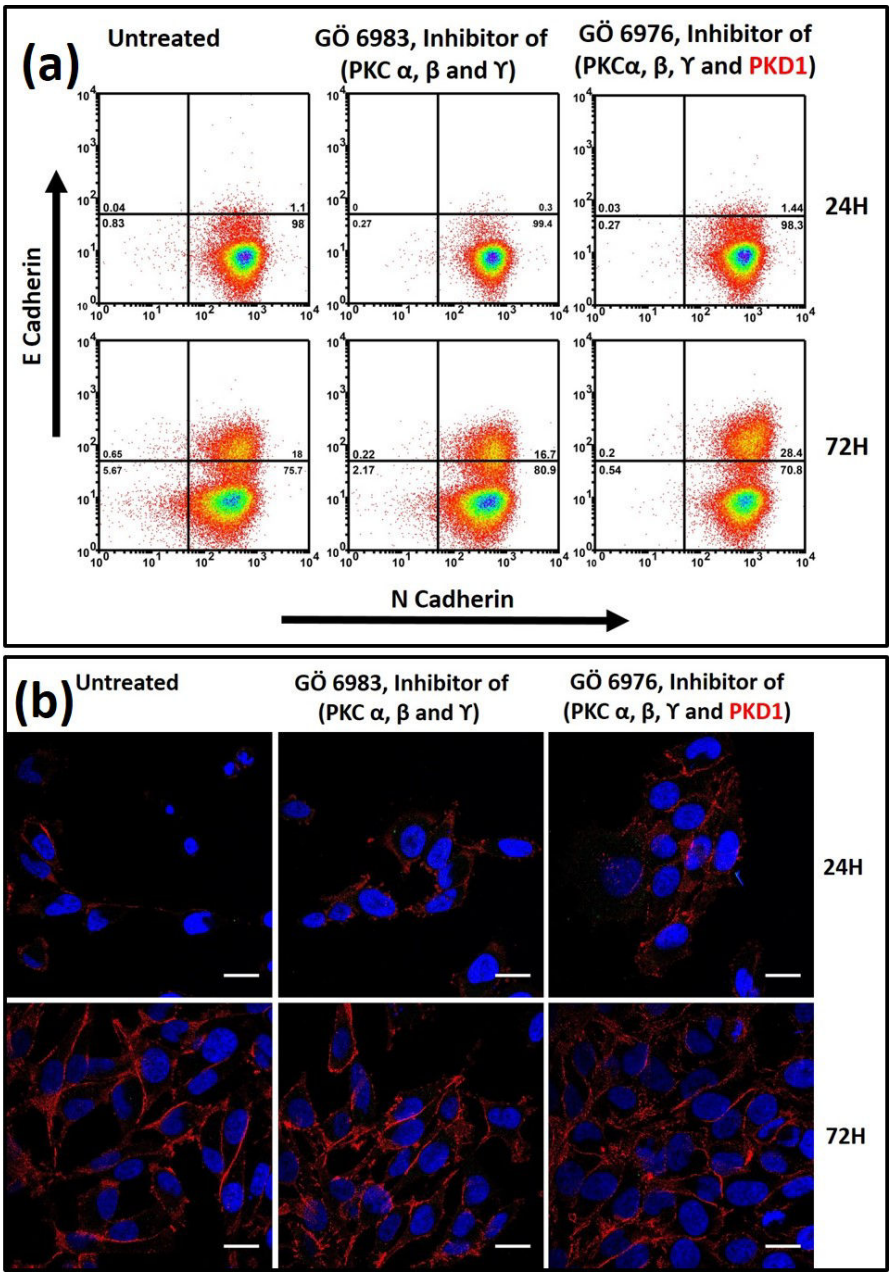

Figure 2.14 : ***Flow cytometry and immunofluorescence labeling of M2 cells after treatment by inhibitors.*** *(a) Cells were labeled by anti E–cadherin APC mouse IgG antibody and anti N–cadherin PE mouse antibody. $X-$ axis represents staining of N–cadherin and $Y-$ axis represents staining of E–cadherin. (b) Confocal images of M2 cells labeled by primary antibodies, anti E–cadherin goat polyclonal antibody + anti N–cadherin mouse monoclonal antibody and anti-goat FITC and anti-mouse AF594 secondary antibodies. Scale: 20μm.*

observed variations in the expression of these proteins depending on the localization of the cell in the cluster (center vs periphery).

In the next chapter, we used an automated epifluorescence microscope-based system

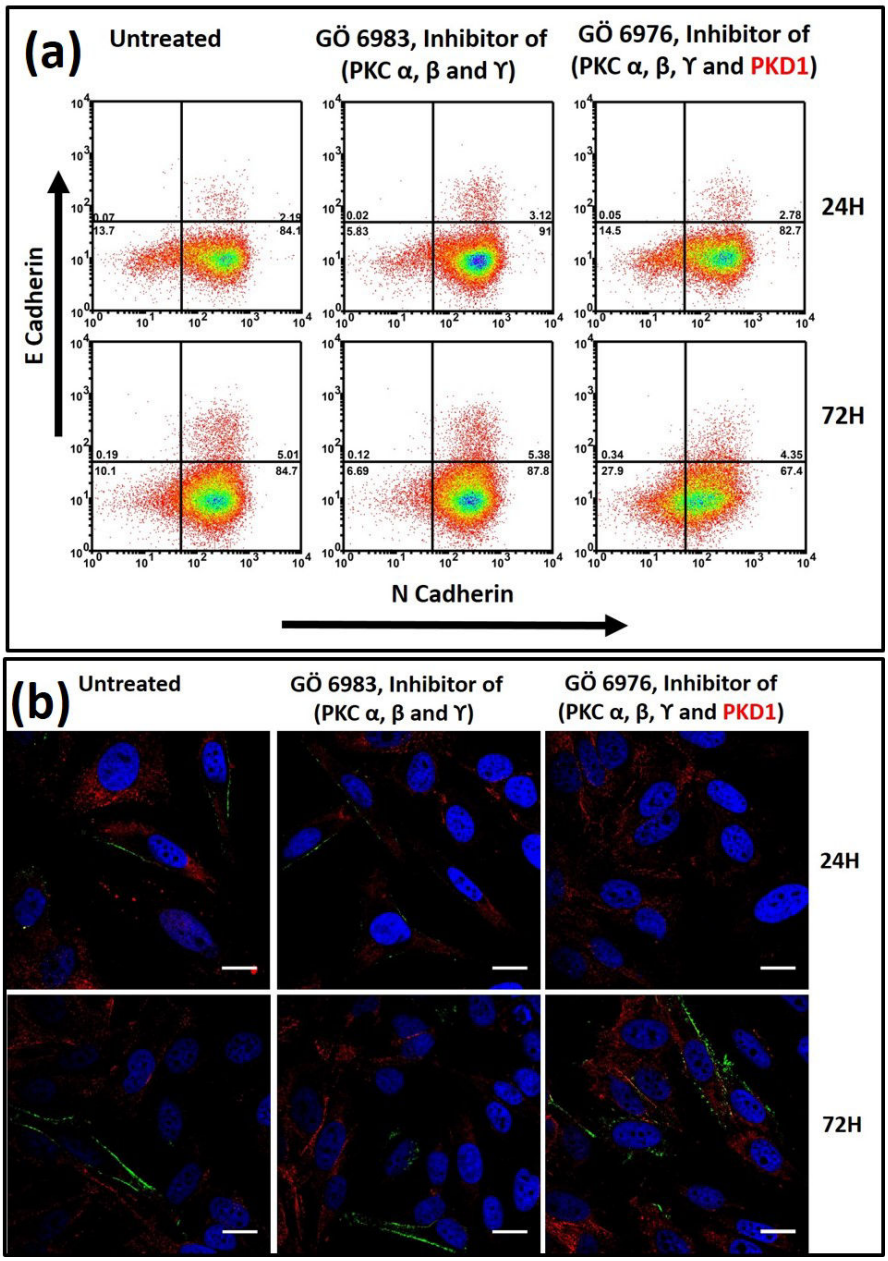

Figure 2.15 : *Flow cytometry and immunofluorescence labeling of G1 cells after treatment by inhibitors.* *(a) Cells were labeled using anti E–cadherin APC mouse IgG and anti N–cadherin PE mouse antibodies. $X-axis$ represents staining of N–cadherin and $Y-axis$ represents staining of E–cadherin. (b) Confocal images of G1 cells labeled by primary antibodies, anti E–cadherin goat polyclonal and anti N–cadherin mouse monoclonal and anti-goat FITC and anti-mouse AF594 secondary antibodies . Scale: 20µm.*

capable of high throughput recording and analysis, in order to identify hybrid cells in a mixed population.

Further studies required to draw any conclusion on the role of PKD1 in morphological

changes observed in the different cell lines.

3 High-throughput phenotype identification of two different co-cultured cell lines

Summary

3.1 Introduction

One of the major goal of the NanoCTC project (to which this PhD work is related) is to develop an automated tools to identify CTCs using fluorescence imaging. This approach relies on the use of IMSTAR S.A. Pathfinder^{TM} system, consisting in (i) an epifluorescence automated microscope, and (ii) a software with custom algorithms optimized by the company in the context of the project in which it is a partner too. This system was developed to provide automated high-throughput recording and analysis of a large amount of cellular immunofluorescence images.

In the context of our researches, we established a protocol to identify two population of cells having different epithelial/mesemchymal phenotypes in co-cultures of them at different proportions. Despite the fact we only tested proportions of each cell which are close to each other (50/50, 25/75), these experiments correspond to the very first step towards the automatic identification of very rare cells of a specific phenotype among a dominant population of a different phenotype. We will present an example where the Pathfinder^{TM} system successfully identified A549 cells among blood cells at very low

concentration in an experiment with the team of Françoise FARACE at *Laboratoire de Recherche Translationel* (IGR, Villejuif), one of the partner in NanoCTC project.

3.2 Experimental procedure and results

In this section, we describe our approach to identify hybrid E– and N–cadherin co-expressing cells (A549 cells) among cells with a different phenotype with which they are co-cultured. We used MCF7 cell line as a model line of E–cadherin expressing cells, while M4T cell line as a model cell line for N–cadherin expressing cells. Optimal immunofluorescence protocols for these three cell lines are described in Chapter 2.

3.2.1 MCF7 and A549 cell co-culture and immunofluorescence labeling

MCF7 and A549 cells co-culture

MCF7 and A549 were cultured in 12 wells plate for 48 hours, using DMEM culture medium. Cells were seeded in two proportions approximately 1:1 and 1:3 (A549:MCF7). Cells were trypsinized, suspended in culture medium, and counted with an hemocytometer.

The seeding density for this experiment is crucial to be able to quantitatively analyzed the imunofluorescence data. The procedure of calculating seeding densities relies on the *American Type Culture Collection* specifications for each cell lines: the doubling time for A549 cells is 22 hours and 29 h for MCF7. So, the increase in the number of cells after 48 h of culture are: $R_{\text{A549}} = 2.18$ times for A549 and $R_{\text{MCF7}} = 1.65$ times for MCF7. The number of each type of cells used in the co-culture was then chosen to get proportions in the range 1:1 and 1:3 for A549:MCF7 cells (see Table 3.1).

Seeded cell number per well (A549:MCF7)	**Cell line**	**Duplication time** (hours)	**Increasing factor** (after 48 h)	**Expected final count of cells**	**Expected final proportion of cells** (%)
60000:80000 (1:1)	A549	22	2.18	283200	52
	MCF7	29	1.65	264000	48
30000:120000 (1:3)	A549	22	2.18	141600	26
	MCF7	29	1.65	396000	74

Table 3.1 : *Seeding parameters of A549:MCF7 cells co-cultures*

Immunolabeling of MCF7:A549 co-culture

For co-culture, fixation and immunolabeling of MCF7 and A549 cells, we followed the same protocol described in appendix B. E-cadherin was fluorescently immunolabeled with anti E–cadherin goat polyclonal primary antibody and anti-goat FITC dye-conjugated secondary antibody, while N–cadherin was labeled with anti N–cadherin mouse monoclonal primary antiboby and AlexaFluor AF594 anti-mouse secondary antibody. DAPI was used to label the nucleus of the cell.

3.2.2 Image acquisition

Images were acquired using the IMSTAR Pathfinder^{TM} system relying on a Nikon Eclipse Ti epifluorescence microscope modified for high throughput cytometry analysis. It is equipped with a motorized translation and a filter stage, 20× and 40× magnification objectives and a CCD array detector. The system acquires series of contiguous images in a large region of interest (ROI) of a cell culture immunofluorescently labeled slide sample in different fluorescent channels, as shown in Figure 3.1(a). The whole system was optimized with the help of Dr Charles Homsy from IMSTAR.

We use three fluorescence channels: **Green:** FITC with filter combination 488/495/520 nm, corresponding to the excitation, beamsplitter and emission central bandpass and high-pass edges wavelengths. The full description of filter set used for this study, provided in Table 3.2. **Red:** AF 594 (545/570/610), and **Blue:** DAPI (375/409/447)

Filterset (# reference, reseller)	**Excitation bandpass filter: central wavelength/width (nm)**	**Dichroic beamsplitter cutoff wavelength edge (nm)**	**Emission bandpass filter: central wavelength/width (nm)**
DAPI (# F36-500, AHF, Germany)	377/25	409	447/60
FITC (# F36-501, AHF)	482/35	506	536/40
AlexaFluor594 (# F46-008, AHF)	560/40	585	630/75

Table 3.2 : *IMSTAR Pathfinder^{TM} filterset used*

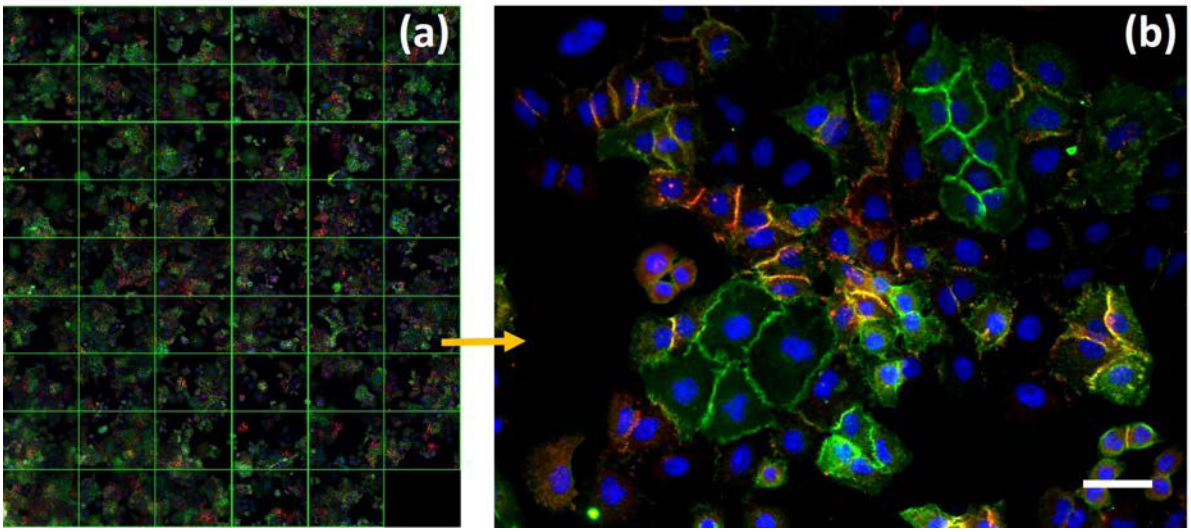

Figure 3.1 : ***Immunofluorescence labeling of co-cultured A549 and MCF7 cell lines.****(a) Metaimage of the total area scanned on the slide, each rectangle corresponding to one field of view.(b) showing one of the field of view (rectangle) of metaimage. Scale bars: 20 µm.*

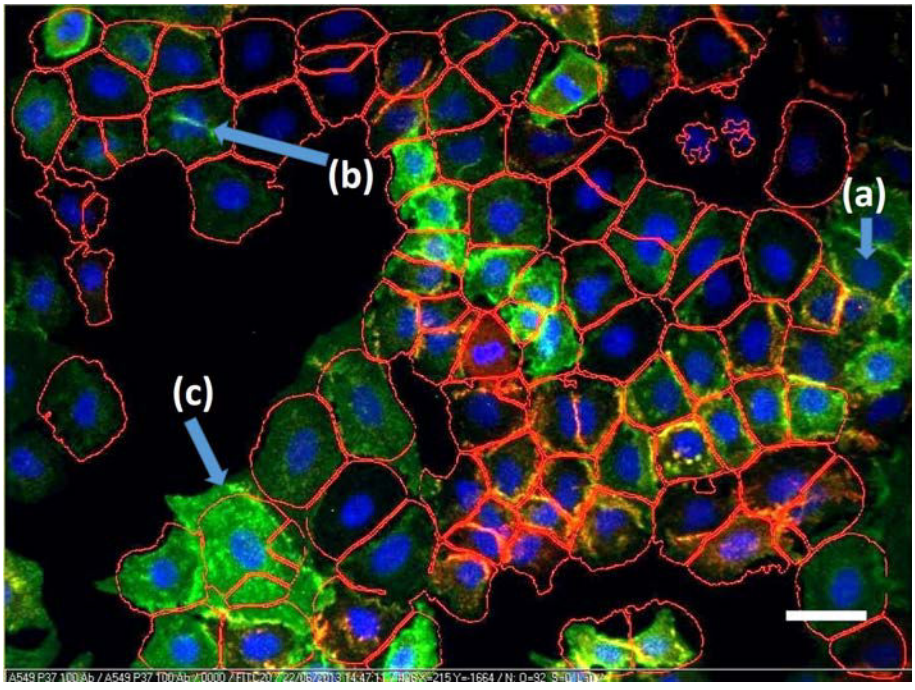

Figure 3.2 : ***Identification of the cell contour by the Pathfinder^{TM} algorithm.*** *(a)-(c) arrows indicate segmentation error discussed in the main text.*

3.2.3 Image processing and analysis

Image segmentation in individual cells

In this study we are interested in identifying cell populations with different phenotypes (characterized by different levels of expression of E– and N–cadherin). The segmentation of the immunofluorescence images in individual cells is done by a system algorithm developed by Dr Alexandre Papine at IMSTAR. This step is critical because fluorescence intensities associated to immunolabelings are then calculated for each delimited area identified as a cell, so that mismatch between the identified region and the actual cell morphology will result in errors or false positive cells in evaluating the expression of the labeled proteins.

The algorithm first identifies the nucleus (labeled with DAPI) and then propagates its contour through the cytoplasm until the cell membrane is detected. The detection of the cell membrane strongly depends on the intensity of the immunofluorescence labeling. In Figure 3.2, the red color contours detected by this algorithm representing cell region. In this figure, some cells were not identified (marked by arrow (a)). In some instance, a dividing cell was identified as a single cell (arrow b). In other occasion, the morphology of cell is not detected properly (arrow c). These segmentation errors of false positive can contribute in mismatch between seeding proportion and final detected proportion.

A549:MCF7 cells fractions inferred from cellular E– and N–cadherin expression levels per cell

Figure 3.3 shows plots of AlexaFluor594-immunolabeled N–cadherin (Y-axis) versus FITC-immunolabeled E–cadherin (X-axis) for three different proportions of A549 and MCF7 cells. The expected proportions after 48 hours of culture are inferred from initial seeding proportion and each cell line growth rate (cf. section 3.2.1), and we would like to check if the Pathfinder^{TM} is capable of retrieving the same proportion automatically.

In Figure 3.3(b) and (c), two cell populations can be identified based on different and well-separated E–cadherin expression levels. We manually selected the region of interest (ROI) corresponding to cells with high expression of E–cadherin and displayed them in yellow (MCF7 cells), while the remaining cells (in orange) co-express E– and N–cadherin (A549 cells). We used the same region of interest for the three different proportions. Note that the control experiments (secondary antibody alone) of Figure 3.3(d-f) show some non-specific binding of the secondary antibody used for N–cadherin but not of the one used for E–cadherin. This non-specific binding may impact the quantification of the

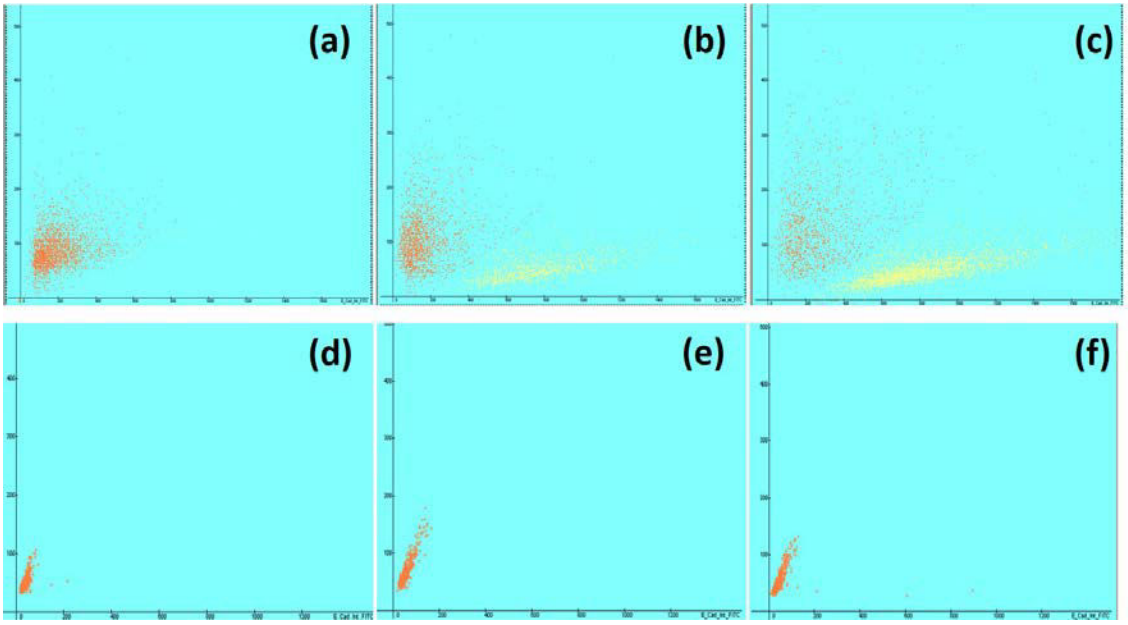

Figure 3.3 : ***E– versus N– cadherin expression levels of each individual cells were measured by IMSTAR system using fluorescent dyes, in co-cultures of MCF7 and A549 cells at different proportions****. (a) culture of A549 alone (100%); (b) co-culture of MCF7 and A549 cells with 52% of A549 cell fraction as inferred from the initial seeding proportion and different cell growth rates; (c) co-culture of MCF7 and A549 (at fraction 26%). We observe a distinct population of cells with high expression of E–cadherin that we have highlighted in a yellow region of interest (ROI). It should correspond to MCF7 cells. A549 cells are displayed in orange. (d-f) control samples with similar A549:MCF7 proportions as in (a-c) (i.e. 100%, 52% and 26% respectively) corresponding to cells treated with dye-labeled secondary antibodies only.*

A549 cells, which is why we chose to evaluate the population of MCF7 instead, using the statistical tools embedded in the Pathfinder^{TM} software.

Table 3.3 shows the results of this analysis and the comparison with the expected fractions of MCF7:A549 cells. The automatic detection yields fractions of 58% and 33% of the hybrid phenotype cells (A549) where we expect 52% and 26% respectively. The larger proportions observed in the automatic detection maybe due to the non-specific binding of the AF594-conjugated secondary antibody used for N–cadhering labeling.

For co-cultured samples, the number of MCF7 cells indicated in column 3 of Table 3.3 corresponds to the number of cells detected in the MCF7 ROI after subtraction of the number of cells counted in the same ROI but for the 100% A549 cells sample (i.e. 44 cells), because these cells are likely to be A549 and not MCF7.

As mentioned, the selection of the region of interest delimiting cell populations is partially arbitrary due to the fact that the two populations slightly overlap in the E–

Expected A549 cells fraction at the seeding stage (%)	**Total number of cells identified**	**Number of detected MCF7 cells**	**Number of inferred A549 cells** (total–MCF7)	**Measured A549 cells fraction** (%)
100	2464	44 (false positive)	2420	98
52	3130	1292	1838	58
26	4958	3237	1721	33

Table 3.3 : Cell proportions in a co-culture of MCF7 and A549. *Comparison of the proportion of cells expected from the seeding parameters and growth rate and the value measured with the Pathfinder^{TM} system, in the case of the ROI population selection corresponding to Figure 3.3.*

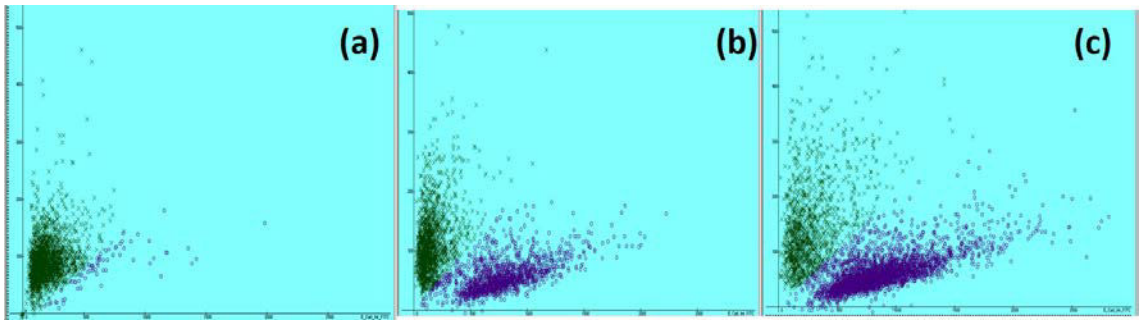

Figure 3.4 : *E– versus N–cadherin expression levels per individual cells as measured by IMSTAR system from immunofluorescently labeled cells, in co-cultures of MCF7 and A549 cells at different proportions*. *Same data as in Figure 3.3 with proportions 100% (a), 52% (b) and 26% (c) of A549, but different ROI selection for MCF7 cell population displayed in purple.*

/N–cadherin plane. In order to estimate the impact of the ROI selection on the cell proportion measurements we selected a larger area of E–cadherin highly expressing cells (see Figure 3.4).

Table 3.4 show the corresponding statistics leading to experimental A549:MCF7 cell proportions closer to the expected ones. Therefore, the selection of MCF7 cell population ROI in the E–/N–cadherin plot is a crucial factor: small changes in the selected ROI of MCF7 cells population results in a few % changes of A549 proportions. The remaining discrepancy has different origins discussed in section 3.2.4.

The software also allows to display the distribution of E– and N–cadherin expression levels for the ROI and compare it to the one of all the cells (Figure 3.5). Fig. 3.5(b)&(e) and (c)&(f) show that the population of cells with the highest E–cadherin expression

Expected A549 cells fraction at the seeding stage (%)	**Total number of cells identified**	**Number of detected MCF7 cells**	**Number of inferred A549 cells** (total–MCF7)	**Measured A549 cells fraction** (%)
100	2464	68 (false positive)	2396	97
52	3130	1413	1717	54
26	4958	3465	1493	30

Table 3.4 : Cell proportions in a co-culture of MCF7 and A549. *Comparison of the proportion of cell expected from the seeding parameters and growth rate and the value measured with the Pathfinder^{TM} system, in the case of the population selection corresponding to Figure 3.4.*

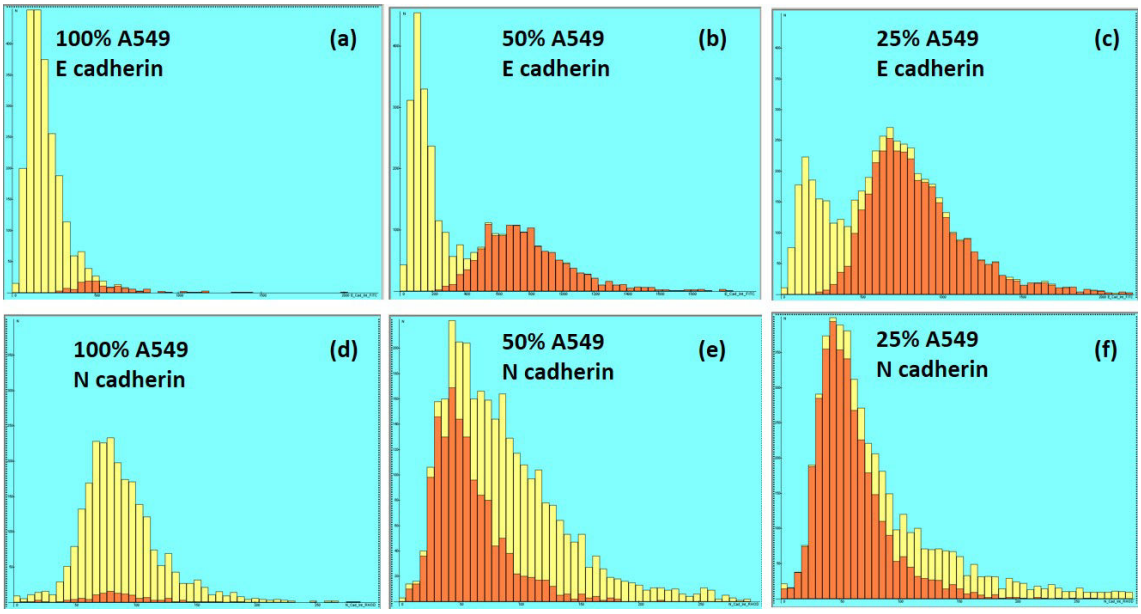

Figure 3.5 : *Histogram of the distribution of E– and N–cadherin expression levels per cell*. *The yellow color bars shows the intensity distribution of all cells, whereas orange bars represents the distribution of the manually selected population shown in Figure 3.3 corresponding to MCF7 cells. (a-c) E–cadherin expression level, and (d-f) N–cadherin expression level for different proportions of A549 cells.*

(considered as MCF7 cells) have the lowest N–cadherin expression, which is nevertheless not negligible due to the non specific binding of the secondary antibody used for N–cadherin labeling.

3.2.4 Discussion

There are possible quantification of false positive cells in the automatic quantitative cellular immunofluorescence measurements due to following reasons;

1. **Wrong cell segmentation** due to the fact that A549 and MCF7 cells, like all epithelial cells form clusters, favoring cell-cell contacts. The later are difficult to detect and the algorithm was improved by Dr Alexandre Papine to better handle this difficulty, by subtracting the non-specific immunofluorescence background. Moreover, the segmentation tools mostly identify dividing cells as single cell even when two nuclei were observed.

2. **Different growth rate** of cells when they are co-cultured compared to their rate in a mono-culture condition

3. **Non-specific binding** to cells of secondary antibody used in N–cadherin labeling.

3.3 Application to the detection of a very small number of cancer cell mixed to blood cells.

The IMSTAR S.A. Pathfinder^{TM} Pathoscan Image Cytometry System was used to scan the whole filter (ISET filter),to identify A549 cells mixed in blood cells, based on a (i) an enrichment step using filtering by size, followed by (ii) a combination of biomarker immunolabeling. The samples were prepared by Benoît Coudert from Dr Françoise Farace's team at Gustave Roussy Institute (partner of the NanoCTC project).

A controlled number of A549 cells (approximately 3000) were trypsinized from the culture (to avoid aggregates) and added to 1 mL suspension of white blood cells ($\approx$ 10 million of cells) in appropriate buffer for 10 min. They were then passed through a polycarbonate filter[1] with 8 μm diameter holes (with a mean density of about one hole per 50 μm^2), letting the blood cells go through (owing to their smaller size than the one of A549 and to their deformation capabilities). A549 cells are expected to be found among the cells remaining on the filter, which still contains intact blood cells and debris.

In order to identify A549 cells as unambiguously as possible, three biomarkers were immunolabeled in addition to the nucleus (labeled with DAPI, blue color on Figure 3.6:

- CD45 immunolabeled with APC dye-antibody conjugate (magenta),

[1] ISET®– Isolation by Size of Tumor cells (RareCells S.A.S., Paris)

- E-cadherin immunolabeled with AlexaFluor488 dye-antibody conjugate (green),
- N-cadherin immunolabeled with AlexaFluor546 dye-antibody conjugate (yellow).

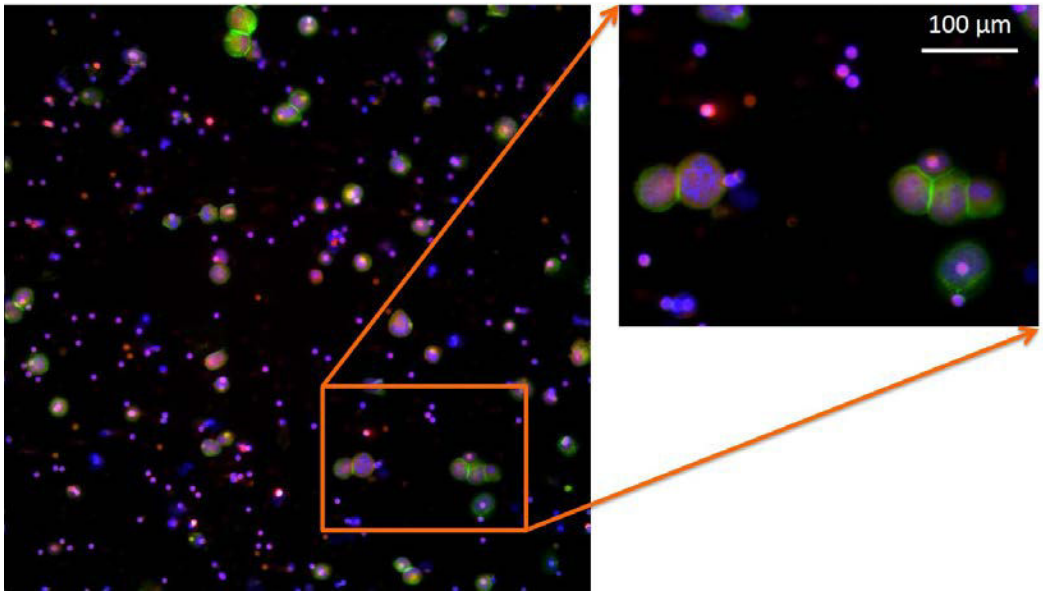

Figure 3.6 : ***Immunofluorescence labeling of blood cells spiked with A549 cells*** *and captured on a ISET® filter [Isolation by Size of Tumor cells (RareCells S.A.S., Paris)]. Small (8 µm diameter) magenta color discs corresponds to the filter holes. Captured cells are mostly located near or on top of these holes.*

White blood cells are positive for CD45 but not A549. Therefore, A549 are searched among CD45$^-$ negative cells. In order to further identify the right cells we added two positive discriminating criteria, which are the co-expression of E– and N–cadherin.

All cells captured on the filter were detected by their nuclei DAPI staining. In the case of aggregated cells, the Pathfinder^{TM} software uses the same segmentation approach as the one described in chapter 3 when dealing with close to confluence cell cultures. After segmentation, the cell membrane and nucleus are delimited by different contours Figure 3.7 allowing to infer quantitative parameters of potential interest (morphometric characterization i.e. the shape and size, intracellular labeling [from the fluorescence intensity]). Note that cells were most frequently superimpose to the filter pores, that later appears in a mixed blue & magenta color because they contain some hematopoietic cells debris (mostly DAPI-labeled DNA). In order to accurately calculate the cell labeling intensity, we exclude the pixels inside the pores. All the cells labeled for E–cadherin are considered as A549 candidates cells.

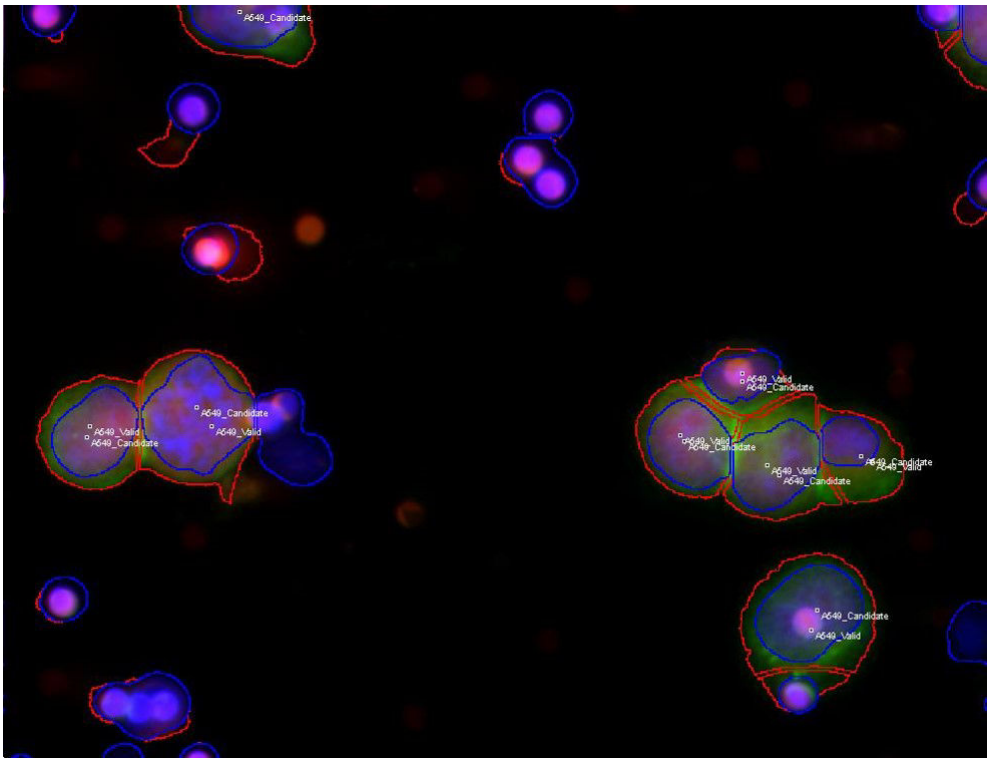

Figure 3.7 : ***Detected objects (cells or debris of cells) are analyzed by the Pathfinder software,*** *which identifies their nucleus and membranes contours for further quantification of protein expressions. A549 candidate cells are the one expressing E– and N–cadherin. They are labeled "A549_candidate" by the software, but they require further validation by an expert operator.*

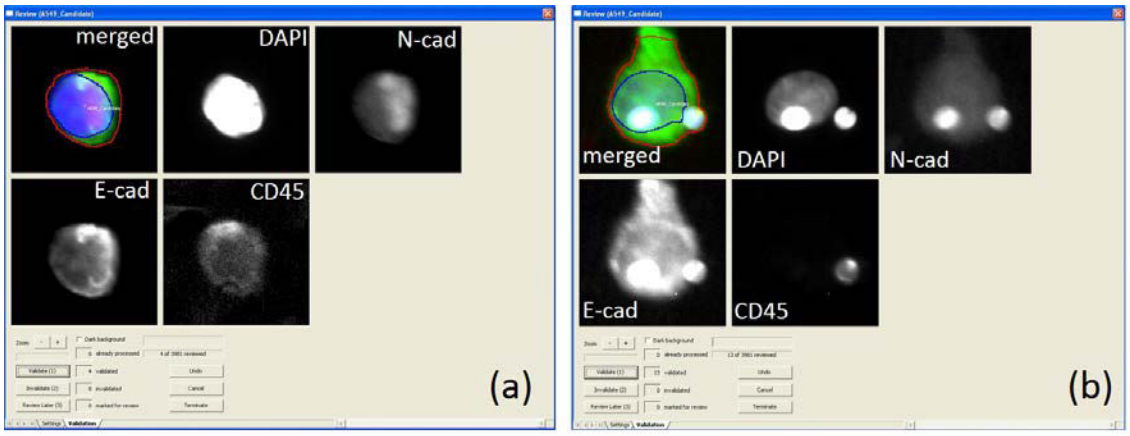

Figure 3.8 : ***Reviewing of A549_candidate cells by an expert****. the software reviewing tool displays DAPI, N–cadherin, E–cadherin and CD45 labeling of A549_candidate cells. (a) One A549_candidate expressing E– and N–cadherin, but since it also expresses CD45, it was finally rejected as a A549 cell. (b) A validated A549 cell on the basis of absence of CD45 labeling.*

The software identifies **A549_candidates** defined by cells with E– and N–cadherin coexpression. To be real A549, the cells should not express CD45, but there is always a background, which is why the opinion of an expert is required to finally validate a A549 candidate as a **A549_validated** cell.

Results: the experiment were carried out on 15-09-2014 consists 103 fields of view, using an objective lens of 20× magnification, corresponding to total area of 57 mm^2. The Pathfinder^{TM} system found 15635 "objects", including pores which are fluorescently labeled due to cellular debris, among which 3981 were detected as **A549_candidate** cells by the algorithm (see an example in Figure 3.8(a), which uses the software reviewing tool displaying the cell images in the 4 fluorescence channels next to each other). Each of these cells were then reviewed for CD45 negative expression by an expert from the IGR team using Pathfinder^{TM} software. From this review, 2850 cells were considered as being **A549_validated** cells (e.g. 3.8(b)), while the initial amount of cells introduced was 3000. We therefore retrieved the number of initial cells introduced with 95% .

As E– and N– cadherin are expressed mostly on the membrane, the quantification based on this expression at this specific location (identified after accurate segmentation), would probably increase the sensitivity because it remains unaffected by the parasitic fluorescence originating from the pores of the filter. This enhanced feature is under development by IMSTAR engineers.

The IMSTAR S.A. Pathfinder^{TM} Pathoscan system provides additional advantages over other systems (i.e. Ariol from Leica, Germany); (i) it can recognizes the pores accurately and corrects for the non-specific background, (ii) the software has an expert model adaptive learning capability, leading to a more reliable identification of A549 cells. Finally, the Pathfinder^{TM} system also provides morphometric characterization i.e. cells and nuclei shape and size.

3.4 Conclusion

We used cell immunofluorescence high throughput automated imaging and processing protocol relying on IMSTAR Pathfinder^{TM} system, to identify a cell population in a co-culture of cells expressing different phenotype. We successfully retrieved within 96% precision the expected proportion after 48 hours in culture.

We also presented the result of IGR team (Partner in the project) and using an upgraded version of IMSTAR Pathfinter^{TM} system adapted to detect a small number of cells with hybrid phenotype mixed with blood cells and then spotted on a polycarbonate

filter. The Pathfinder^{TM} system also allows further analysis on each cell which is necessary for a complete phenotype identification (and to do other analysis like Fluorescence *In Situ* Hybridization). To this respect, this experiments represents a initial step to validate the system using sample close to clinical sample, more precisely A549 cell mixed in blood.

While the combination of different fluorescent markers expression contributes to identify a cell phenotype more precisely, there is always some background that can be responsible for either a large number of false positives or no detection at all, depending on detection threshold level. In the following chapter, we introduce the time-gated fluorescence resonance energy transfer (TG-FRET) technique that we used in order to improve the signal over background detection of rare cells having a highly specific signature.

4 Fluorescence Resonant Energy Transfer to detect E/N–cadherin pairs at cell membrane

Summary

The aim of the NanoCTC project was to take advantage of nanotechnologies to improve the specific identification of CTCs, based on their phenotypic characteristics. Fluorescent Resonant Energy Transfer (FRET) is one of these technologies. It is capable of confirming the nanometer-separated coexistence of two proteins at the cell membrane, relying on dipole–induced dipole energy transfer which depend on the distance R between two well-chosen fluorophores as $1/R^6$.

Moreover, the use of photon donor with long radiative lifetime (2.7 ms) like lanthanide complex (e.g. terbium ones) allows to implement time-gated imaging to significantly decrease the short lifetime ($\approx$ 2 ns) cell autofluorescence, resulting in an increased signal-over-background ratio in immunofluorescence labeling.

In this chapter, we investigated the time-gated FRET between the terbium as a donors conjugated to E–cadherin and fluorophores as acceptors conjugated to N–cadherin. E– and N–cadherin nanoscale co-expression at the membrane was measured by exciting the terbium donors and time-resolved detection the emission by the fluorophore acceptors. If these proteins form nanoscale clusters/dimers we expect a FRET signal that could be specific to the cell line.

4.1 Co-expression of E– and N–cadherin at A549 cell membrane

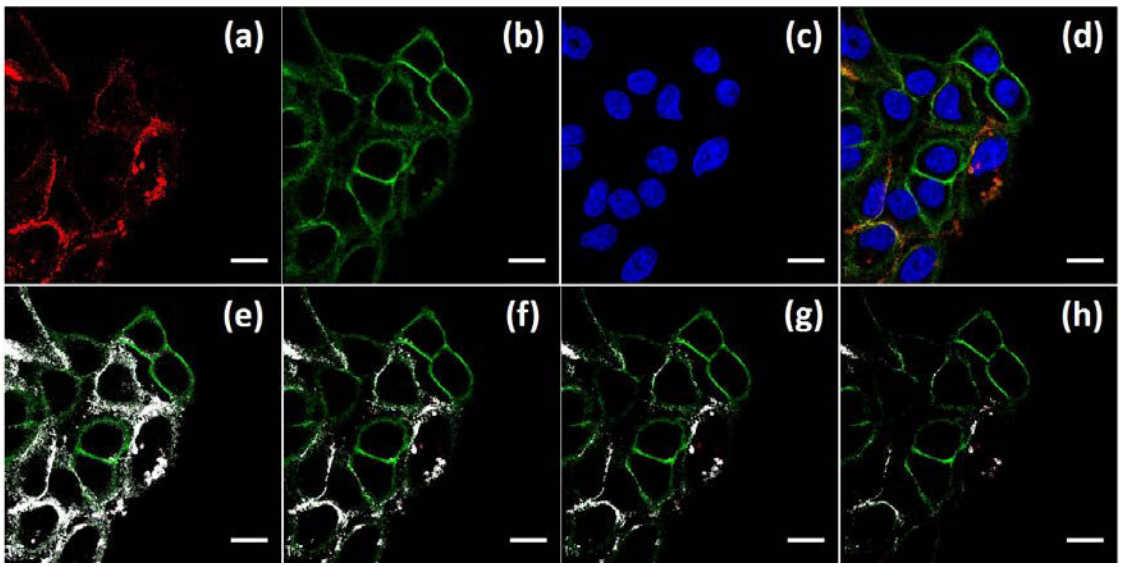

Figure 4.1 : Confocal raster scans of Immunofluorescently labeled E– and N–cadherin in A549 cells, to quantify the co-expression of these proteins. *(a) N–cadherin, (b) E–cadherin, (c) nucleus and (d) overlay of (a) to (c). Images (e)-(h) were processed using the colocalization Image J plugin (JACoP). White dots correspond to co-localized pixels of E– and N–cadherin. From (e) to (h) we increased the intensity level to be considered as the fluorescence background. A549 cells were exposed to primary antibodies, anti-E–cadherin goat polyclonal, and anti-N–cadherin mouse monoclonal and then secondary antibodies FITC (green channel (b)) dye conjugated anti-goat and Alexa Fluor 594 (red channel, (a)) dye conjugated anti-mouse, respectively. Cell nuclei were also labeled with DAPI (blue channel (c)). Scale bars: 20 µm.*

In order to see if FRET can applied to detect E–/N–cadherin clusters in A549 cell membrane, we first checked whether these proteins are expressed at this same location. This was done on A549 cultured cells in which we immunolabeled E– and N–cadherin with non spectrally overlapping dyes (Figure 4.1(a)-(d)). We did a co-localization analysis on images acquired by confocal microscopy. To avoid drawbacks and prejudice of visual based analysis, the image analysis tool JACoP (Just another Co-localization Plugin) was used to perform quantitative co-localization analysis of proteins at the subcellular level [98].

E–cadherin and N–cadherin were labeled with fluorescent probes, FITC (green) and AF594 (red) respectively and the images of Figure 4.1 were acquired at the appropriate excitation and emission wavelengths by using a confocal microscope equipped with 63×,

numerical aperture 1.32 oil objective lens. The overlay of E– and N–cadherin images shown in (d) displays only few places (in yellow) where these two proteins are colocalized. These images were processed by JACoP plugin for colocalization of E-/N- cadherin. Visually there are very few places where we see the co-localization of E and N–cadherin in yellow color (green+red). However, a more objective quantification with JACoP allows to evidence a larger number of colocalized pixels, displayed in white in figure 4.1(e-h), at increasing background fluorescence intensities. This tool also provides a quantification of the colocalization in terms of the Manders' coefficients: $M_1 = 0.945$ (defined as the fraction of AF594 pixels overlapping FITC pixels) and $M_2 = 0.479$ (fraction of FITC pixels overlapping AF594 pixels). These results suggest a partial colocalization of E– and N–cadherin at A549 membrane, which justify further investigation by FRET.

4.2 Time-gated FRET (TG-FRET)

4.2.1 Principle of TG-FRET

We used a Terbium (Tb) complex made of a ligand and a central Tb^{3+} ion (Lumi4-Tb, Lumiphore Inc., USA) as a donor and organic fluorophores as acceptors (see Fig. 4.2(a) with the example of Alexa Fluor 568 acceptor).

The lanthanide elements have many unique properties adapted to TG-FRET: (i) 2.6 ms very long radiative lifetimes, (ii) large Förster radius (up to 10-12 nm), (iii) excitation in the wavelength range 340-390 nm with multiple narrow transitions in the range 500 to 700 nm far from each other providing a broad choice or acceptor dyes, and finally (iv) a high resistance to photobleaching and oxidation [99].

In TG-FRET a time-delay larger than the acceptor radiative lifetime is introduced between the donor pulsed excitation and the acceptor emission detection, as displayed on Fig. 4.2(b). Both the acceptor fluorophore and cell autofluorescence having a short radiative lifetime (maximum of a few tens of ns in the case of semiconductor nanocrystals), no photon coming from their direct excitation will be detected. The detected photons only come from the FRET process, improving the FRET signal-to-background ratio.

4.2.2 TG-FRET Microscopy setup

The TG-FRET setup shown in figure 4.3(a) consists of an epifluorescence microscope equipped with (i) A light emitting diode (LED) emitting at 365 nm (Prizmatix, Israel) and collimated, (ii) a delay generator (DG645, Stanford Research Systems, Sunnyvale, CA)

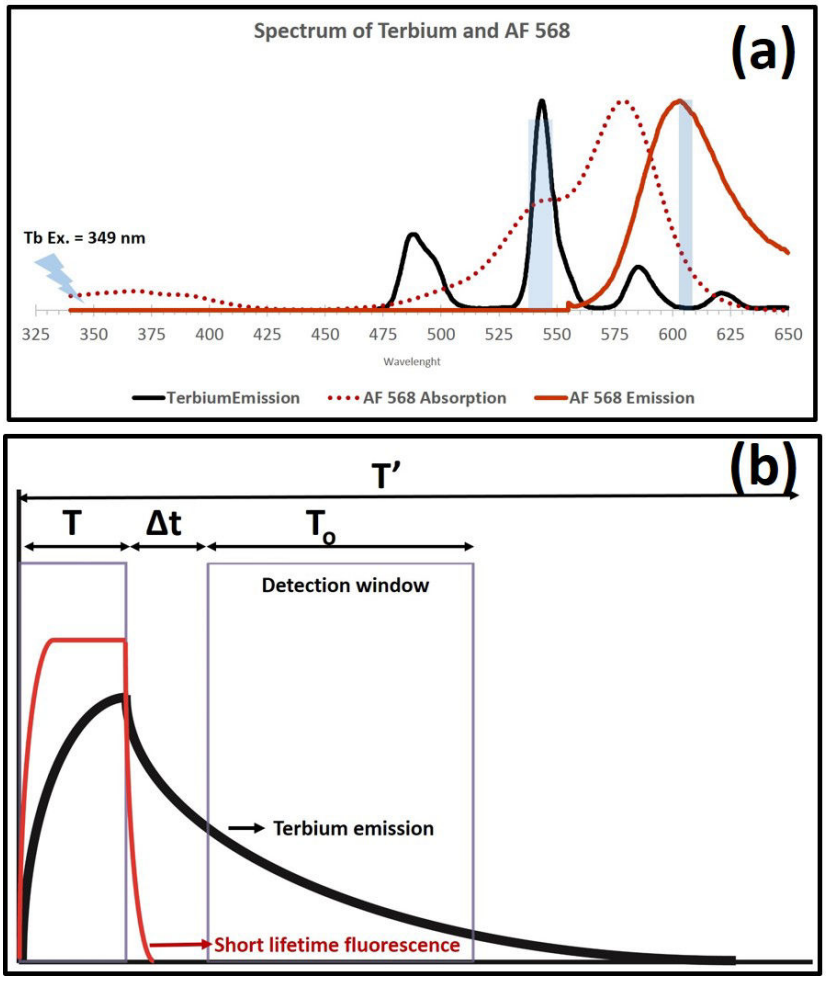

Figure 4.2 : ***Schematic representation of TG-FRET detection.*** *(a) Terbium complex donor fluorescence spectrum (black) after excitation at 365 nm wavelength. Absorption (irregular red line) and emission (regular red line) spectra of AF568 acceptor. Bandpass filter detection range is displayed in light blue. (b) Principle of time-gated FRET.*

delivering pulses at controlled moments, (iii) an intensified CCD (ICCD) array detector (Princeton Instruments, NJ, USA) mounted on the microscope, and a (iv) a computer board controlling the ICCD.

In the TG-FRET system, the delay generator triggers the LED excitation and ICCD acquisition. The adjustable parameters are $T', T, \Delta t$, and T_0, corresponding to repetition period, excitation pulse duration, time-delay, and detection gate-width respectively. Multiple cycles images (about 400) are integrated on the ICCD to improve the signal-to-noise ratio. Figure 4.3(b) shows the pulse sequence of TG-FRET. Typical parameters are: $T = 600$ μs, $\Delta t = 10$ μs, and $T = 2.5$ ms.

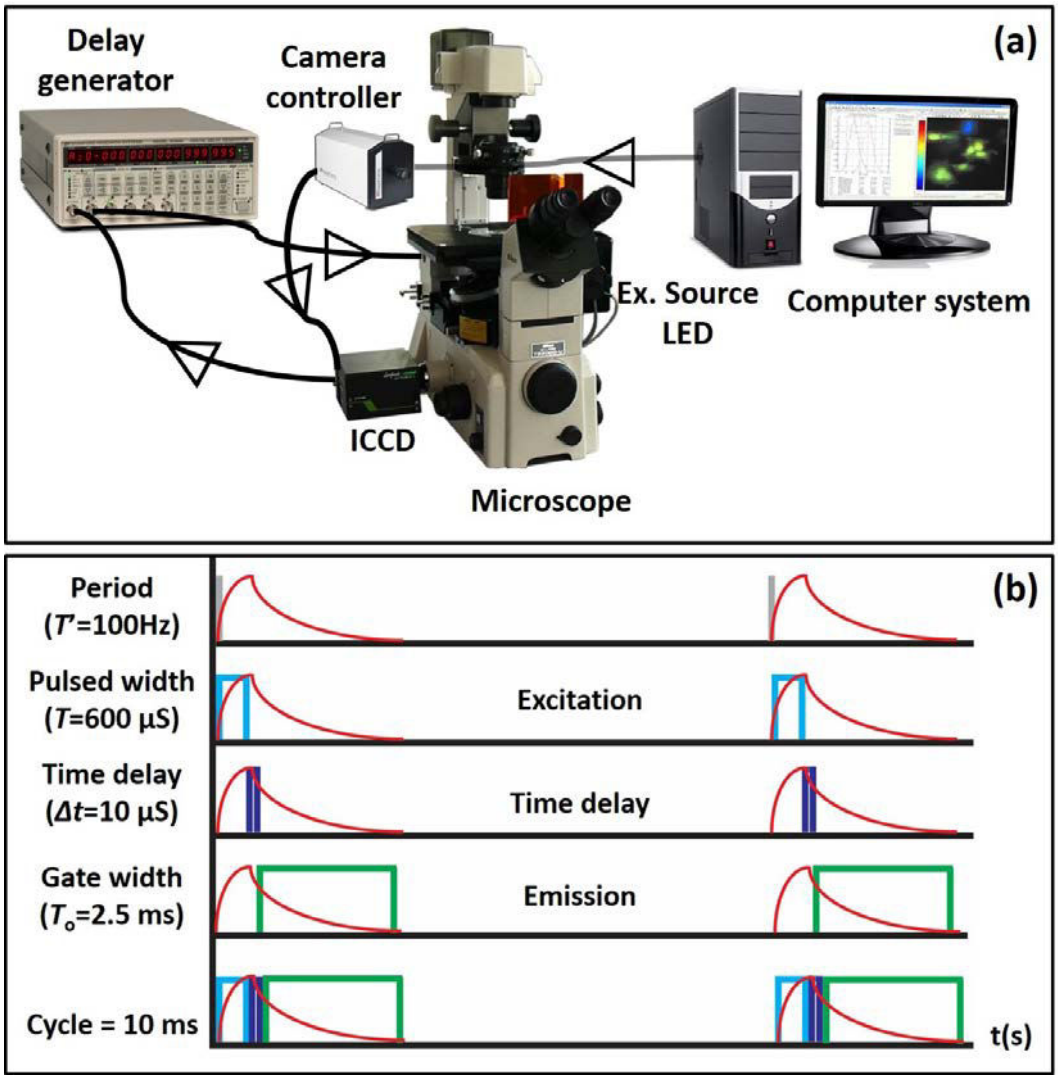

Figure 4.3 : *TG-FRET Microscopy setup.* *(a) Experimental setup of TG-FRET relying on an epifluorescence microscope with an excitation LED light source emitting in UV range, an intensified CCD array detector (ICCD) and a delay generator to synchronize the acquisition. (b) Pulse sequence of TG-FRET including the duration of each pulse.*

4.2.3 Methodology of TG-FRET implementation in cell microscopy

We used 3 different tumor cell lines in our TG-FRET experiments: A549, MCF7 and M4T. If E–cadherin and N–cadherin are within a few nanometers range at the cell membrane, we expect to observe energy transfer between their fluorescent immunolabels, as shown in figure 4.4.

E–cadherin being more abundant than N–cadherin in A549 cell line (see section 2.3),

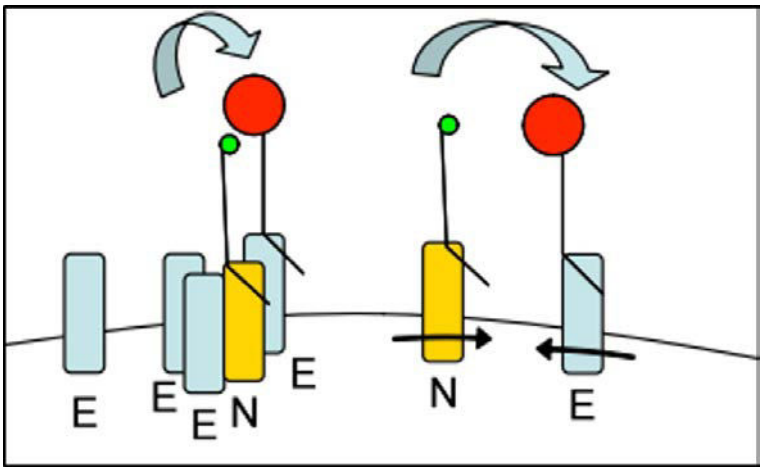

Figure 4.4 : ***Shows the targeting of protein by photoluminescent label of FRET pairs***

we chose to label E–cadherin with Terbium donor (using primary antibody goat polyclonal and secondary anti-goat antibody).

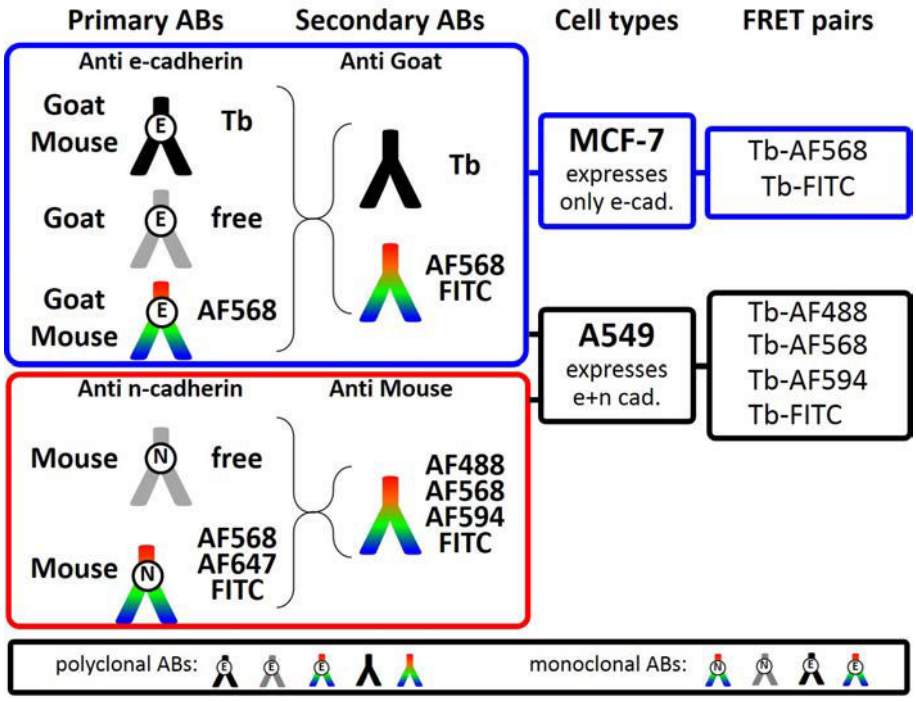

Figure 4.5 : ***Combination of FRET donor-acceptor fluorophores conjugated to E– and N–cadherin used in our study.***

We conjugated various FRET pairs of fluorophore to antibodies (either to primary or secondary ones). Figure 4.5 shows the combinations we realized to study the organization

of E– and N–cadherin at cancer cell membrane by FRET.

4.3 Time-gated FRET between fluorophores conjugated to E–cadherin

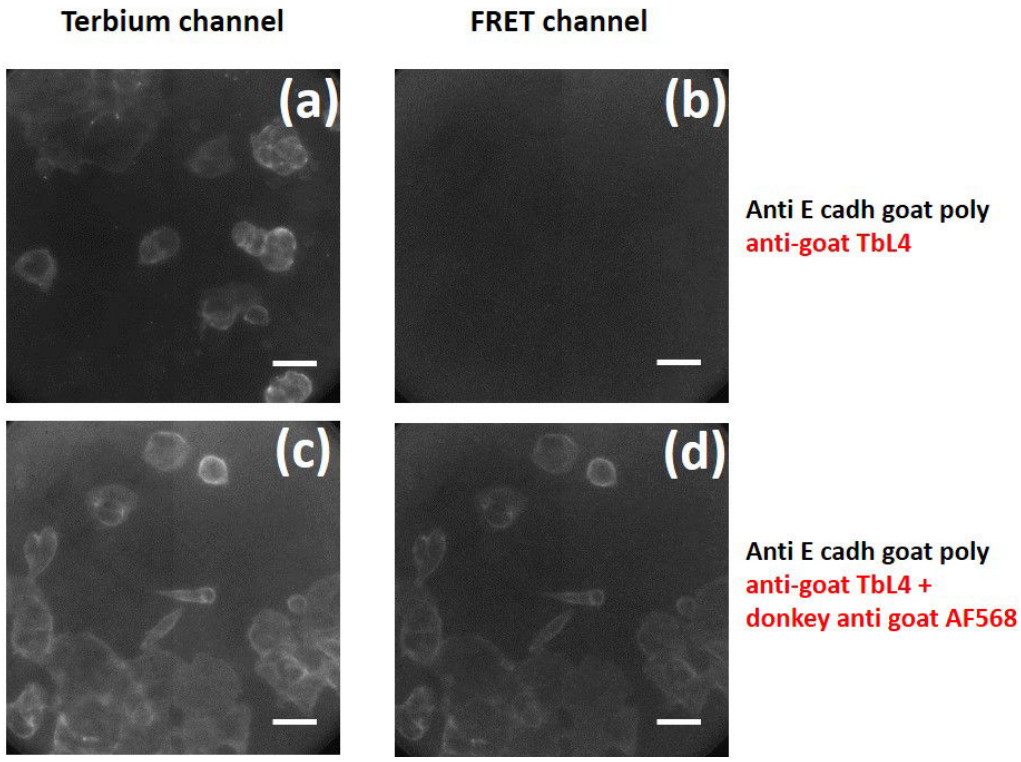

Figure 4.6 : *Imaging E–cadherin at MCF7 cell membrane by FRET*. *Lumi4-Tb labeled E–cadherin only, observed in the donor (Terbium, TbL4=Lumi4-Tb) channel (a) or in the Alexa Fluor 568 acceptor channel (b). The samples (c) and (d) were labeled with primary antibody and both the secondary FRET pair (anti-goat TbL4 and anti-goat AF568). (d) FRET signal between Terbium and AF568. Scale bars: 20 µm.*

As demonstrated previously MCF7 cells strongly express E–cadherin. This cell line is an interesting system to validate the FRET protocol and test the sensitivity of the detection system.

After fixation of MCF7 cell with PAF and blocking, cells were incubated for 1 hour with primary antibody and then again for 1 hour with secondary antibody conjugated with the terbium complex or with Alexa Fluor 568 dye. Then the coverslip were mounted on a glass slide for the analysis.

We then imaged the sample fluorescence in two different channels: terbium complex donor (detection centered at 542 nm with a bandwidth of 10 nm) and Alexa Fluor 568

acceptor (detection centered on 607 nm, bandwidth of 4 nm). The observations of figure 4.6 indicate that there is FRET at the cell membrane between terbium and AF 568. A similar experiment where AF568 was replaced by FITC reached the same conclusion

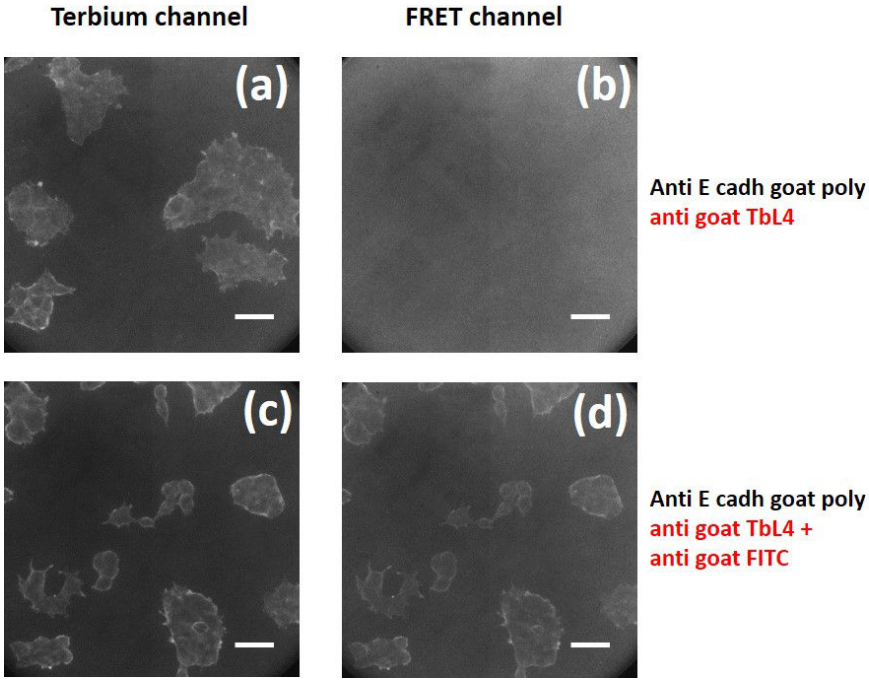

Figure 4.7 : *Imaging E–cadherin at MCF7 cell membrane by FRET*. *Lumi4-Tb labeled E–cadherin only, observed in the donor (Terbium) channel (a) or in the FITC acceptor channel (b). The samples (c) and (d) were labeled with primary antibody and both the secondary FRET pair (anti-goat TbL4 and anti-goat FITC). (d) Observation of FRET signal between Terbium and FITC. Scale bars: 20 μm.*

(see figure 4.7). For this experiment, we used two different channels: donor centered on 490 nm (bandwidth of 12 nm), and acceptor centered at 520 nm (bandwidth of 7 nm).

From the above observations one can conclude that an energy transfer only takes place between Tb and dye fluorophores attached to either two different E–cadherin (forming a cluster) as displayed on figure 4.8(a) or to a single E–cadherin (fig.4.8(b)). The later possibility cannot be excluded at this stage due to the fact that we used polyconal anti-E–cadherin antibody.

To figure out which explanation is correct we targeted two different E–cadherin with Tb- and dye-labeled **monoclonal** primary antibodies, and did not observed any FRET signal as shown on figure 4.9(c).

This result was rather unexpected because it has been reported that at adherens junctions cadherin are packed in a quasi-crystalline structure with a mean distance between molecules of 7 nm [100]. One possible explanation of the missing FRET signal would

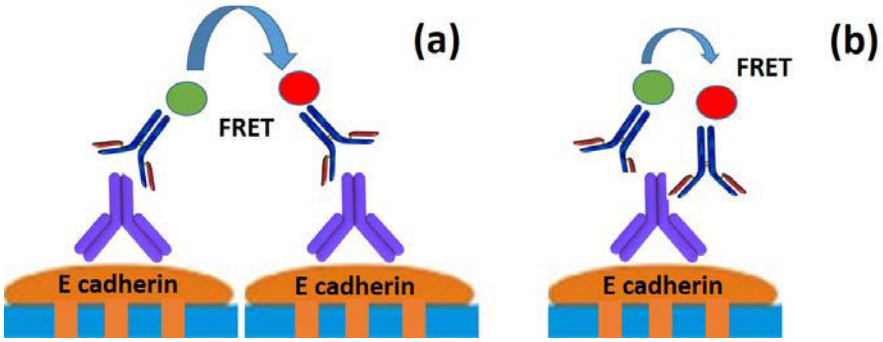

Figure 4.8 : *The two possible configurations of fluorophore-labeled secondary antibody explaining FRET observation in MCF7 E–cadherin immunolabeling of figures 4.6 and 4.7.*

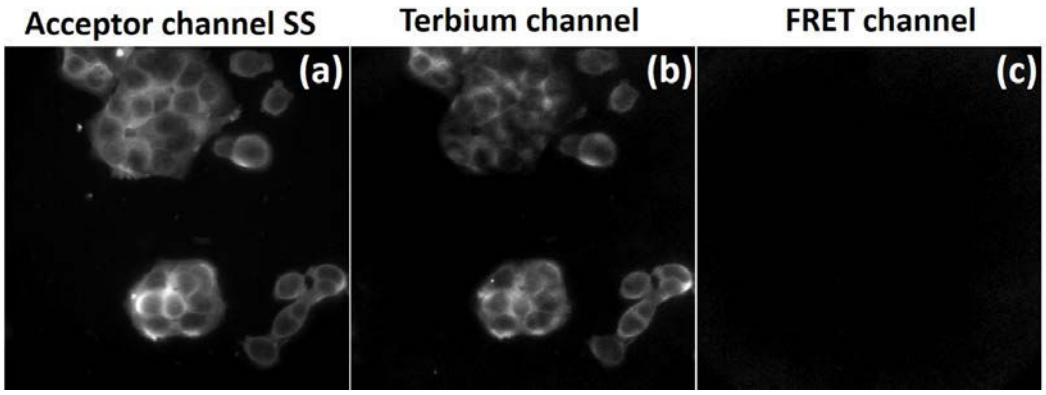

Figure 4.9 : *Investigation of E-/-E cadherin Tb-to-dye FRET in MCF-7 cells.Anti-E cadherin monoclonal antibody is conjugated with AF568 and TbL4,the staining of E cadherin with TbL4 and AF568 shown in (a) and (b) respectively. No FRET signal is observed in (c).*

be the unavailability of the E–cadherin for efficient antibody recognition at the adherens junctions due to steric hindrance. Moreover, the E-cadherin located in other parts than the cell junctions have a larger inter-protein distance which may exceed the FRET range.

Despite this negative result, we investigated the possibility of E– and N–cadherin clusters at A549 cell membrane by the same approach, as reported in the next section.

4.4 Time-gated FRET between fluorophores conjugated to E– and N–cadherin in A549 cells

To explore the presence of E–/N–cadherin clusters at A549 cell membrane, we followed the similar immunostaining protocol as for E–cadherin labeling, and used up to three

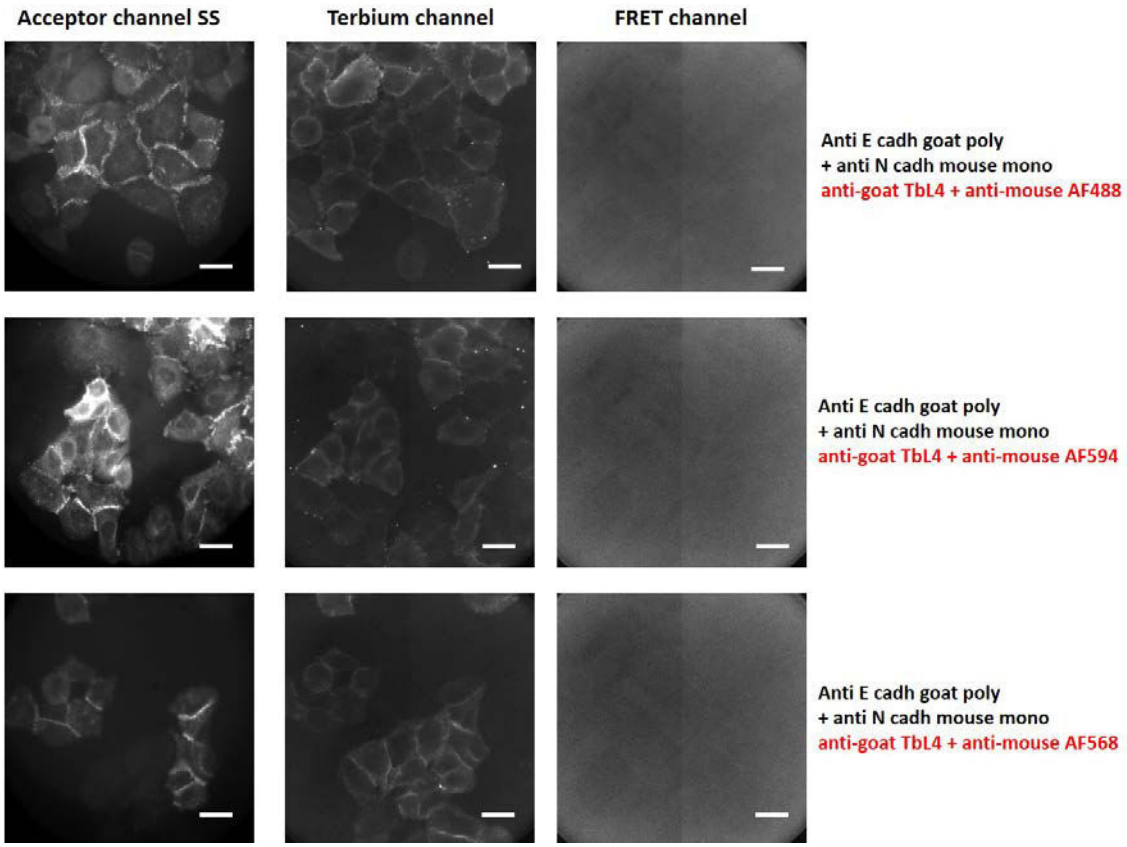

Figure 4.10 : Investigation E– and N–cadherin cluster formation at A549 cell membrane by FRET. *Acceptor channel shows the labeling of N–cadherin with different dyes in steady state mode (left column). Donor terbium channel shows the labeling of E–cadherin with Lumi4-Tb in time-gated mode (central column) and FERT channel shows energy exchange signal between fluorophores (right column). (top row) FRET between Lumi4-Tb and Alexa Fluor 488, (middle row), between Lumi4-Tb and Alexa Fluor 594, and (bottom row) between Lumi4-Tb and Alexa Fluor 568. No FRET signal is observed between fluorophores labeling E– and N–cadherin in A549 cell. Scale bars: 20 µm.*

different dye acceptors (Alexa Fluor 488, 594 and 568).

Figure 4.10 shows an efficient labeling of N–cadherin with the dye acceptors, and a good labeling of E–cadherin with Lumi4-Tb complex, observed in different samples and with a clear membrane localization. In spite of both protein expression on A549 cells, Time-gated FRET from Lumi4-Tb to dyes could not be observed in any of the antibody combinations.

The missing FRET signal may have different origins. First, E– and N–cadherin may not be co-expressed in clusters, which would result in E–N cadherin distances beyond the maximum detectable FRET distance of 10 to 12 nm. Another possibility is that E– and N–cadherin may be so close to each other that efficient binding of the antibodies to E–

and N–cadherin organized in clusters is not possible.

4.5 Conclusion

We have developed time-gated FRET cellular immunofluorescence microscopy to study the organization of E– and N–cadherin at the membrane. We used Lumi4-Tb(donor)–dye(acceptor) pairs with the advantage of (i) a high photostability of the donor, (ii) a low autofluorescence backgroung owing to the time-gated detection made possible by the millisecond radiative lifetime of Tb complex, resulting also in (iii) no crosstalk between the acceptor and donor channels.

The TG-FRET was used to investigate the presence of clusters of E–cadherin in MCF7 cells (expressing only E-cadherin), and E– and N–cadherin in A549 cells (co-expressing the two proteins). Unfortunately we did not observe FRET between the fluorophores used as labels, which does not prove alone the absence of clusters. However, despite the numerous studies on cadherins there is only one conclusive report of FRET between dyes labeling two cadherins [101]. To investigate in more details E– and N–cadherin membrane organization experiments involving single-molecule based superresolution fluorescence microscopy techniques like Stochastic optical reconstruction microscopy (STORM) [102] or Photoactivated localization microscopy [103] are necessary.

5 Immunofluorescence labeling of E–cadherin using photoluminescent semiconductor nanocrystals

Summary

Photoluminescent semiconductor nanocrystals (Quantum Dots, QDots) have many advantages as bioimaging labels: (i) it can be synthesized to emit at a controlled wavelength (related to their core size), with a narrow ($\approx 10-20$ nm width) emission spectrum, (ii) it has high resistance to photobeaching, (iii) it's surface chemistry can be tailored to facilitate biomolecule conjugation [104, 105].

In this chapter we present the results of immunofluorescence labeling of E–cadherin using custom-made, functionalized QDots (produced by the team of Thomas Pons, at ESPCI, Paris).

5.1 Bio-functionalization of QDots

Bio-functionalization of QDots is still a major challenge, because the conjugation of biomolecule like protein and antibodies to QD can compromise the stability of the colloidal suspension and/or the biomolecules function.

Before the bioconjugation is done, we first have to pass the QDots from its "natural" organic solvent, into water. This is done by ligand exchange [106]. This method consists in exchanging the hydrophobic molecules present at the QDot surface (as a result of the colloidal synthesis) with bifunctional molecules, having an hydrophilic part on one end

and an hydrophobic one on the other end. The most often used hydrophobic head groups reactive to the surface of QDots are thiol (-SH), while carboxyl groups (-COOH) are used at hydrophilic ends.

Once the QDots are dispersed in an aqueous suspension, crosslinking molecules are used to covalently couple the biomolecule of interest to the ligand taking advantage of reactive groups, such as -COOH, -NH_2, or –SH [107]. Since our goal was to use the QDots as fluorophores in E– or N–cadherin immunolabeling experiments, we first had to covalently bind appropriate biomolecules to QDots, as detailed in the next section.

5.2 Immunofluorescence labeling of E–cadherin using QDots

We used different strategies: (i) one relying on the well known biotin-streptavidin very high affinity, and requiring the conjugation of streptavidin to QDots and the use of biotinylated antibody, and (ii) the other consisting in a covalent coupling of an antibody (either the secondary or primary) to the QDots.

5.2.1 Biotin–streptavidin binding

For cell culture immunolabeling we first used an anti E–cadherin goat polyclonal primary antibody *biotinylated* and then we added the streptavidin-QD580 conjugate relying on a QDot with an emission centered at 580 nm.

A core/shell CdSe/CdS/ZnS nanoparticles was synthesized by following well established protocols [47,106,108] yielding particles of an average diameter of 7 nm (determined by Transmission Electron Microscopy, TEM) and absorbance/photoluminescence (PL) characteristics corresponding to an emission maximum at 580. This emission wavelength is well-suited for fluorescence microscopy imaging and FACS (Fluorescence Activated Cell Sorting) with a standard Texas Red filter. The same QD580 were used in first and third strategy. The synthesis and bioconjugation of QDots was done by Mariana Tasso from Thomas Pons's group at ESPCI ParisTech (partner of the NanoCTC project).

Briefly, the synthesis protocol is as follows:

- Core CdSe nanoparticles were obtained by reaction of triocylphosphine selenide and cadmium oleate in a mixture of octadecene, oleylamine and trioctylophosphine oxide [47].

- For the shell, three monolayers of CdS followed by two monolayers of ZnS were grown onto the core CdSe nanoparticles using cadmium oleate, zinc oleate and sulfur precursors dissolved in octadecene, as per the SILAR[1] procedure [108].
- The core/shell CdSe/CdS/ZnS nanoparticles were stored in hexane until use.

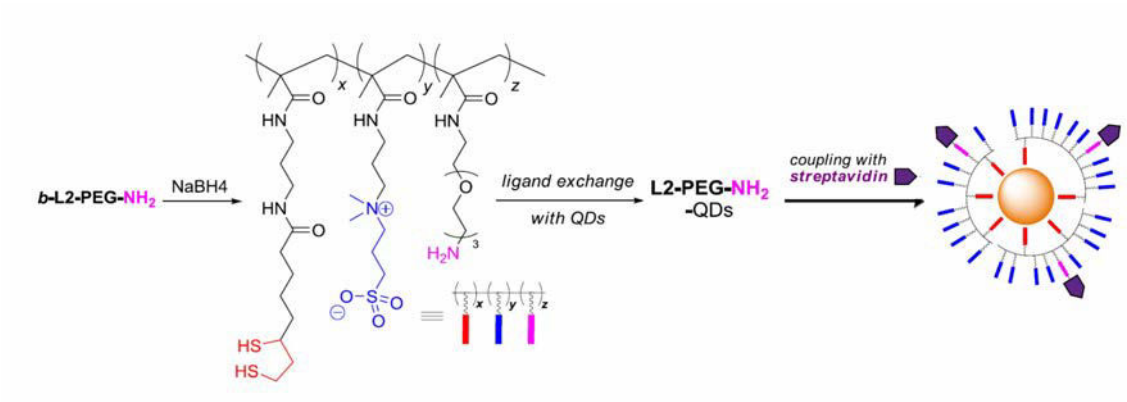

Figure 5.1 : ***Schematic representation of ligand exchange and conjugation of QDots to streptavidin [106]***

Figure 5.1 shows the schematic representation of the ligand exchange and conjugation process of streptavidin to QDot, obtained with the following steps:

- A terpolymer L2-PEG-NH_2 amine reactive group was synthesized and coupled to the ligand
- After ligand exchange, L2-PEG-NH_2-capped QDots were bio-conjugated, via the amine function, to streptavidin, using a peptide coupling based on a thiol/maleimide reaction.

Figure 5.2 shows the results of immunofluorescence and flow cytometry experiments performed in MCF7 cell, using QDots–streptavidin conjugates and biotinylated anti-E–cadherin antibodies. Immunofluorescence shows the specific labeling of E–cadherin with QDots, with the expected cell membrane localization of the protein. Flow cytometry confirms the result of IF.

Since one of our aims is to use QDots as an acceptor in FRET experiments, the additional cross-linking of biotin-streptavidin may significantly impede the FRET efficiency. In order to minimize the distance between donor and acceptor we tested other strategies involving a direct coupling of the antibody to the QDots.

[1]Successive Ionic Layer Adsorption and Reaction

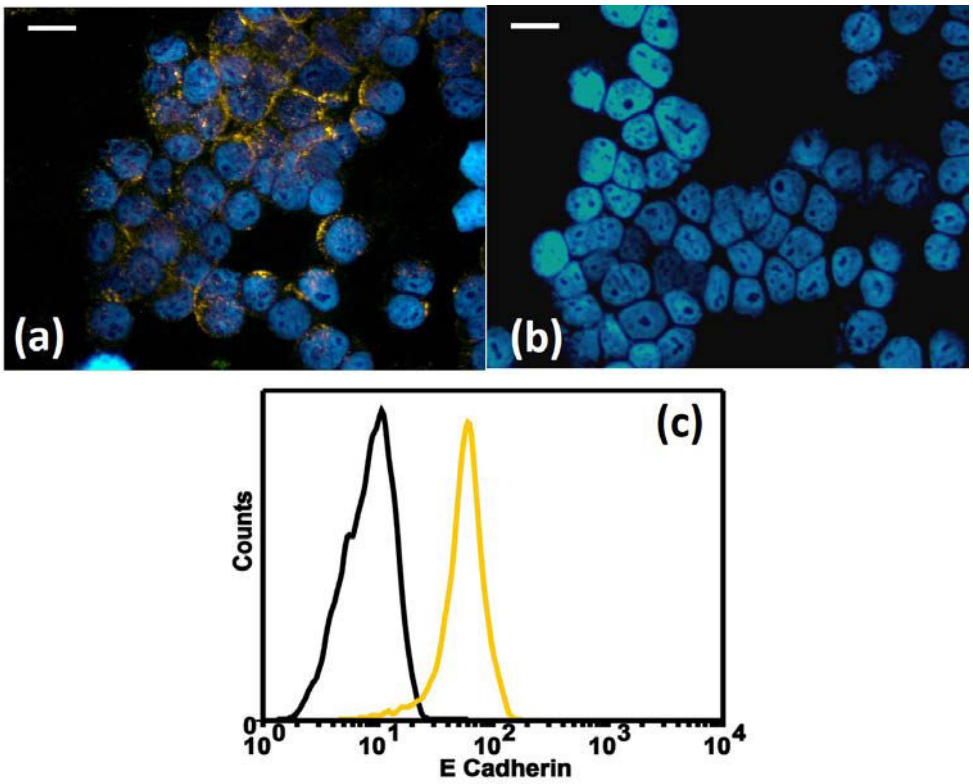

Figure 5.2 : ***E–cadherin immunofluorescence labeling of MCF7 cell using QDots conjugated to streptavidin.*** *(a) Epifluorescence microscopy analysis of E–cadherin immunolabeling by QD580 streptavidin complex appearing in yellow while blue represents cell nucleus labeling with DAPI. We used a biotinylated anti-E–cadherin primary antibody goat polyclonal and streptavidin-QD580 conjugates. (b) Control experiment, without primary antibody. (c)shows results of flow cytometry analysis, the yellow line corresponding to the sample incubated with the primary antibody and QD-streptavidin and the regular black line representing the control sample (without the primary antibody). Scale bars in (a) and (b): 20 µm.*

5.2.2 Simple covalent binding

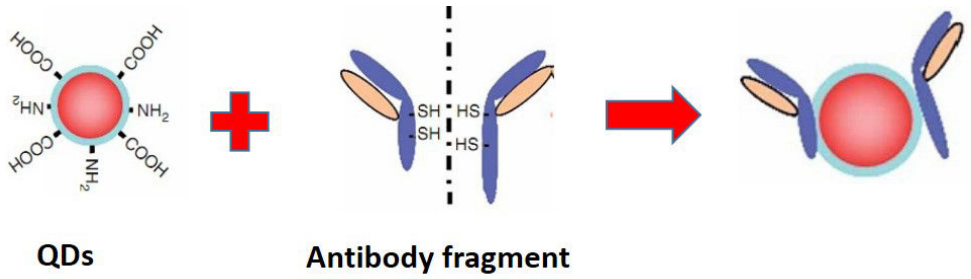

Figure 5.3 : ***Conjugation of QDots to secondary antibodies with free sulfhydryl (thiol) groups.***

We used commercial QDots with free (-COOH, and -NH) groups and a secondary antibody (donkey polyclonal antibody goat IgG - H& L (ref # ab7120, abcam , MA, USA) with free sulfhydryl (thiol) groups. The conjugation was performed using the eFluor ®Nanocrystal Sulfhydryl-Reactive conjugation kit (see Figure 5.3). The use of a linker is avoided to conjugate quantum dots and antibodies in order to minimize the distance between them.

The QDots-antibodies were then used to detect E–cadherin in MCF7 cells. Fixed cells were incubated during 1 hour with the primary antibody and 1 hour with the secondary antibody conjugated with commercial QD650 (central emission wavelength 650 nm). The results of immunofluorescence and flow cytometry experiments are shown in Figure 5.4. The IF image (Fig. 5.4(a)) corresponds to sample incubated with anti-E cadherin goat polyclonal antibodies and anti-goat QD650, we can see E–cadherin localized at the plasma membrane. However, we do observer some fluorescence emission due to the aggregation of QDot which is not localized at the plasma membrane. Also, the control sample (Fig 5.4(b))incubated with QDot conjugated to anti-goat antibodies clearly shows aggregation of QDots with some non-specific binding. This non-specific binding and aggregates can be interpret from the flow cytometry experiment result (Fig. 5.4(c)), where clear difference in signal can be observed from autoflourescence, control and specific samples represented in image by irregular black line, regular black line and red line respectively. However, The difference in the red and regular black line indicate the detection of E cadherin in MCF7 cells using QDots.

5.2.3 Oriented conjugation of antibody to QDot using protein A/G

In this strategy we used the recombinant protein A/G which has a very high affinity for the Fc domain of immunoglobins (IgG). In this method, we first covalently coupled protein A/G to the QDots, before adding the primary anti-E–cadherin goat polyclonal antibody. The QDot-protein A/G binds to the primary antibody in a spatially oriented manner, preserving the antibody structure and its antigen-recognition site (see Figure 5.5). The total hydrodynamic diameter of the complex is around 30 nm. We noticed a slight decrease in the fluorescence intensity of QDots, before and after the conjugation process. These QDots were equally stable when used in flow cytometry.

The detailed method of conjugation is as follows;

1. Surface-accessible Lysine residues in IgG binding domains of Protein A/G are mod-

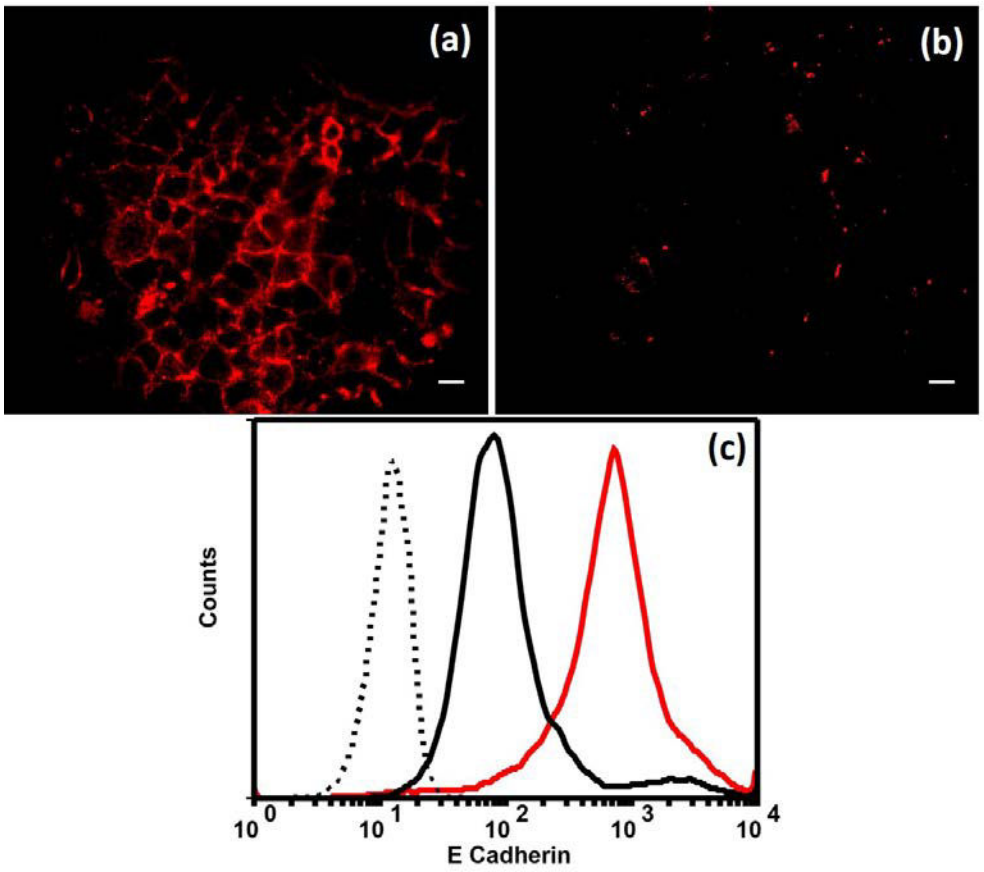

Figure 5.4 : *E–cadherin immunofluorescence labeling in MCF7 cells using QD650 conjugated to the secondary antibody.* *Images were acquired by epifluorescence microscopy. QD650 was excited in UV range and detected window centered at 650 bandwidth 20nm. (a)Labeling of QD650 appears in the sample was incubated with anti E–cadherin goat polyclonal primary antibody and the anti-goat antibodies QD650 conjugates. (b) Control experiment without primary antibody labeling. (c) Flow cytometer analysis, the red line representing the sample incubated with the primary and secondary antibodies conjugated with Qd650, the regular black line represents control sample incubated with only anti-goat antobodies QD650 conjugates. The irregular black line represents autofluorescence, this sample was incubated with washing buffer (PBS+2%SVF). Scale bars in (a) and (b) images correspond to 20 μm.*

ified with the hetero-bifunctional linker SMCC[2].

2. The conjugate SMCC-protein A/G is bound to accessible sulfhydryl groups present in the QDots copolymer ligand.

3. Unbound Protein A/G is separated via ultracentrifugation.

4. Protein A/G-functionalized QDots are bound to antibodies through strong affinity

[2]succinimidyl 4-[N-maleimidomethyl]cyclohexane-1-carboxylate

interactions.

5. Unbound antibodies are separated via ultracentrifugation

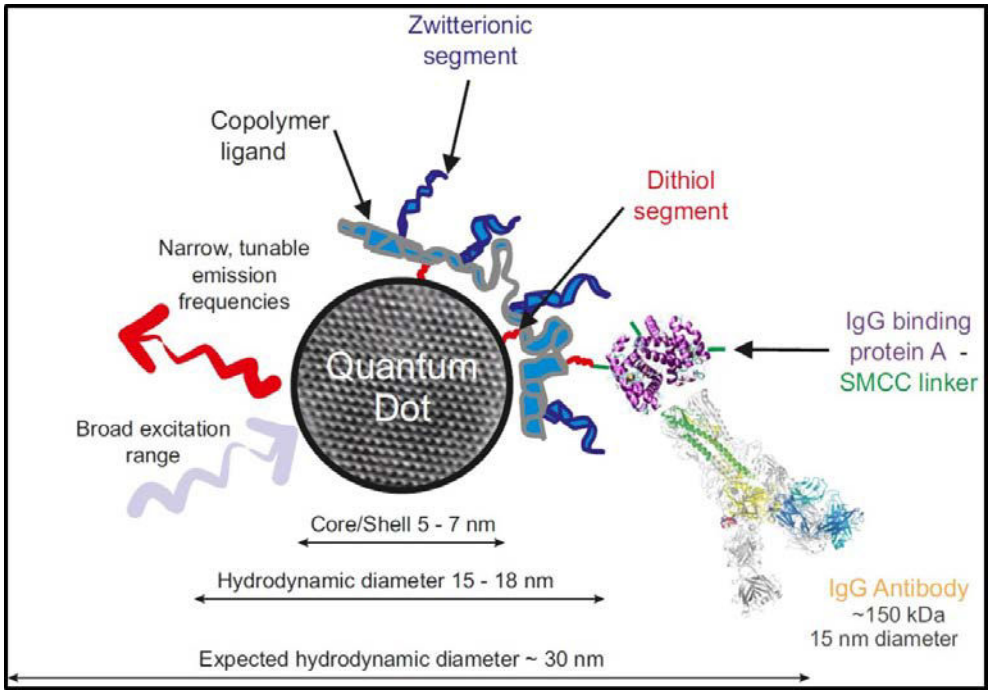

Figure 5.5 : ***Oriented conjugation of primary antibodies to QDots using protein A/G.***

Anti-E–cadherin goat polyclonal antobody-protein A/G-QDots were used to label MCF7 cells in culture. We tested this sample at 3 different concentrations (0.2 μM, 1 μM, and 3 μM). At 3 and 1 μM, we observed a clear membrane labeling but at 3 μM we also detected a signal in cytoplasm (data not shown). Moreover, the concentration of 0.2 μM was not appropriate due to the presence of QDots aggregates in the initial solution. We therefore concluded that the optimal concentration is 1 μM (Figure 5.6), for which the direct conjugation of anti-E–cadherin to protein A/G-modified QDots does lead to a specific E-cadherin membrane labeling.

In the same series of experiments we also conjugated **anti-N–cadherin** mouse polyclonal antibodies to QD580 with protein A/G. Figure 5.7(a) shows the labeling of N–cadherin using their conjugates in M4T cells by flow cytometry, where we observe some QDots aggregation (not visible in histogarms due to saturation of detector). To investigate further, the same cells were projected on a coverglass by a Cytospin^{TM} (ThermoFischer, USA) system and then labeled with DAPI and examined by epifluorescence microscopy (Fig. 5.7(b)). We observed some QDots aggregates along with the specific

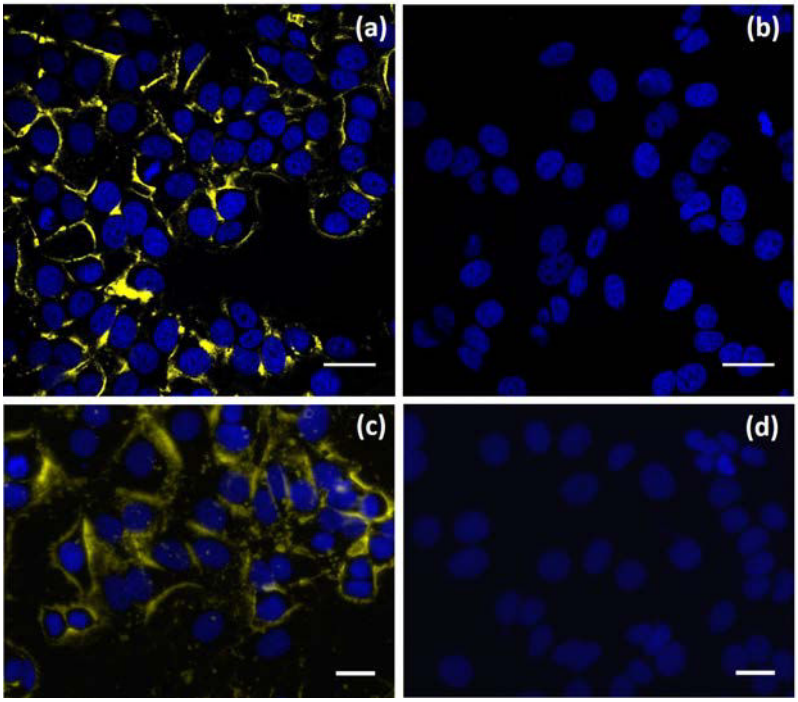

Figure 5.6 : ***E–cadherin immunofluorescence labeling in MCF7 cells, using QD580 conjugated to the primary antibody in a spatially oriented manner through protein A/G.*** *Antibody concentration: 1 µM. (a) Labeling by QD580 antibodies conjugates is displayed in yellow color, while the nucleus is labeled in blue by DAPI. (b) Control sample treated with Protein A/G-QD580 alone (i.e. no primary antibody). (a-b) Images acquired by confocal microscopy. QD580 was excited with a laser emitting at 458 nm; detection window centered at 580 nm, bandwidth 20 nm. (c-d) Images acquired with IMSTAR Pathfinder^{TM} epifluorescence microscope. Scale bars: 20 µm.*

membrane labeling. The aggregation of the QDots resulted in decreasing the concentration of staining solution which eventually resulted in weak membrane labeling of N–cadherin. Figure 5.7(c) shows a control experiment, with no sign of QDots aggregation as observed in the control sample histogram in figure 5.7(a).

In order to get rid of aggregation we repeated the N–cadherin labeling using a secondary antibody (anti-mouse) conjugated to the QD580 through protein A/G. The result of this experiment is not presented here: we observed larger amount of aggregates and very poor N–cadherin labeling. We also found that the aggregation of QDots took place after the ultra-centrifugation step. Ultra-centrifugation step is a critical step to remove unbound antibodies. The ESPCI team, who developed the conjugation method and the QDots, is working to solve this issue.

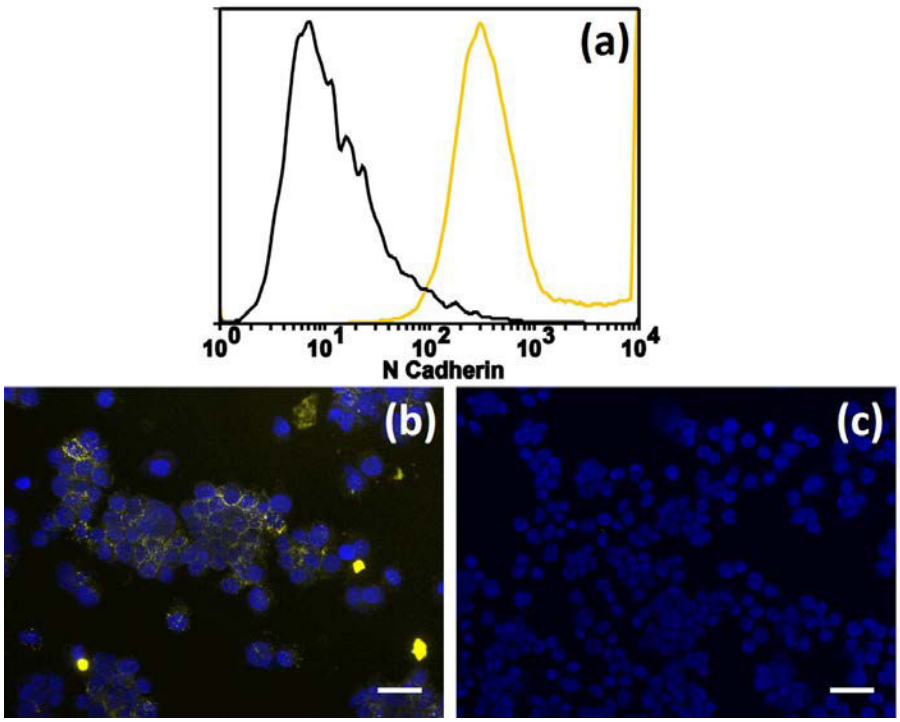

Figure 5.7 : *N–cadherin immunofluorescence labeling in M4T cells, using QD580 directly conjugated to the primary antibody.* *(a) Flow cytometry analysis of N–cadherin labeling by QD580 conjugated to anti-N cadherin mouse monoclonal through protein A/G (yellow color); control sample was incubated with protein A/G QD (black color). (b-c) Same sample were spincoated on a coverglass with Cytospin^{TM}, and then labeled with DAPI. (b) Anti-N–cadherin antibodies conjugated to QD580. Images were acquired by IMSTAR epifluorescence microscope. (c) Control sample incubated with Protein A/G-QD 580 conjugates only (no primary antibodies). Scale bars (b-c): 20 µm.*

5.3 QDot as a FRET acceptor

The extraordinary optical properties of QDots makes it a good candidates for FRET, in particular with terbium complex as donor, for the following reasons:

- The use of terbium as donor and QDots as acceptors in FRET assays provide a large spectral overlap integral, leading to a large Förster radius of about 12 nm(as compared to about 6 nm for traditional organic dye [109]

- Terbium has four well separated emission peaks which can excite four different QDots acceptor (see figure 5.8(b)). Therefore, Tb-QDots FRET allows multiplexing imaging relying on a single donor molecule and several acceptors molecules [110].

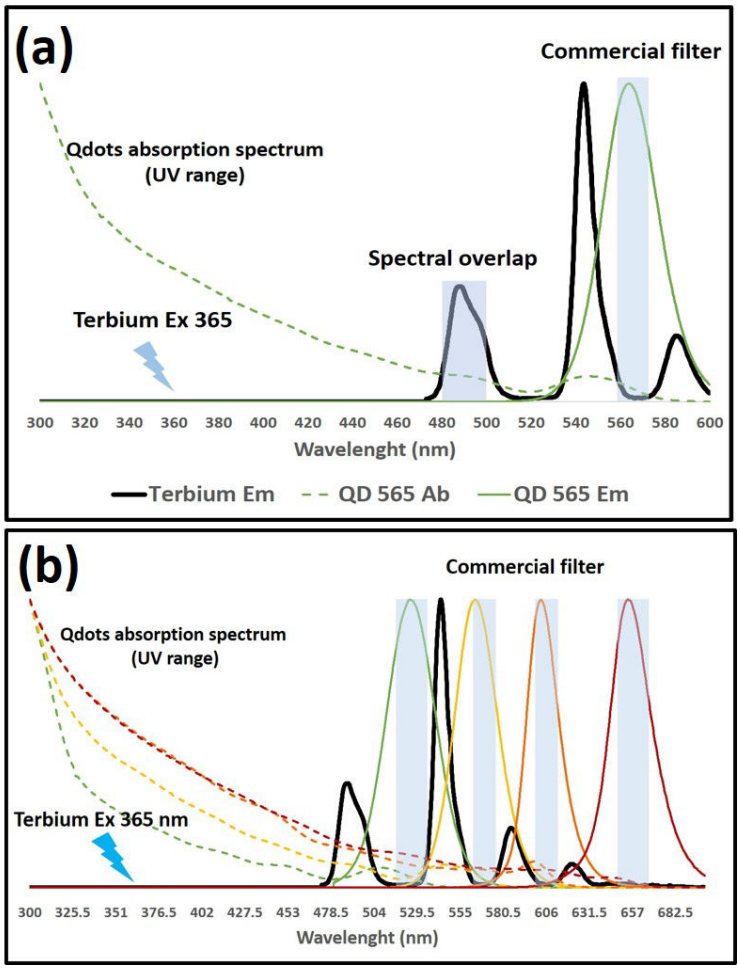

Figure 5.8 : *Depicts the spectral overlap of terbium and QDots.* *(a) shows the spectral overlap between emission spectrum of terbium and excitation overlap of QD565. The first emission peak of terbium can be used to excite QD565 and emitted light can collected using appropriate commercial optical filters. (b) shows that single terbium molecule as a donor can be used to excite atleast 4 different acceptor QDots (i.e. QD-525,565,605 and 650) using appropriate optical filters to allow multiplex imaging.*

5.4 Conclusion

The use of fluorescent nanoparticles for bioimaging is still under development. We experienced some advantages of QDots over conventional fluorophores, among which a much better photostability. We detected E–cadherin using QDots with different emission spectra and using different conjugation methods. Out of three different conjugation strategies, conjugation through protein A/G produced the best results with specific membrane labeling.

The successful bio-conjugation of QDots provides an opportunity to use them as acceptors in FRET experiments. Apart from that, QDots can be used as efficient donors

in steady-state FRET experiments. It has been reported that QDots effectively increase the FRET efficiency when used as donors with a dye as an acceptor [111]. Finally, owing to their high photostability, QDots-antibodies conjugates are very well adapted to targeted single particle tracking experiments.

6 Conclusion and Prospects

In this thesis we have developed fluorescence–based methodologies that could be used to improve the identification and characterization of Circulating Tumor Cells. CTC are currently the focus of many studies since, as mandatory intermediates in tumor dissemination, they have the potential to provide diagnostic and prognostic information as well as to be a unique window on the biology of the metastatic process. Although in most cases cancers give rise to none or only a few metastases many tumors continuously spew cells into the circulation providing a steady flow of CTC. Thus, even if CTC are rare among hematopoietic cells (typically one in a few millions), their relative abundance and their phenotype could be monitored over time to assess the evolution of the disease and its response to therapy. This is all the more attractive considering that taking a blood sample is a much less invasive intervention than standard biopsies – when they can be performed.

Identifying and characterizing CTC is still a challenge because of their low abundance and of the need to distinguish them from hematopoietic cells. The epithelial mesenchymal transition and the reverse transition provide a convincing biological framework to explain how carcinoma cells can egress from the tumor and become motile and invasive. At the same time, if during the intravasation process tumor cells have a fully mesenchymal phenotype it could be very difficult to distinguish them from the hematopoietic cells. Thus most approaches for detecting CTC have intrinsic biases as illustrated by the only clinically approved CTC test, CellSearch®, which relies on epithelial markers to detect CTC. Understanding the Epithelial(E)/Mesenchymal(M) status of CTC is therefore of key importance for clinical studies as well as for understanding the underlying biology.

In this work we have chosen to focus on cells with a hybrid phenotype, i.e. expressing both epithelial and mesenchymal markers, as they are prime candidates for CTC with a high metastatic potential. Cell surface proteins are versatile markers since they can be detected on living cells or cells fixed but not permeabilized. Here we have used E– ad N–cadherin as prototypic markers of Epithelial and Mesenchymal cells with two main goals: (i) developing a high throughput image analysis in order to identify hybrid cells among a larger population of mesenchymal cells and (ii) testing whether E– and N–cadherin were

in sufficiently close proximity to achieve a FRET between antibodies targeting them.

We started by identifying a cancer cell line (human lung cancer cell, A549) bearing such hybrid E/M characteristics, that we then used to validate our new detection methods. E, M and hybrid E/M phenotypes were characterized by measuring the levels of expression of E– and N–cadherins by conventional immunofluorescence and flow cytometry. Apart from A549 cells, we used purely epithelial and mesemchymal cell lines too, as controls.

In cooperation with IMSTAR S.A. we implemented a **high-throughput immunofluorescence-based detection** of A549 cells cocultured with purely epithelial cells, in initial proportion down to 25:75 respectively. This experiment yielded a A549 cell detection efficiency of 96%. The 4% false positive can be explained by the high degree of clustering of the cells in culture, complicating the automatic cell segmentation.

However, in patient samples, CTC and blood cells are individual cells in suspension. They do not form clusters, so that in the clinical sample analysis conditions cell segmentation is no more an issue of image processing. To get closer to these conditions, IMSTAR and us tested with the team of Françoise Farace (Translational Research Laboratory, Institut Gustave Roussy, Villejuif, France) the capacity of the Pathfinder^{TM} system to recover the correct number of A549 cells mixed in small proportion (3000 A549 cells added to 1 mL of blood) in a sample, after filtration by size and automatic immunofluorescence analysis of the filter membrane. Using an advanced algorithm developed by IMSTAR engineers capable of integrating an expert opinion during a training phase, we were able to identify on the ISET filter 95% of the initial A549 cells added.

The analysis of tumor cells on ISET filters is time consuming and requires a lot of input from trained personnel including anatomopathologists, the time of which is in high demand. While we have not yet implemented the image analysis protocol on CTC samples from patients, our preliminary study suggests that it has the potential to significantly reduce the number of candidate cells which should be examined by trained personnel. This will require training the algorithm on patient samples with the supervision of an anatomopathologist in order to optimize and validate the implemented criteria.

In this work we also addressed the improvement of the sensitivity of complex phenotype detection, by fluorescence techniques. We used **time-gated FRET** to investigate the presence of clusters of E– and N–cadherins, at A549 cells membrane. Energy transfer range in FRET being of the order of a few nanometers, the existence of such a signal would have revealed a molecular scale proximity of both types of cadherin. Moreover, such a FRET would have been a clear signature with a high signal over background ratio,

of an hybrid phenotypic character. Unfortunately we did not observe such a discriminant signal, despite the fact that both cadehrins are co-expressed at the cell membrane. Further investigations by superresolution fluorescence imaging would be necessary to identify whether this reflects an insufficient proximity or a restricted access to antibodies within cadherin clusters.

While here we have considered only two phenotypic markers it is obvious that phenotypic characterization of cells whether for clinical of fundamental purpose would be dramatically improved by an ability to measure a larger number of markers in a single experiment. Thus, a molecular signature of CTC could allow to simultaneously (i) characterize the genetic make up of tumor cells for choosing the appropriate treatment, (ii) accumulate prognostic information through the Epithelial/Mesenchymal status, and (iii) measure other biological markers once they have been validated. Figure 6.1 shows for example a CTC identified in patients with metastatic non-small cell lung cancer though the presence of high keratin and vimentin expression [75]. Adding to this biomarker expression measurements the ones of E– and N–cadherins, would complement the CTC signature.

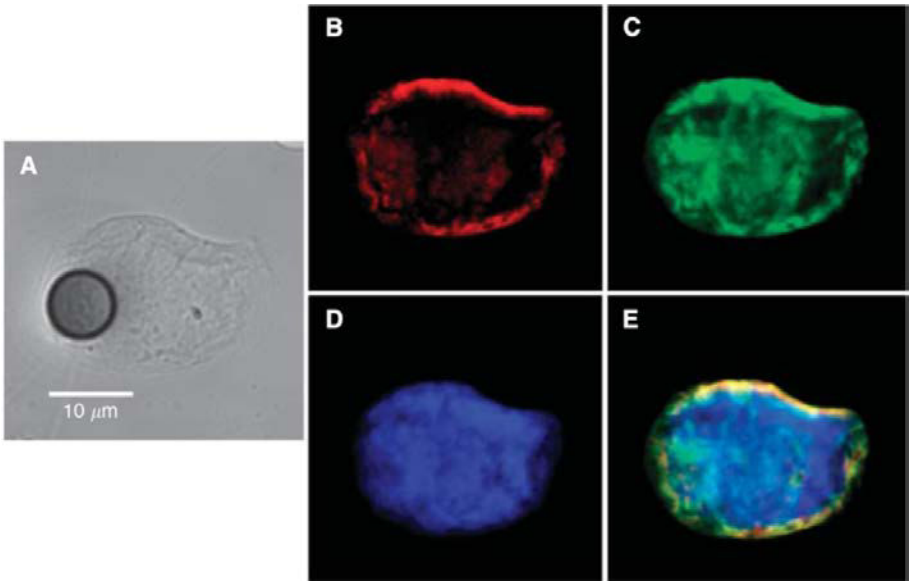

Figure 6.1 : ***Immunofluorescence analysis of CTCs expressing hybrid phenotype (Keratins and vimentin.*** *. (A) Bright field image, (B) Keratins, (C) vimentin, (D) nucleus and (E) merged of B-D. (Source: Ref. [75])*

To achieve this goal we need to improve the multiplexing capabilities of fluorescence microscopy. We contributed to this domain by evaluating E– and N–cadherin immunolabeling with **quantum dots–antibody conjugates**. This work was done in close

cooperation with the team of Thomas Pons (Laboratoire de Physique et d'Étude des matériaux, ESPCI ParisTech, Paris) which made the synthesis. The objective was to take advantage of the QDots remarkable properties: (i) a 10 nm width emission spectrum, with a central wavelength tunable by the size of the nanocrystas, (ii) quantum efficiency and photostability larger than the ones of organic dyes. Compared to organic fluorophores which have an emission spectrum width $\approx$ 50 nm, the narrow-band emission of QDots allows multiplexing as shown for example on Figure 5.8.

We have successfully demonstrated the detection of E–cadherin at high signal over background ratios, high photostability and high specificity, using three different QDot bio-functionalization schemes. In the case of N–cadherin we have faced aggregation of the conjugate. Therefore, there is still an important need for the optimization of QDdots bioconjugation before this tool can deliver its full potential. Moreover QDots used as acceptors in FRET with lanthanide as donor, has a large Förster radius ($\approx$ 12 nm), offering new possibilities to test protein-protein arrangements at the nanoscale.

Altogether, the different methods developed in this thesis should allow to address efficiently crucial questions in the field of CTC but also, more generally, to characterize the phenotypic diversity in normal tissues.

Appendices

A Article Reprint

"Terbium-Based Time-Gated Förster Resonance Energy Transfer Imaging for Evaluating Protein-Protein Interactions on Cell Membranes,"
Linden, S., Singh, M.K., Wegner, K.D., Regairaz, M., Dautry, F., Treussart, F., and Hildebrandt, N., **Dalton Trans.** (2015), doi: 10.1039/c4dt02884h

Dalton Transactions

PAPER

View Article Online
View Journal

Cite this: DOI: 10.1039/c4dt02884h

Terbium-based time-gated Förster resonance energy transfer imaging for evaluating protein–protein interactions on cell membranes†

Stina Lindén,[a] Manish Kumar Singh,[b,c,d] K. David Wegner,[a] Marie Regairaz,[d] François Dautry,[d] François Treussart[b] and Niko Hildebrandt*[a]

Received 23rd September 2014,
Accepted 14th January 2015

DOI: 10.1039/c4dt02884h

www.rsc.org/dalton

Fluorescence imaging of cells and subcellular compartments is an essential tool to investigate biological processes and to evaluate the development and progression of diseases. In particular, protein–protein interactions can be monitored by Förster resonance energy transfer (FRET) between two proximal fluorophores that are attached to specific recognition biomolecules such as antibodies. We investigated the membrane expression of E- and N-cadherins in three different cell lines used as model systems to study epithelial to mesenchymal transition (EMT) and a possible detection of circulating tumour cells (CTCs). EMT is a key process in cancer metastasis, during which epithelial markers (such as E-cadherin) are down-regulated in the primary tumour whereas mesenchymal markers (such as N-cadherin) are up-regulated, leading to enhanced cell motility, intravasation, and appearance of CTCs. Various FRET donor–acceptor pairs and protein recognition strategies were utilized, in which Lumi4-Tb terbium complexes (Tb) and different organic dyes were conjugated to several distinct E- and N-cadherin-specific antibodies. Pulsed excitation of Tb at low repetition rates (100 Hz) and time-gated (TG) imaging of both the Tb-donor and the dye-acceptor photoluminescence (PL) allowed efficient detection of the EMT markers as well as FRET in the case of sufficient donor–acceptor proximity. Efficient FRET was observed only between two E-cadherin-specific antibodies and further experiments indicated that these antibodies recognized the same E-cadherin molecule, suggesting a limited accessibility of cadherins when they are clustered at adherens junctions. The investigated Tb-to-dye FRET systems provided reduced photobleaching compared to the AlexaFluor 488-568 donor–acceptor pair. Our results demonstrate the applicability and advantages of Tb-based TG FRET for efficient and stable imaging of antibody–antibody interactions on different cell lines. They also reveal the limitations of interpreting colocalization on cell membranes in the case of lacking FRET signals.

Introduction

Circulating tumour cells (CTCs), *i.e.* cells in the bloodstream originating from a solid tumour, are currently actively studied as a potential source of information on the tumour, its genetic alterations, and its response to treatment.[1] One major difficulty is to identify CTCs since they are present at a very low abundance in comparison with white blood cells (typically 10^{-5}–10^{-6}). For tumours of epithelial origin, which constitute the major types of cancer, it is assumed that cells cannot efficiently egress from the tumour unless they undergo an epithelial to mesenchymal transition (EMT), which reduces the strength of cell–cell interactions and endow them with migratory capacities (Fig. 1A).[2] One of the hallmarks of EMT is the replacement of E-cadherin (epithelial marker) by N-cadherin (mesenchymal marker) at the surface of cells. Cadherins are transmembrane proteins that play a crucial role in cell–cell interactions, mostly through the organization of adherens

[a]NanoBioPhotonics, Institut d'Electronique Fondamentale, Université Paris-Sud, CNRS, Orsay, France. E-mail: niko.hildebrandt@u-psud.fr; http://www.nanofret.com
[b]Laboratoire Aimé Cotton, UMR 9188 CNRS, Université Paris-Sud and ENS Cachan, 91405 Orsay, France
[c]Laboratoire de Photonique Quantique et Moléculaire, UMR 8537 CNRS and ENS Cachan, 94235 Cachan, France
[d]Laboratoire de Biologie et de Pharmacologie Appliquée, UMR 8113 CNRS and ENS Cachan, 94235 Cachan, France

†Electronic supplementary information (ESI) available: Results of cadherin expression from flow cytometry (Fig. S1 and S2); PL decay curve and determination of PL decay time of Tb antibodies (Fig. S3); additional TG microscopy images of control experiments for E-cadherin expression on MCF-7 cells (Fig. S4); PL decay curves of solution-phase assays demonstrating Tb-antibody and dye-antibody binding to the same primary antibody (Fig. S5 and S6); additional TG and SS microscopy images showing that there is no crosstalk of Tb PL in the FRET channel (AF568) in the case of the E-cadherin cluster investigations using FRET and MCF-7 cells (Fig. S7); additional TG and SS microscopy images of control experiments for E/N-cadherin co-expression on A549 cells (Fig. S8 to S10); additional TG and SS microscopy images showing photobleaching, problems in serial donor–acceptor image acquisition, and successful co-labelling of N-cadherin with Tb and dye antibodies on M4-T cells (Fig. S11 and S12). See DOI: 10.1039/c4dt02884h

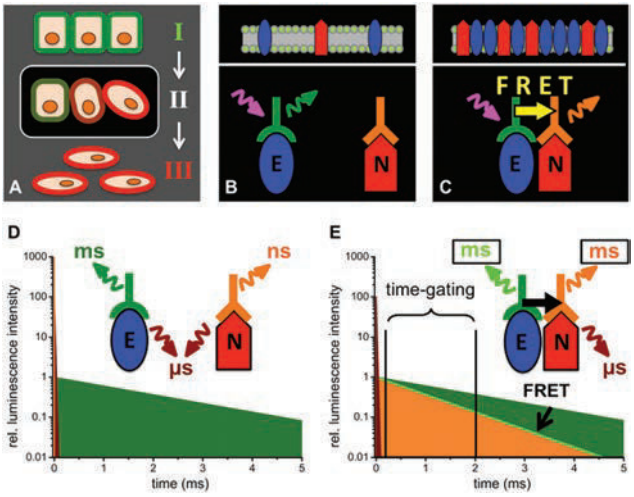

Fig. 1 Schematic presentations of EMT (A, cells in epithelial (I), intermediate (II) and mesenchymal (III) state) and the distinction between E-cadherin and N-cadherin coexpression (B and D) and E/N-cadherin clustering (C and E) by TG FRET using Tb-donor antibody (green) excitation (magenta arrow) and dye-acceptor antibody (orange) emission (orange arrow). (D) When E- and N-cadherins are not in a close distance (>20 nm) UV-excitation of the immunostained cells leads to long-lifetime Tb PL (green), a strong nano- to microsecond autofluorescence (brown) and a weak short-lived (nanoseconds) acceptor PL. (E) Clustering of E- and N-cadherins brings the Tb-donor and dye-acceptor in close proximity, which causes Tb-to-dye FRET. As the FRET efficiency η_{FRET} depends on the PL decay times of the pure Tb-donor (τ_D) and the one of the Tb-dye donor–acceptor pair (τ_{DA}) by $\eta_{FRET} = 1 - (\tau_{DA}/\tau_D)$,[23] FRET leads to millisecond Tb and dye emission (light green and orange, respectively) that is shorter than the pure Tb PL decay time. TG detection of the FRET quenched Tb-donor PL and FRET-sensitized dye-acceptor PL intensities several microseconds after the excitation pulse leads to specific PL signals for E/N clustering.

junctions made of dynamic patches of these molecules.[3] Within a patch, molecules are organized through *cis* interactions between cadherins (*i.e.* between molecules in the same membrane) and *trans* interactions (*i.e.* between molecules on apposed membranes).[4] While classical cadherins mediate homophilic interactions, heterophilic interactions between E- and N-cadherin have been observed *in vitro* and in some cases *in vivo*.[5] However, it is unclear how E- and N-cadherins are distributed in the cell membrane when they are co-expressed. By itself, the expression of N-cadherin cannot be used to detect CTCs since hematopoietic cells also express the protein. On the other hand, relying solely on E-cadherin expression would bias the study in favour of purely epithelial cells, which are unlikely to be the most aggressive ones. The only FDA (U.S. Food and Drug Administration)-approved test for CTC detection (Cell Search from Johnson & Johnson)[6] relies on the expression of epithelial markers and detects fewer cells than an assay that enriches in CTC on the basis of their larger size compared to most hematopoietic cells (ISET from Rarecells).[7] While during development EMT seems to be a toggle between two states, cancer cells behave in a less clear cut manner and can simultaneously express epithelial and mesenchymal markers.[8–10] Indeed, we have observed that some tumour cell lines express both E- and N-cadherins, in agreement with recent publications.[11] Being able to detect cells coexpressing E- and N-cadherins would allow to monitor the presence of cells that are likely to be more relevant to the metastatic process than purely epithelial cells.

While the detection of E- and N-cadherin expression with antibodies coupled to two distinct fluorophores should in principle allow the identification of cells with an intermediate epithelial/mesenchymal phenotype, such an approach cannot provide any information about the E/N-cadherin distances and their possible interactions in clusters. Alternatively, one can combine immunolabelling with Förster resonance energy transfer (FRET) to reveal with a high specificity the presence of the two molecules in close proximity. FRET is a non-radiative energy transfer from an excited donor to a proximal (*ca.* 1 to 20 nm) ground-state acceptor and requires spectral overlap of donor emission and acceptor absorption.[12–15] Thus FRET could produce an ideal signature of E/N-cadherin clustering if the two molecules were close enough to each other in the cell membrane. Many donor–acceptor pairs using organic dyes, metal complexes, nanoparticles, fluorescent proteins, and other fluorophores are available for FRET experiments.[16–19] In a typical cellular imaging setup for the analysis of protein–protein interactions the donor and acceptor fluorophores are conjugated to two different biological recognition molecules (antibodies in most cases),[20,21] which are specific for the two interacting proteins. Once the antibodies bind to their protein targets, donor and acceptor can interact by FRET, which can be detected by quenching of the donor photoluminescence (PL) and/or sensitization of the acceptor PL.[22,23] One major drawback of conventional dyes and fluorescent proteins is their susceptibility to photobleaching,[24–27] which makes long excitation and emission cycles almost impossible and causes difficulties in FRET analysis due to donor and/or acceptor bleaching. Because changes in donor and acceptor PL intensities and/or lifetimes are used for FRET analysis, alterations due to photobleaching can strongly interfere with the analysis of FRET signals. Luminescent nanoparticles, such as semiconductor quantum dots (QDs), can overcome photobleaching problems.[27,28] However, their relatively large sizes compared to biomolecules may perturb biological function and although QDs allow for relatively large Förster distances (R_0, donor–acceptor distance at which the FRET efficiency is 50%)[29] and high FRET efficiencies in case of direct attachment of dyes to water-soluble uncoated QDs,[30] the often applied thick polymer or lipid-based surface coatings result in increased donor–acceptor distances.[31–33]

An alternative approach consists in using time-gated (TG) or time-resolved (TR) imaging with lanthanides, taking advantage of their long PL lifetimes (in the μs to ms range). Such imaging techniques involve pulsed excitation at low repetition rates (Hz to kHz range), which leads to fewer excitation-emission cycles per unit time than for fluorophores with short (ns range) PL lifetimes, such as organic dyes, and therefore to a reduced photobleaching. Moreover, PL detection can be performed several microseconds after the excitation pulse when

autofluorescence of other components (*e.g.* endogenous fluorophores in biological samples, in particular in tissues)[34,35] has already occurred and therefore significantly reduce background signals. TG and TR microscopy approaches with long-lived fluorophores were already developed more than 20 years ago[36,37] but they have never become standard imaging tools. Technological advances and improved lanthanide-based fluorophores have led to a recent revival of time-gated imaging, which includes applications on standard wide-field microscopes equipped with pulsed UV excitation sources and time-gated cameras,[38–42] time-gated scanning luminescence using optical choppers and PMT detection,[43] time-gated orthogonal scanning automated microscopy (OSAM),[44] which was also applied for multiplexed imaging using upconversion nanocrystals,[45] and pinhole shifting lifetime imaging microscopy (PSLIM) and temporal sampling lifetime imaging microscopy (TSLIM) for the use on conventional confocal laser scanning microscopes in both TG and TR imaging.[46] Apart from detection of only the lanthanide PL, FRET from lanthanide donors to different dye acceptors has also been demonstrated in several spectroscopy and imaging studies.[46–54]

Here, we present an extensive TG-FRET imaging investigation of different model cell lines, which express E-cadherin, N-cadherin, or both, using immunostaining with luminescent Tb complexes (Tb) as FRET donors and various organic dyes as FRET acceptors to demonstrate the usability of TG-FRET imaging for the detection of protein–protein interactions at the cell membranes. Moreover, we also show the limitations of FRET imaging to interpret these interactions when no FRET signal is detected.

Results and discussion

E- and N-cadherin expression in the different cell lines

The main goal of our biological study was to distinguish between a simple coexpression of E- and N-cadherins (Fig. 1 B and D) and cadherin clustering at the FRET-imaging scale of *ca.* 1 to 10 nm (Fig. 1 C and E). For this purpose we investigated three tumour-derived cell lines: MCF-7 (from a breast carcinoma) expressing only E-cadherin, A549 (from a lung carcinoma) expressing E- and N-cadherin, and M4-T (from a melanoma) expressing only N-cadherin. MCF-7 was selected to evaluate the performance of our TG-FRET imaging system. We expected to be able to detect FRET between two E-cadherins for the MCF-7 cells because it was reported that E-cadherins at adherens junctions are packed in a quasi-crystalline structure with a mean distance between molecules of *ca.* 7 to 8 nm.[55,56] Flow cytometry experiments (Fig. S1 in the ESI†) confirmed the expression of E-cadherin but not N-cadherin at the cell membrane of MCF-7 cells. A549 cells were selected due to their ability of expressing both E- and N-cadherin as confirmed by confocal microscopy (Fig. 2) and flow cytometry (Fig. S2 in the ESI†). The confocal microscopy images clearly show coexpression of both cadherins on the cell membranes but as the spatial resolution is diffraction-limited they do not allow a determination of the E/N-cadherin distances. Because most dye acceptors were used to label N-cadherin-specific antibodies we selected the purely N-cadherin expressing M4-T cells to compare Tb-to-dye FRET to dye-to-dye FRET for an evaluation of background fluorescence suppression and photobleaching.

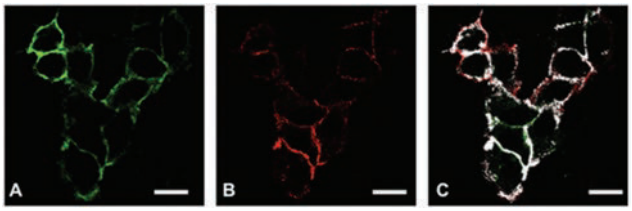

Fig. 2 Confocal images of A549 cells, which coexpress E-cadherin (A, FITC dye) and N-cadherin (B, AlexaFluor 594 dye). The overlay image (C) shows colocalization (indicated by the white pixels) with Mander's overlap coefficients of M_1 = 0.95 (fraction of AF594 pixels overlapping FITC pixels) and M_2 = 0.48 (fraction of FITC pixels overlapping AF594 pixels) but does not contain any information about the E/N-cadherin distances (E/N-cadherin clusters). Scale bars correspond to 20 μm.

Antibody-fluorophore conjugates and FRET properties

FRET imaging studies using immunostaining with donor and acceptor antibodies require many control experiments to allow determination of the origin of the different donor and acceptor PL signals as well as decreased PL signals, which can possibly occur due to insufficient staining or too large donor–acceptor distances (no FRET) caused by the protein expression levels and/or the FRET antibodies. We tested many different antibodies for efficient E- and N-cadherin targeting and selected those with the best selectivity to be combined with the Tb-complex Lumi4®-Tb[57] as FRET donor and different dyes as FRET acceptors. Some of the antibodies were readily available as dye-conjugates whereas others were conjugated in-house (*cf.* Experimental section). It should be noted that despite its strong and well-known susceptibility to photobleaching fluorescein isothiocyanate (FITC) is still a frequently applied dye for fluorescence immunostaining because many antibody-FITC conjugates are commercially available. Fig. 3 shows the different combinations of primary and secondary antibodies with Tb and various dyes for specific recognition of E- or N-cadherin and the resulting FRET pairs. E-cadherin was selected to be stained with Tb donor antibodies for studying both E-to-E and E-to-N cadherin FRET experiments between Tb and dye antibodies. Accordingly, one type of goat polyclonal and one type of mouse monoclonal primary antibodies were conjugated with Tb and AlexaFluor 568 (AF568) and secondary antibodies were labelled with Tb (anti-goat), Alexa Fluor dyes AF488, AF568, AF594, or FITC (anti-goat and anti-mouse). For N-cadherin (acceptor protein) a mouse monoclonal primary antibody was conjugated with AF568, AF647, or FITC and the same dye-conjugated anti-mouse antibodies as for E-cadherin staining were used as secondary antibodies. The various combinations led to two different Tb-dye FRET pairs for TG imaging of E-cadherin expression on MCF-7 cells, five different Tb-dye FRET pairs for TG imaging of E- and N-cadherin

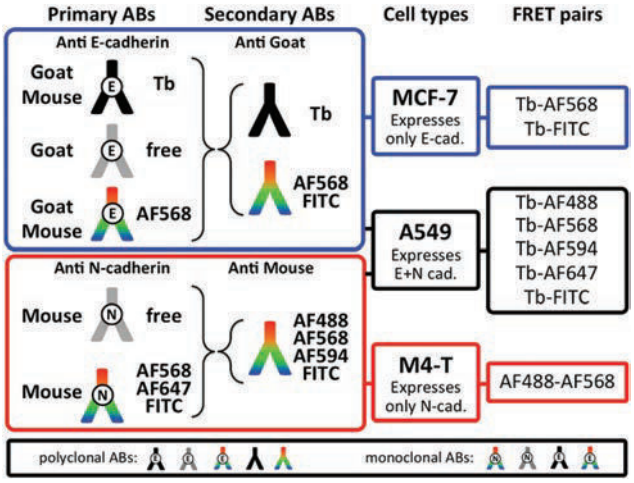

Fig. 3 Overview of available Lumi4-Tb and dye antibody conjugates, cell lines, and FRET pairs used for PL imaging experiments in our study. The black box on the bottom shows the different antibodies that were available as polyclonals and/or monoclonals.

expression on A549 cells, and one dye–dye FRET pair for steady-state (SS) imaging of N-cadherin expression on M4-T cells.

The chemical and photophysical properties of Lumi4-Tb and its advantages as Tb FRET donors have been discussed in detail elsewhere.[54,57,58] Briefly, they consist of unpolarized emission and extremely long excited-state lifetimes of 2.6 ms (Fig. S1 in the ESI†), which justify the orientation factor approximation of $\kappa^2 = 2/3$, and multiple and well-separated PL emission bands, which allow FRET to several different dyes for spectral multiplexing. The absorbance and emission spectra of Tb and the different dyes are shown in Fig. 4. Using the spectral overlap of Tb donor emission and the dye acceptor absorbance, the Förster distances were calculated by eqn (1),

$$R_0 = 0.02108(\kappa^2 \Phi_D n^{-4} J)^{1/6} \text{ nm} \quad (1)$$

where $\kappa^2 = 2/3$ is the orientation factor between the Tb emission and dye absorption transition dipole moments, $\Phi_D = 0.75$ is the PL quantum yield of the central Tb-ion, $n = 1.33$ is the refractive index of the aqueous buffer, and J (in M^{-1} cm^{-1} nm^4) is the spectral overlap integral as defined by eqn (2),

$$J = \int \bar{I}_D(\lambda)\varepsilon_A(\lambda)\lambda^4 d\lambda \quad (2)$$

where $\bar{I}_D(\lambda)$ (with $\int \bar{I}_D(\lambda) = 1$) is the intensity normalized emission of Tb and $\varepsilon_A(\lambda)$ is the molar absorptivity (or extinction coefficient) of the dye. The R_0 values of the different Tb-dye FRET pairs are in the 5 to 6 nm range (Fig. 4), which should provide a maximum detectable distance of approximately 10 to 12 nm ($2 \times R_0$).[23]

TG imaging for evaluating TG-FRET and E/E-cadherin clustering on MCF-7 cell membranes

To demonstrate the efficiency of TG Tb-to-dye FRET for imaging protein–protein interactions, we first performed a series of experiments on MCF-7 cells. Fixed cells were incubated for 3 h with primary antibodies against E-cadherin and for an additional 2 h with secondary antibodies. The cells were then washed and mounted on microscopy slides for imaging. As shown in Fig. 5A, TG imaging of MCF-7 cells targeted with both polyclonal Tb- and dye-labelled primary antibodies led to efficient FRET (positive TG dye signals upon Tb excitation). Similar experiments were performed with secondary Tb and dye antibodies, which also led to bright FRET signals (Fig. 5B and Fig. S4 in the ESI†) and very good evidence for efficient Tb-to-dye FRET.

As shown in the schemes of Fig. 5A and B, such positive FRET signals may arise from binding of the two antibodies to either the same protein (E-cadherin or primary antibody) or to two different ones. To reveal which binding scenario was responsible for the FRET signals we performed a series of control experiments. Time-resolved spectroscopy using unlabelled primary E-cadherin antibodies and secondary Tb

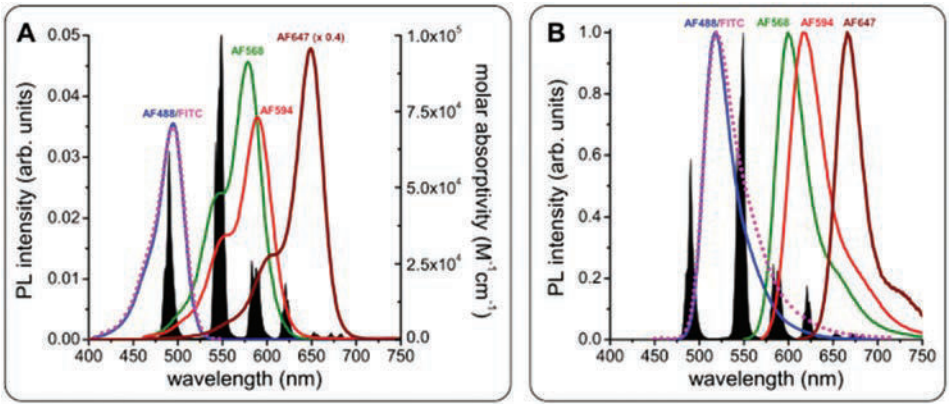

Fig. 4 PL emission spectrum of Tb (black in A and B) and absorbance (A) and PL emission (B) spectra of FITC (magenta), AF488 (blue), AF568 (green), AF594 (red), and AF647 (brown, molar absorptivity spectrum in A multiplied by 0.4 for better visibility of all spectra). Förster distances of the different FRET pairs were calculated using eqn (1) and (2): R_0(Tb-FITC) = 4.9 nm, R_0(Tb-AF488) = 4.9 nm, R_0(Tb-AF568) = 6.1 nm, R_0(Tb-AF594) = 5.9 nm, R_0(Tb-AF647) = 5.9 nm, and R_0(AF488-AF568) = 6.2 nm.

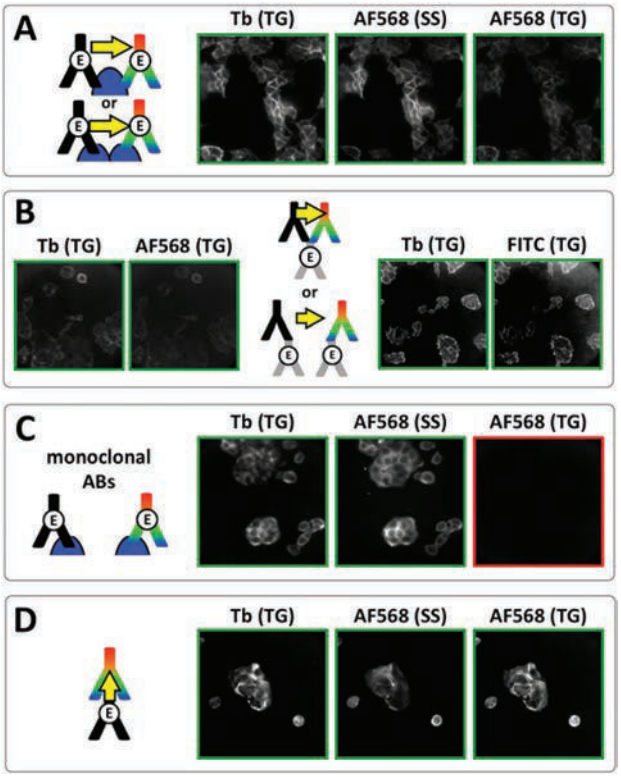

Fig. 5 Investigation of E/E-cadherin clustering in MCF-7 cells by Tb-to-dye FRET. For better clarity, positive signal images have green frames whereas negative signal images have red frames. (A) Time-gated (TG, 0.01–2.51 ms after excitation pulse) and steady-state (SS, excited at 520 ± 14 nm) images in the Tb detection channel (Tb, 542 ± 10 nm) and the AF568 detection channel (AF568, 607 ± 5 nm) using polyclonal primary Tb and AF568 antibodies resulted in positive TG Tb, SS AF568 and TG AF568 (FRET) PL signals, which could be caused by antibody-protein recognition on the same or different E-cadherins (top or bottom scheme, respectively). (B) Similar results as in A were found when using unlabelled polyclonal antibodies against E-cadherin and Tb and AF568 (left) or FITC (right) secondary antibodies, which offers again two possible binding scenarios (top and bottom scheme, respectively). (C) Using monoclonal Tb and AF568 primary antibodies led to efficient costaining but no FRET signal (TG AF568) due to too large distances (>*ca.* 12 nm) between Tb and AF568 antibodies (scheme). (D) For a verification of efficient TG Tb-to-dye FRET Tb primary antibodies and AF568 secondary antibodies (against the Tb primaries) were used for immunostaining. Efficient costaining as well as FRET due to antibody–antibody recognition (scheme) are clearly visible in the TG Tb, SS AF568, and TG AF568 PL images, respectively. Control experiments using only primary Tb antibodies showed that the TG AF568 signal is not caused by spectral cross-talk from the Tb PL (Fig. S7 in the ESI†).

and dye antibodies in solution (without any cells) showed that several secondary antibodies could bind to the same primary antibody, which was evidenced by FRET-sensitization of the dye acceptor secondary antibodies by the Tb donor secondary antibodies (Fig. S5 and S6 in the ESI†). We further prepared Tb- and dye-labelled monoclonal antibodies against E-cadherin. In contrast to the polyclonal antibodies, which can bind to different epitopes of E-cadherin and therefore enable multiple-antibody binding to the same E-cadherin, monoclonal antibodies are specific against the same epitope, which strongly reduces the possibility of multiple-antibody binding to the same E-cadherin. Despite very bright Tb and dye antibody staining on the same cells, no FRET was detected (Fig. 5C). Taking into account the expected distances of *ca.* 7 to 8 nm between clustered E-cadherins at adherens junctions (*vide supra*), this result was somewhat unexpected. A possible explanation for the lack of FRET is the unavailability of two different clustered E-cadherins for efficient antibody recognition. Such steric hindrance does not exist for unclustered E-cadherins or E-cadherins located on cell surfaces outside of cell junctions, where the density of molecules is much lower. Therefore multiple polyclonal antibody binding to the same E-cadherin or primary antibody (and FRET) becomes possible (top schemes in Fig. 5A and B), whereas the monoclonal antibodies can bind only to single E-cadherins, which are separated by distances beyond the FRET range (scheme in Fig. 5C).

Despite the limitations of our FRET analysis to quantify the distances between E-cadherins in fixed MCF-7 cells, the successful TG-FRET imaging experiments for FRET donor and acceptor antibody binding to the same protein (E-cadherin or primary antibody) clearly demonstrate the feasibility of efficient protein proximity detection using TG Tb-to-dye FRET microscopy. This was further confirmed by efficient FRET on the MCF-7 cells between Tb-labelled primary antibodies and dye-labelled secondary antibodies (Fig. 5D).

TG imaging for evaluating E/N-cadherin clustering on A549 cell membranes

For the different TG-FRET imaging experiments to study E- and N-cadherin co-expression, the immunolabelling was performed similarly to the one of MCF-7 cells. Fig. 6 (and Fig. S8 to S10 in the ESI†) shows TG and SS images of various antibody combinations for FRET immunostaining. Independent of the applied combination of Tb- and dye-labelled antibodies, A549 cells showed positive PL signals for both E-cadherin (TG Tb signals) and N-cadherin (SS dye signals) immunostaining, with a clear membrane localization and some intracellular signal. Despite this double protein expression, FRET from Tb to dyes (TG dye signals) could not be observed in any of the various antibody combinations. Taking into account the results from the MCF-7 cell imaging, the absence of FRET was certainly caused by too long distances between the Tb and dye antibodies. From the biological point of view the lack of FRET signals prevents any quantification of colocalization and/or clustering. Nevertheless, different qualitative interpretations are possible. First, E- and N-cadherins may not be coexpressed in clusters, which would result in E–N cadherin distances beyond the maximum detectable FRET distance of *ca.* 10 to 12 nm. Second, clustered E- and N-cadherins may be in such a close proximity that efficient binding of the antibodies in E/N clusters is not possible (or at least very inefficient). Third, the antibodies may be able to bind to the cadherins but the antibody-protein recognition sites place the two antibodies at a distance beyond the detectable FRET range.

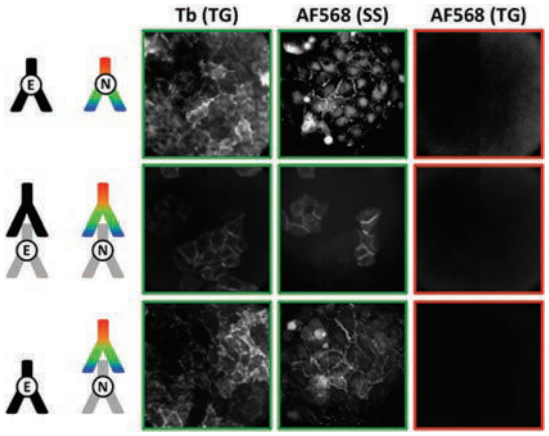

Fig. 6 TG (0.01–2.51 ms after excitation pulse) and SS (excited at 520 ± 14 nm) images in the Tb detection channel (Tb, 542 ± 10 nm) and the AF568 detection channel (AF568, 607 ± 5 nm) of different FRET-pair antibody combinations to detect a possible E/N-cadherin clustering. Costaining of Tb-antibodies (against E-cadherin) and AF568-antibodies (against N-cadherin) is clearly visible in the TG Tb and SS AF568 PL images. However, no FRET signal (TG AF568 signal) was detected, which shows that Tb-donor and dye-acceptor are not in close (<*ca.* 12 nm) proximity. For better clarity, positive signal images have green frames whereas negative signal images have red frames. Control experiments using FITC, AF647, AF488, and AF594 antibodies against N-cadherin as acceptors and different primary/secondary antibody combinations led to the same results (Fig. S8 to S10 in the ESI†).

Comparison with steady-state dye-to-dye FRET imaging using N-cadherin expression on M4-T cell membranes

Apart from short-lived autofluorescence background of the cells as one possible disadvantage of SS imaging, many dyes are prone to photobleaching, which limits their application for imaging cellular processes on longer time scales. During initial TG-FRET imaging experiments, in which we recorded first Tb-TG, dye-SS, and then dye-TG images, we discovered a significant decrease of the dye PL intensity during the acquisition of the SS images. We therefore adapted our acquisition series and always took the TG-images (of both Tb and dyes) before the SS images, which significantly improved the TG-dye image acquisition. It should be noted that different dyes provide different photostabilities and that the conditions of the cell medium may be optimized by deoxygenation or the addition of different chemicals. However, the selection of matching FRET pairs, the varying availability of selective antibodies conjugated with different dyes, and a possible sensitivity of the cells to chemical treatment (in view towards live cell or *in vivo* imaging) usually limit the possibilities to achieve a fully optimized system. We therefore decided to perform a comparison of Tb-to-dye FRET imaging and dye-to-dye FRET imaging under similar conditions, which implied to use the same acceptor dye AF568 and identical staining procedures. To also match the Förster distance to the Tb-to-dye system we

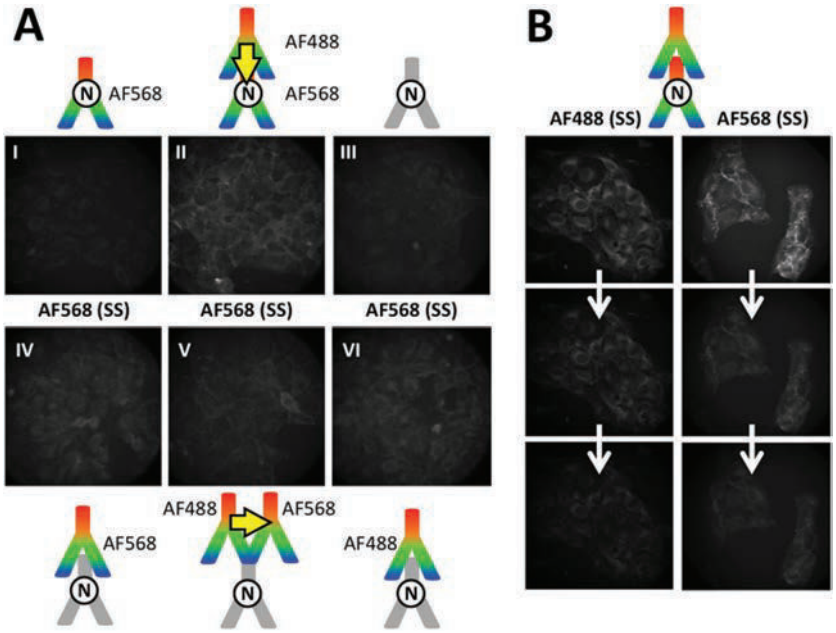

Fig. 7 (A) SS images of different combinations of AF488 donor antibodies with AF568 acceptor antibodies on M4-T cells were recorded in the AF568 PL emission channel upon excitation of AF488 (438 ± 12 nm, no significant direct excitation of AF568). Although the two possible AF488–AF568 FRET combinations (II and V) led to positive PL signals, the dye–dye FRET pair could not provide clear evidence for FRET because direct excitation of AF568 (I and IV), spectral crosstalk of AF488 PL in the AF568 detection channel (VI), and autofluorescence of immunostained cells without any dyes (III) also led to positive PL signals. Control experiments using specific excitation of only AF488 antibodies and AF568 antibodies confirmed that both dye-labelled antibodies were bound to the cell membranes (Fig. S12 in the ESI†). (B) Strong photobleaching (three serial image acquisitions from top to bottom) of both AF488 (excitation *via* 438 ± 12 nm and detection *via* 522 ± 6 nm transmission filters, 100 ms acquisition per image) and AF568 (excitation *via* 542 ± 10 nm and detection *via* 607 ± 5 nm transmission filters, 350 ms acquisition per image) with both dye-labelled antibodies against N-cadherin or with only one type of each dye-labelled antibody (Fig. S11 in the ESI†).

selected the AF488-AF568 donor–acceptor pair with a Förster distance of approximately 6.2 nm.[19]

The fluorescence images of M4-T cells in Fig. 7A show SS AF568 PL signals upon AF488 excitation at 438 ± 12 nm. This wavelength range is not optimal for AF488 excitation but it was selected to avoid any significant direct AF568 excitation (Fig. 4A), which is an important requirement for SS FRET experiments to distinguish between direct and FRET-sensitized acceptor PL. Although the most efficient FRET scenario of direct primary–secondary antibody binding (*cf*. Fig. 5D) provided the brightest PL signal (Fig. 7A II), unconjugated primaries (Fig. 7A III), AF568 primaries (Fig. 7A I), AF568 secondaries (Fig. 7A IV), AF488 secondaries (Fig. 7A VI), and both FRET secondaries (Fig. 7A V, with lower PL intensity than the non-FRET images IV and VI) also provided more or less strong PL signals in the AF568 detection channel upon AF488 excitation. Such unwanted PL background signals impede the analysis of FRET because they cannot be distinguished from the FRET signals. In addition to background PL, photobleaching is very problematic for both measurements over long time periods and the quantitative analysis of FRET. Fig. 7B shows a series of images of photobleaching of the AF488- and AF568-labelled antibodies against N-cadherin in M4-T cells. Both AF488 (upon AF488 excitation) and AF568 (upon AF568 excitation) show strongly decreased PL intensities within only three image acquisition cycles. Similar bleaching was found in M4-T cells that were stained with only one of the antibodies (AF488 or AF568, Fig. S11 in the ESI†). The necessity to image donor and acceptor PL on the same cells in a serial manner (unless image splitters for the simultaneous detection of two colours are used) further complicates a precise evaluation of dye-to-dye FRET because the acceptor PL images contain a convolution of donor photobleaching and FRET sensitization by the photobleached donor (Fig. S12 in the ESI†). It should be noted that the use of a different cell line (M4-T) and the detection of only N-cadherins does not allow a direct comparison with the TG Tb-to-dye FRET images taken on A549 and MCF-7 cells using E- and N-cadherin immunostaining. Nevertheless, the similar experimental conditions demonstrate the problematic PL background and photobleaching issues in dye-to-dye FRET imaging and underline the efficiency of TG Tb-to-dye FRET imaging with high signal-to-background ratios, stable PL intensities, and high photostability over longer measurement times compared to standard SS imaging with organic dyes.

Conclusions

In this study we have shown that TG Tb-to-dye FRET microscopy can be an efficient imaging tool for the analysis of protein–protein interactions. In particular, the strong reduction of short-lived PL background from sample autofluorescence and direct acceptor excitation and of donor spectral crosstalk in combination with low excitation repetition rates and reduced photobleaching provide significant advantages of Tb-to-dye FRET analysis compared to conventional dye-to-dye systems. Concerning A549 cells used as a model of membrane E- and N-cadherin co-expression for a possible distinction of CTCs, we could not detect FRET using immunostaining with Tb and dye antibody conjugates. There are two main interpretations of these results: (i) although E-and N-cadherins colocalize at distances that cannot be accessed with diffraction-limited optical resolution (Fig. 2), they are in fact separated by distances larger than our FRET range (max. 12 nm), (ii) the dense packing achieved in adherens junctions does not allow antibody binding to adjacent molecules. This second possibility is supported by the absence of FRET between two E-cadherin molecules in MCF-7 cells although in culture these cells have extensive cell–cell contacts through adherens junctions. In spite of the numerous studies on cadherins there is only one conclusive report of FRET between two cadherins,[59] which is based on the expression of engineered N-cadherins that contain fluorescent proteins inserted in the second extracellular domain next to the dimerization domain. Notably, this approach was designed to circumvent the issue of accessibility by using genetically modified cells expressing the fluorescent reporters. Moreover, when the fluorescent protein was inserted in a domain proximal to the membrane the FRET efficiency was greatly reduced, which illustrated that the packed cadherins are in an extended conformation in agreement with the large distance between the two membranes of the apposed cells at adherens junction (15 to 30 nm).[4] Although our TG-FRET study could unfortunately not provide conclusive results concerning the clustering of E- and/or N-cadherins on the membranes of different cell lines, efficient FRET between Tb and dye antibodies bound to the same target (E-cadherin or primary antibody) demonstrated the advantages of TG Tb-to-dye FRET in comparison to dye-to-dye FRET using the well-known AF488–AF568 FRET-pair for cellular imaging. We believe that these results will be even more relevant for FRET imaging in tissues, which suffer from significantly higher autofluorescence background, and that TG Tb-to-dye FRET can serve to efficiently image protein–protein interactions *via* immunolabelling with antibodies that are able to target complementary epitopes at distances below *ca.* 12 nm.

Experimental

Cell culture and immunofluorescence labelling for confocal microscopy

Cells were cultured on glass coverslips at the bottom of 12-well plates for 48 h in Dulbecco's Modified Eagle Medium (DMEM-Glutamax, Life Technologies) with 10% FBS and antibiotics (Penicillin–Streptomycin, Life Technologies) at 37 °C and 5% CO_2. Then cells were fixed with 3% formaldehyde. Formaldehyde was removed and the wells were rinsed with 1 M glycine, followed by two washes with blocking solution (10 mM HEPES with 2% fetal bovine serum, FBS) and a final incubation with the blocking solution for 30 min at 37 °C. After removal of the blocking solution, 60 μL of either 1/100 (anti-E-cadherin) or 1/200 (anti-N-cadherin) dilution of the

primary antibodies (see references below) in HEPES were added. The coverslips were then rinsed three times with HEPES and exposed for 1 h at 37 °C to 60 μL of the fluorophore-labelled secondary antibodies at 1/100 dilution in HEPES. Slides were mounted with Fluoromount-G (ref. 0100-01, Southern Biotech, Alabama, USA).

Cell culture and immunofluorescence labelling for time-gated imaging

Cells were grown on coverslips for 48 h in DMEM (Sigma-Aldrich) supplemented with 10% FBS, 2 mM L-glutamine (Life Technologies) and antibiotics (1× Anti Antibiotic-Antimycotic, Gibco) at 37 °C with 5% CO_2. The cells were fixed in 4% formaldehyde in PBS and rinsed with a 1 M glycine solution. The cells were blocked for 30 min with 2% FBS in PBS. The samples were then incubated with antibody solutions at 37 °C (primaries 3 h, secondaries 2 h) for the appropriate experiment (see antibodies below), rinsed with PBS, and mounted on microscopy slides using Fluoro-Gel (Electron Microscopy Sciences). *Primary antibodies*: Anti-E cadherin goat polyclonal (ref. AF648, R&D Systems, Minneapolis, USA), anti-N Cadherin [8C11] antibody (ref. ab19348, Abcam, Cambridge, UK), pan Cadherin Antibody (3F4) (ref. H00000999-M01, Novus Biologicals). *Secondary antibodies*: donkey anti-goat IgG-FITC (ref. sc-2024, Santa Cruz Biotechnology Inc., Dallas, USA), Alexa Fluor® 594 Donkey Anti-Mouse IgG(H + L) (ref. A-21203, Life Technology, USA), Alexa Fluor 488 Donkey Anti-Mouse IgG (H + L) (ref. A-21202 Life Technology, USA), Donkey Anti-Mouse IgG H&L (FITC) preadsorbed (ref. ab7057 Abcam).

Antibody conjugation

Primary and secondary antibodies, (AF648 from R&D Systems, H00000999-M01 from Novus Biologicals, ab19348, ab7120 and ab7056 from Abcam) were labelled with amine-reactive dyes (Alexa Fluor 568 NHS ester and Alexa Fluor 647 NHS ester from Life Technologies and NHS-Fluorescein from Thermo Fisher Scientific) or TbL4 (Lumi4®-Tb-NHS, Lumiphore), both in concentration excess to the antibody solutions, in 100 mM carbonate buffer at pH 9.0. The mixtures were incubated while rotating at 25 rpm (Intelli-Mixer, ELMI) for 5 h at room temperature. The samples were purified using 30 kDa filter centrifugal devices (Amicon Ultra 0.5 mL filters) and stored in 100 mM Tris-HCl buffer, pH 7.2.

Confocal laser-scanning immunofluorescence microscopy

Cells were imaged using a TCS SP2 inverted microscope (Leica Mikrosysteme, Wetzlar, Germany) using a 63×/1.32 NA immersion oil objective. LCS MicroLab (Leica) and ImageJ (National Institute of Health, USA) softwares were used for acquisition and image processing respectively. FITC dye was excited with the wavelength 488 nm line of an argon laser; FITC selected detection range was 520–540 nm. AF594 dye was excited with the wavelength 543 nm line of a helium–neon laser, and the selected detection range was 610–650 nm. The exposure time was 5 μs per pixel for all scans.

Steady-state (SS) and time-gated (TG) widefield immunofluorescence microscopy

Cells were imaged using an inverted microscope (Olympus IX71). For steady-state fluorescence images the samples were excited using a mercury lamp (X-Cite 120Q, Lumen Dynamics) and images acquired with a scientific CMOS camera (PCO). For time-gated images the samples were excited from on top by a pulsed laser at 100 Hz (Spectra-Physics), triggering an ICCD camera (PI-MAX3, Princeton Instruments). The settings for acquisition were kept at 10 μs delay, 2.5 ms gatewidth, 400–800 gates per exposure and gain 100. Image processing was done using ImageJ (National Institute of Health, USA, http://imagej.nih.gov/ij/).

Acknowledgements

We thank Lumiphore, Inc. for the gift of Lumi4®-Tb-NHS reagent and Christian Auclair and Gérald Peyroche for fruitful discussions. This work was supported by the French « Investment for the Future » program managed by Agence Nationale de la Recherche, grant ANR-10-Nano-05.

References

1 T. A. Yap, D. Lorente, A. Omlin, D. Olmos and J. S. de Bono, *Clin. Cancer Res.*, 2014, **20**, 2553.
2 J. P. Thiery, H. Acloque, R. Y. J. Huang and M. A. Nieto, *Cell*, 2009, **139**, 871.
3 W. Meng and M. Takeichi, *Cold Spring Harbor Perspect. Biol.*, 2009, 1.
4 J. Brasch, O. J. Harrison, B. Honig and L. Shapiro, *Trends Cell Biol.*, 2012, **22**, 299.
5 P. Katsamba, K. Carroll, G. Ahlsen, F. Bahna, J. Vendome, S. Posy, M. Rajebhosale, S. Price, T. M. Jessell, A. Ben-Shaul, L. Shapiro and B. H. Honig, *Proc. Natl. Acad. Sci. U. S. A.*, 2009, **106**, 11594.
6 M. Cristofanilli, G. T. Budd, M. J. Ellis, A. Stopeck, J. Matera, M. C. Miller, J. M. Reuben, G. V. Doyle, W. J. Allard, L. W. M. M. Terstappen and D. F. Hayes, *New Engl. J. Med.*, 2004, **351**, 781.
7 F. Farace, C. Massard, N. Vimond, F. Drusch, N. Jacques, F. Billiot, A. Laplanche, A. Chauchereau, L. Lacroix, D. Planchard, S. Le Moulec, F. Andre, K. Fizazi, J. C. Soria and P. Vielh, *Br. J. Cancer*, 2011, **105**, 847.
8 M. Yu, A. Bardia, B. S. Wittner, S. L. Stott, M. E. Smas, D. T. Ting, S. J. Isakoff, J. C. Ciciliano, M. N. Wells, A. M. Shah, K. F. Concannon, M. C. Donaldson, L. V. Sequist, E. Brachtel, D. Sgroi, J. Baselga, S. Ramaswamy, M. Toner, D. A. Haber and S. Maheswaran, *Science*, 2013, **339**, 580.
9 W. L. Tam and R. A. Weinberg, *Nat. Med.*, 2013, **19**, 1438.
10 A. Lecharpentier, P. Vielh, P. Perez-Moreno, D. Planchard, J. C. Soria and F. Farace, *Br. J. Cancer*, 2011, **105**, 1338.

11 T. Celia-Terrassa, O. Meca-Cortes, F. Mateo, A. Martinez de Paz, N. Rubio, A. Arnal-Estape, B. J. Ell, R. Bermudo, A. Diaz, M. Guerra-Rebollo, J. J. Lozano, C. Estaras, C. Ulloa, D. Alvarez-Simon, J. Mila, R. Vilella, R. Paciucci, M. Martinez-Balbas, A. Garcia de Herreros, R. R. Gomis, Y. Kang, J. Blanco, P. L. Fernandez and T. M. Thomson, *J. Clin. Invest.*, 2012, **122**, 1849.
12 J. R. Lakowicz, *Principles of Fluorescence Spectroscopy*, 3rd edn, Springer, New York, 2006.
13 I. L. Medintz and N. Hildebrandt, *FRET-Förster Resonance Energy Transfer. From Theory to Applications*, Wiley-VCH, Weinheim, 2013.
14 B. Valeur and M. N. Berberan-Santos, *Molecular Fluorescence: Principles and Applications*, Wiley-VCH, Weinheim, 2nd edn, 2012.
15 N. J. Turro, V. Ramamurthy and J. C. Scaiano, *Modern molecular photochemistry of organic molecules*, University Science Books, 2010.
16 K. E. Sapsford, L. Berti and I. L. Medintz, *Angew. Chem., Int. Ed.*, 2006, **45**, 4562.
17 B. Hötzer, I. L. Medintz and N. Hildebrandt, *Small*, 2012, **8**, 2297.
18 K. E. Sapsford, B. Wildt, A. Mariani, A. B. Yeatts and I. L. Medintz, in *FRET-Förster Resonance Energy Transfer. From Theory to Applications*, ed. I. L. Medintz and N. Hildebrandt, Wiley-VCH, Weinheim, 2013.
19 A. G. Byrne, M. M. Byrne, G. Coker, K. Boeneman-Gemmill, C. Spillman, I. L. Medintz, S. L. Sloan and B. W. van der Meer, in *FRET-Förster Resonance Energy Transfer. From Theory to Applications*, ed. I. L. Medintz and N. Hildebrandt, Wiley-VCH, Weinheim, 2013.
20 G. T. Hermanson, *Bioconjugate Techniques*, Academic Press, London, 3rd edn, 2013.
21 R. P. Haugland, *The Molecular Probes® Handbook - A Guide to Fluorescent Probes and Labeling Technologies*, Life Technologies Corporation, USA, 11th edn, 2010.
22 A. Periasamy and R. N. Day, *Molecular imaging: FRET microscopy and spectroscopy*, Oxford University Press, Inc., New York, 2005.
23 N. Hildebrandt, in *FRET-Förster Resonance Energy Transfer. From Theory to Applications*, ed. I. L. Medintz and N. Hildebrandt, Wiley-VCH, Weinheim, 2013.
24 L. Y. Lee, S. L. Ong, J. Y. Hu, W. J. Ng, Y. Feng, X. Tan and S. W. Wong, *Appl. Environ. Microbiol.*, 2004, **70**, 5732.
25 J. Mahmoudian, R. Hadavi, M. Jeddi-Tehrani, A. R. Mahmoudi, A. A. Bayat, E. Shaban, M. Vafakhah, M. Darzi, M. Tarahomi and R. Ghods, *Cell J.*, 2011, **13**, 169.
26 J. E. Berlier, A. Rothe, G. Buller, J. Bradford, D. R. Gray, B. J. Filanoski, W. G. Telford, S. Yue, J. Liu, C.-Y. Cheung, W. Chang, J. D. Hirsch, J. M. Beechem, R. P. Haugland and R. P. Haugland, *J. Histochem. Cytochem.*, 2003, **51**, 1699.
27 U. Resch-Genger, M. Grabolle, S. Cavaliere-Jaricot, R. Nitschke and T. Nann, *Nat. Methods*, 2008, **5**, 763.
28 W. R. Algar, H. Kim and U. J. Krull, in *FRET-Förster Resonance Energy Transfer. From Theory to Applications*, ed. I. L. Medintz and N. Hildebrandt, Wiley-VCH, Weinheim, 2013.
29 W. R. Algar, H. Kim, I. L. Medintz and N. Hildebrandt, *Coord. Chem. Rev.*, 2014, **263–264**, 65.
30 A. Yahia-Ammar, A. M. Nonat, A. Boos, J.-L. Rehspringer, Z. Asfari and L. J. Charbonnière, *Dalton Trans.*, 2014, **43**, 15583.
31 K. D. Wegner, F. Morgner, E. Oh, R. Goswami, K. Susumu, M. H. Stewart, I. L. Medintz and N. Hildebrandt, *Chem. Mater.*, 2014, **26**, 4299.
32 K. D. Wegner, P. T. Lanh, T. Jennings, E. Oh, V. Jain, S. M. Fairclough, J. M. Smith, E. Giovanelli, N. Lequeux, T. Pons and N. Hildebrandt, *ACS Appl. Mater. Interfaces*, 2013, **5**, 2881.
33 K. D. Wegner, Z. Jin, S. Lindén, T. L. Jennings and N. Hildebrandt, *ACS Nano*, 2013, **7**, 7411.
34 N. Billinton and A. W. Knight, *Anal. Biochem.*, 2001, **291**, 175.
35 M. S. Viegas, T. C. Martins, F. Seco and A. do Carmo, *Eur. J. Histochem.*, 2007, **51**, 59.
36 H. J. Tanke, *J. Microsc.*, 1989, **155**, 405.
37 G. Marriott, R. M. Clegg, D. J. Arndt-Jovin and T. M. Jovin, *Biophys. J.*, 1991, **60**, 1374.
38 L. J. Charbonnière, N. Hildebrandt, R. F. Ziessel and H.-G. Löhmannsröben, *J. Am. Chem. Soc.*, 2006, **128**, 12800.
39 K. Hanaoka, K. Kikuchi, S. Kobayashi and T. Nagano, *J. Am. Chem. Soc.*, 2007, **129**, 13502.
40 M. Rajendran, E. Yapici and L. W. Miller, *Inorg. Chem.*, 2014, **53**, 1839.
41 H. E. Rajapakse, N. Gahlaut, S. Mohandessi, D. Yu, J. R. Turner and L. W. Miller, *Proc. Natl. Acad. Sci. U. S. A.*, 2010, **107**, 13582.
42 R. Pal and A. Beeby, *Methods Appl. Fluoresc. Spectrosc.*, 2014, **2**, 037001.
43 Y. Lu, D. Jin, R. C. Leif, W. Deng, J. A. Piper, J. Yuan, Y. Duan and Y. Huo, *Cytometry, Part A*, 2011, **79A**, 349.
44 Y. Lu, P. Xi, J. A. Piper, Y. Huo and D. Jin, *Sci. Rep.*, 2012, **2**, 837.
45 Y. Lu, J. Zhao, R. Zhang, Y. Liu, D. Liu, E. M. Goldys, X. Yang, P. Xi, A. Sunna, J. Lu, Y. Shi, R. C. Leif, Y. Huo, J. Shen, J. A. Piper, J. P. Robinson and D. Jin, *Nat. Photonics*, 2014, **8**, 32.
46 A. Grichine, A. Haefele, S. Pascal, A. Duperray, R. Michel, C. Andraudd and O. Maury, *Chem. Sci.*, 2014, **5**, 3475.
47 K. R. Kupcho, D. K. Stafslien, T. DeRosier, T. M. Hallis, M. S. Ozers and K. W. Vogel, *J. Am. Chem. Soc.*, 2007, **129**, 13372.
48 T. Kokko, T. Liljenbäck, M. T. Peltola, L. Kokko and T. Soukka, *Anal. Chem.*, 2008, **80**, 9763.
49 T. Kokko, L. Kokko and T. Soukka, *J. Fluoresc.*, 2009, **19**, 159.
50 S. H. Kim, J. R. Gunther and J. A. Katzenellenbogen, *J. Am. Chem. Soc.*, 2010, **132**, 4685.
51 T. Hilal, V. Puetter, C. Otto, K. Parczyk and B. Bader, *J. Biomol. Screening*, 2010, **15**, 268.

52 H. E. Rajapakse and L. W. Miller, *Methods Enzymol.*, 2012, **505**, 329.
53 D. Geißler, S. Stufler, H.-G. Löhmannsröben and N. Hildebrandt, *J. Am. Chem. Soc.*, 2013, **135**, 1102.
54 D. Geißler, S. Lindén, K. Liermann, K. D. Wegner, L. J. Charbonnière and N. Hildebrandt, *Inorg. Chem.*, 2014, **53**, 1824.
55 O. J. Harrison, X. Jin, S. Hong, F. Bahna, G. Ahlsen, J. Brasch, Y. Wu, J. Vendome, K. Felsovalyi, C. M. Hampton, R. B. Troyanovsky, A. Ben-Shaul, J. Frank, S. M. Troyanovsky, L. Shapiro and B. Honig, *Structure*, 2011, **19**, 244.
56 B.-A. Truong Quang, M. Mani, O. Markova, T. Lecuit and P.-F. Lenne, *Curr. Biol.*, 2013, **23**, 2197.
57 J. Xu, T. M. Corneillie, E. G. Moore, G.-L. Law, N. G. Butlin and K. N. Raymond, *J. Am. Chem. Soc.*, 2011, **133**, 19900.
58 N. Hildebrandt, K. D. Wegner and W. R. Algar, *Coord. Chem. Rev.*, 2014, **273–274**, 125.
59 S. A. Kim, C.-Y. Tai, L.-P. Mok, E. A. Mosser and E. M. Schuman, *Proc. Natl. Acad. Sci. U. S. A.*, 2011, **108**, 9857.

Electronic Supplementary Material (ESI) for Dalton Transactions.

Terbium-Based Time-Gated Förster Resonance Energy Transfer Imaging for Evaluating Protein-Protein Interactions on Cell Membranes

Stina Lindén, Manish Kumar Singh, K. David Wegner, Marie Regairaz, François Dautry, François Treussart, and Niko Hildebrandt

SUPPORTING INFORMATION

Cell membrane E- and N-cadherin expression for MCF-7 and A549 cell lines, measured by flow cytometry

Flow cytometry immunolabelling protocol. Culture flasks were washed once with PBS. Versene solution (ref. 15040-066, Life Technologies) was then used to dissociate cells at 4°C. Aliquots of 5-6 x 10^5 dissociated cells were prepared and washed twice with PBS + 2% FBS (washing buffer). Cells were then incubated with the washing buffer for 30 minutes at 4°C as a protein blocking step. After removing the washing buffer, the fluorophore-labelled primary antibodies APC anti-human CD324 E-Cadherin (ref. 324108, BioLegend, San Diego, USA) and PE anti-human CD325 N-Cadherin (ref. 350805, BioLegend) were added. For the control, we used the corresponding fluorophore conjugated isotype APC Mouse IgG1, κ Isotype Ctrl (ref. 400122, BioLegend) and antibody PE Mouse IgG1, κ Isotype Ctrl (ref. 400114, BioLegend) diluted in the washing buffer. Aliquots were then kept at 4°C for one hour. The samples were washed 3 times with the washing buffer before the flow cytometry measurements. The flow cytometer used is a guava easyCyte model (EMD Millipore, Massachusetts).

Results

MCF-7 cells (human breast cancer cell line) were used as a reference for strong expression of E-cadherin at the membrane. Figure S1 shows flow cytometry detection of E-cadherin in MCF-7 cells. The experiment was performed on living cells, and staining and blocking were performed at 4°C to keep metabolic activity low (see protocol above). Flow cytometry also confirmed the co-expression of E- and N-cadherins at the cell membrane in A549 cells. Moreover, two populations of A549 cells were observed: cells located in the first quadrant of Figure S2(a) are positive for both E- and N-cadherins (E^+/N^+), whereas cells in the second quadrant are positive for E-cadherin but negative for N-cadherin (E^+/N^-).

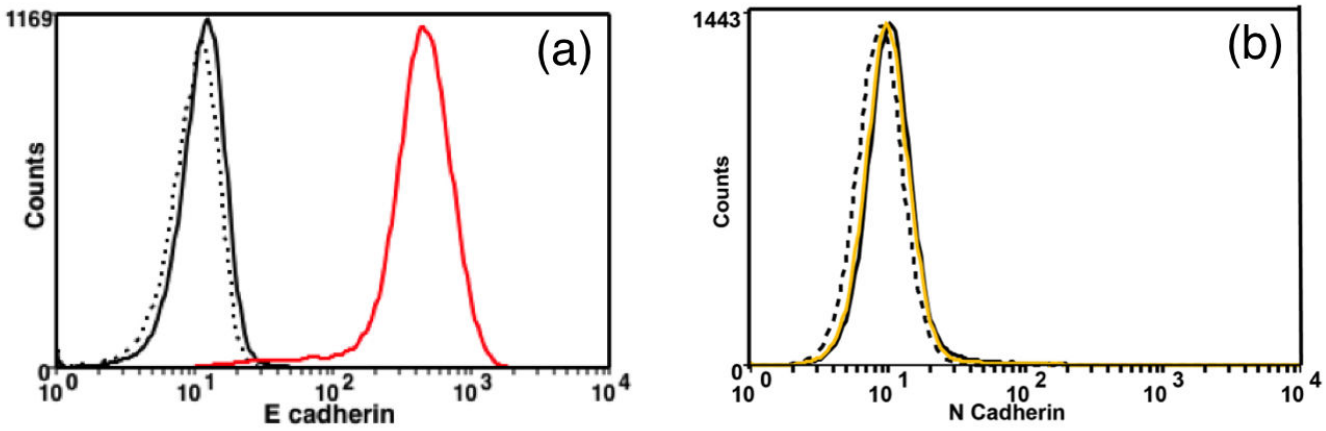

Figure S1: Flow cytometry measurement of (a) E-cadherin and (b) N-cadherin proteins membrane expression for MCF-7 cells. For E-cadherin labeling, MCF-7 cells were targeted with APC anti-human CD324 (E-Cadherin) Antibody (red line). Control sample was treated with APC Mouse IgG1, κ Isotype Ctrl (black regular line). For N-cadherin labeling, MCF-7 were treated with PE anti-human CD325 (N-Cadherin) antibody (yellow line). Control sample was treated with PE Mouse IgG1, κ Isotype Ctrl (black regular line). Autofluorescence samples for E- and N-cadherin experiments were exposed to the washing buffer (dashed lines). These results show that MCF-7 cells express E cadherin but not N-cadherin.

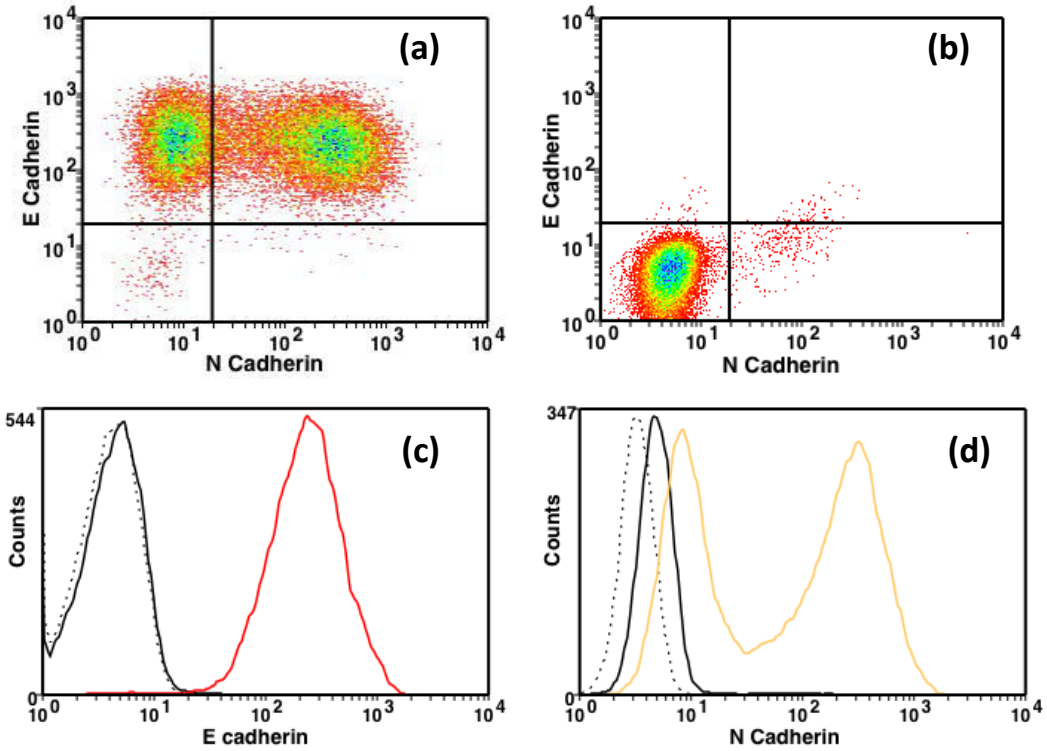

Figure S2: Flow cytometry measurement of E-cadherin and N cadherin expressions in A549 cells. (a) Dot plot showing A549 cells labelled simultaneously with APC anti-human CD324 (E-Cadherin) antibody and PE anti-human CD325 (N-Cadherin) antibody. (b) Control samples treated with APC Mouse IgG1, κ Isotype Ctrl and Antibody PE Mouse IgG1, κ Isotype Ctrl. Comparing the results (a) and (b), it can be concluded that the labelling of both proteins is highly specific. The observation of two cell populations indicates the presence of different phenotypes in the cell line. The major population, which represents approximately 55% of the total cells, expresses both proteins. (c) Histogram of E-cadherin expression, APC anti-human CD324 (E-Cadherin) Antibody (red line), control sample was treated with APC Mouse IgG1, κ Isotype Ctrl (black regular line) and autofluorescence sample was exposed to the washing buffer (dashed line) and (d) Histogram of N-cadherin expression, PE anti-human CD325 (N-Cadherin) Antibody (yellow line). Control sample was treated with PE Mouse IgG1, κ Isotype Ctrl (black regular line). Autofluorescence sample was exposed to the washing buffer (dashed line).

PL decay (and average decay times) of Tb-labelled antibodies

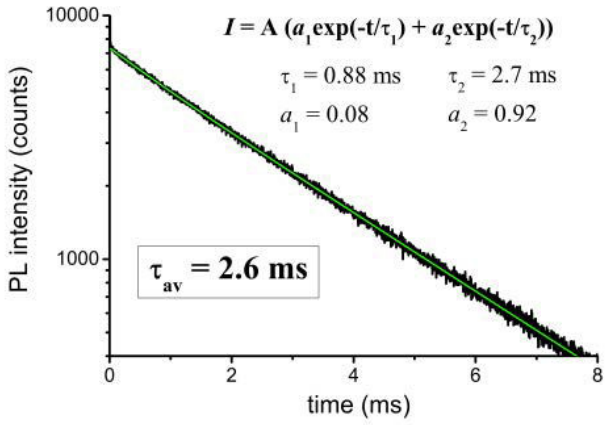

Figure S3: PL decay curve and determination of PL decay time of Tb-labelled antibodies

Additional TG imaging and control experiments

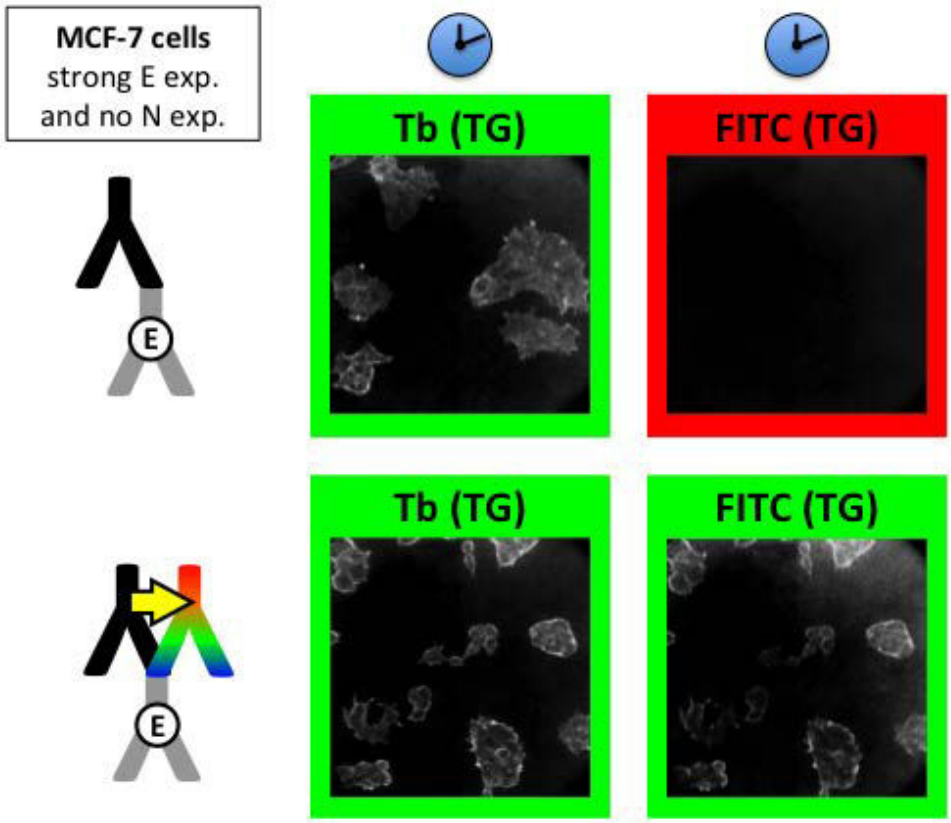

Figure S4: Time-gated FRET microscopy images of control experiments for E-cadherin expression on MCF-7 cells, using FITC-labelled acceptor secondary antibodies.

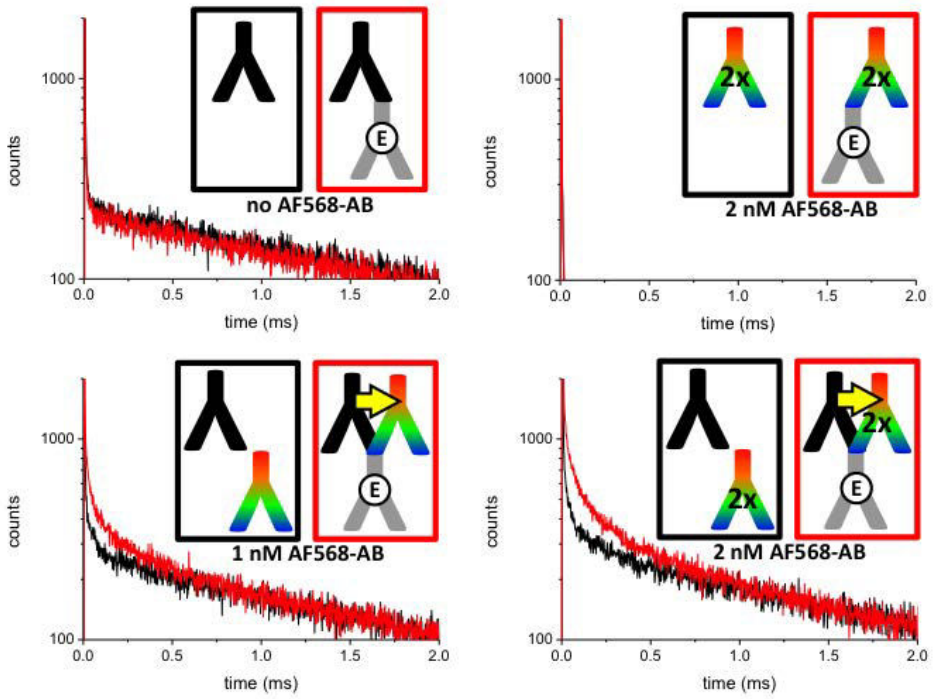

Figure S5: PL decay curves of solution-phase assays demonstrating Tb-antibody and AF568 dye-antibody binding to the same primary antibody.

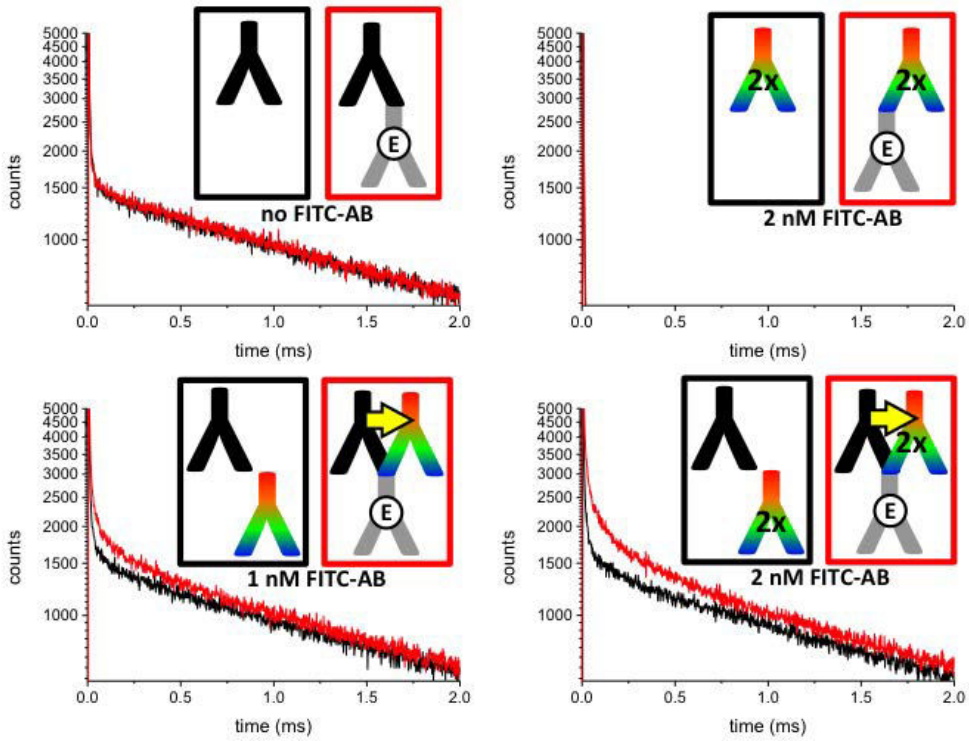

Figure S6: PL decay curves of solution-phase assays demonstrating Tb-antibody and FITC dye-antibody binding to the same primary antibody.

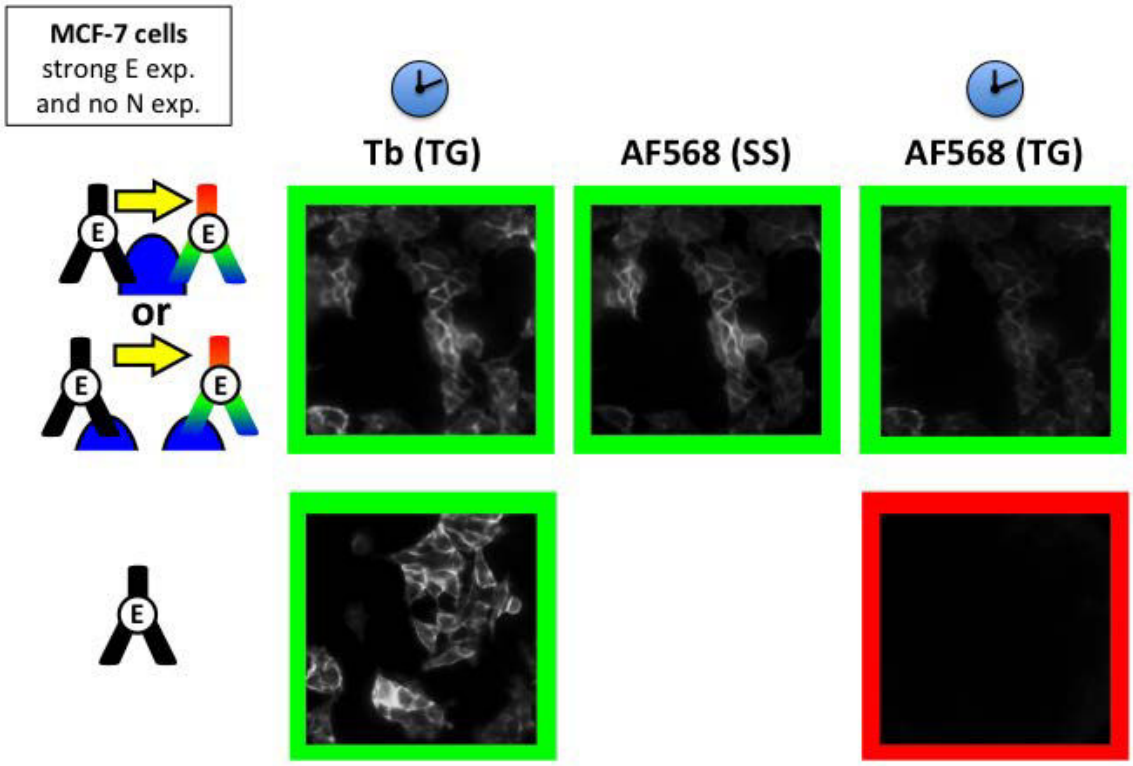

Figure S7: Control experiments showing that there is no crosstalk of Tb PL in the FRET channel (AF568) in the case of the E-cadherin cluster investigations using FRET and MCF-7 cells.

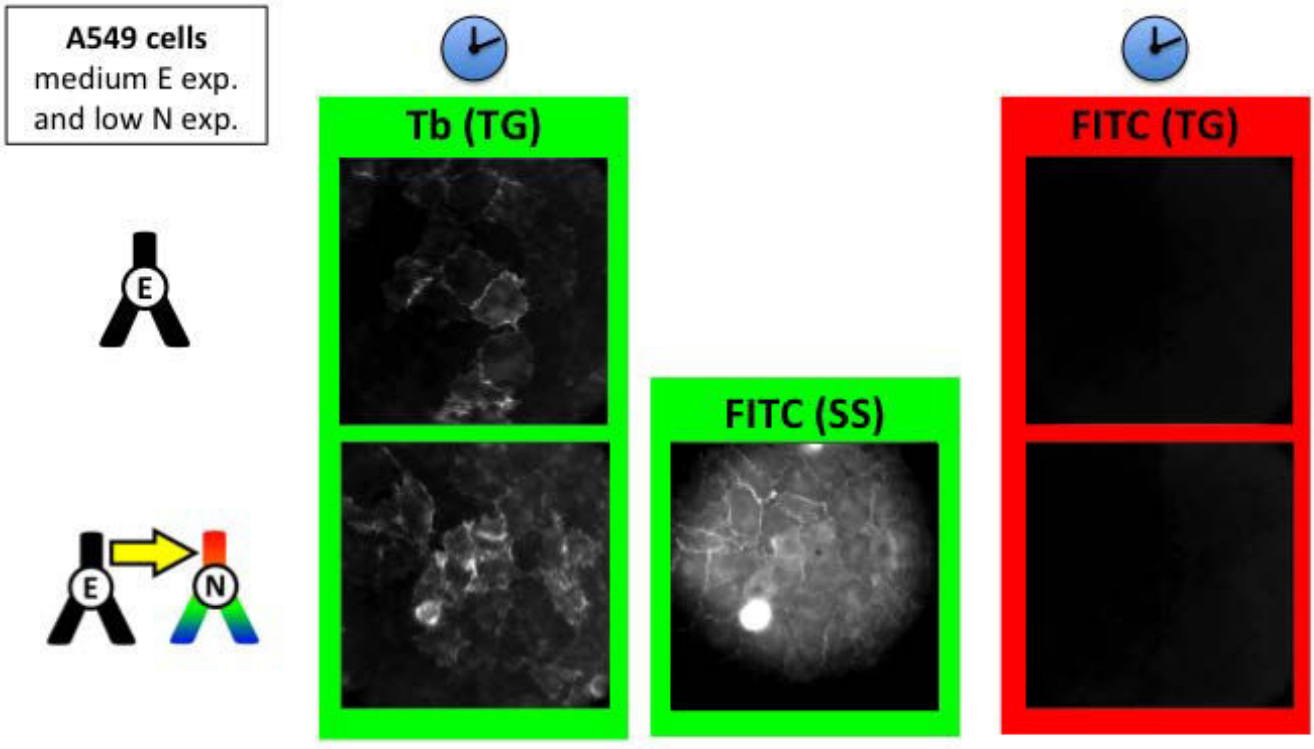

Figure S8: Time-gated and steady-state microscopy images of control experiments for E/N cadherin co-expression on A549 cells, using FITC-labelled N-cadherin primary antibodies.

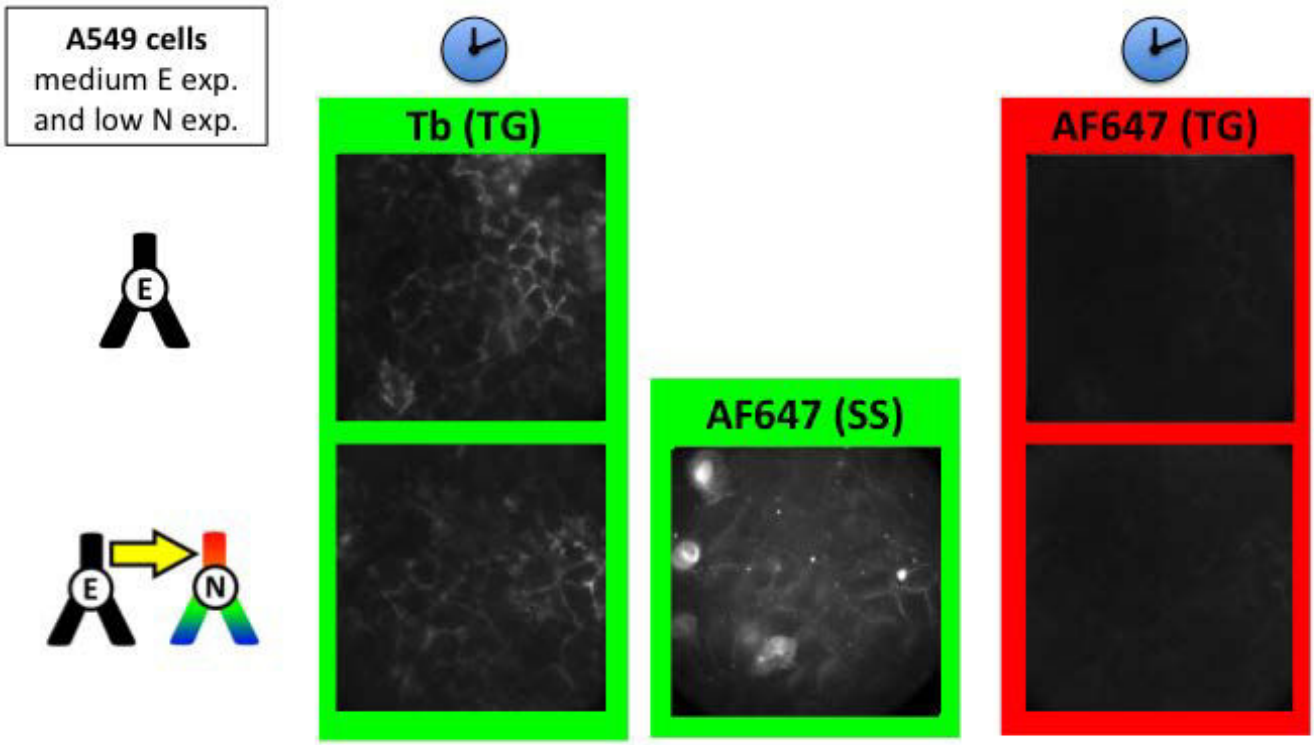

Figure S9: Time-gated and steady-state microscopy images of control experiments for E/N cadherin co-expression on A549 cells, using AF647-labelled N-cadherin primary antibodies.

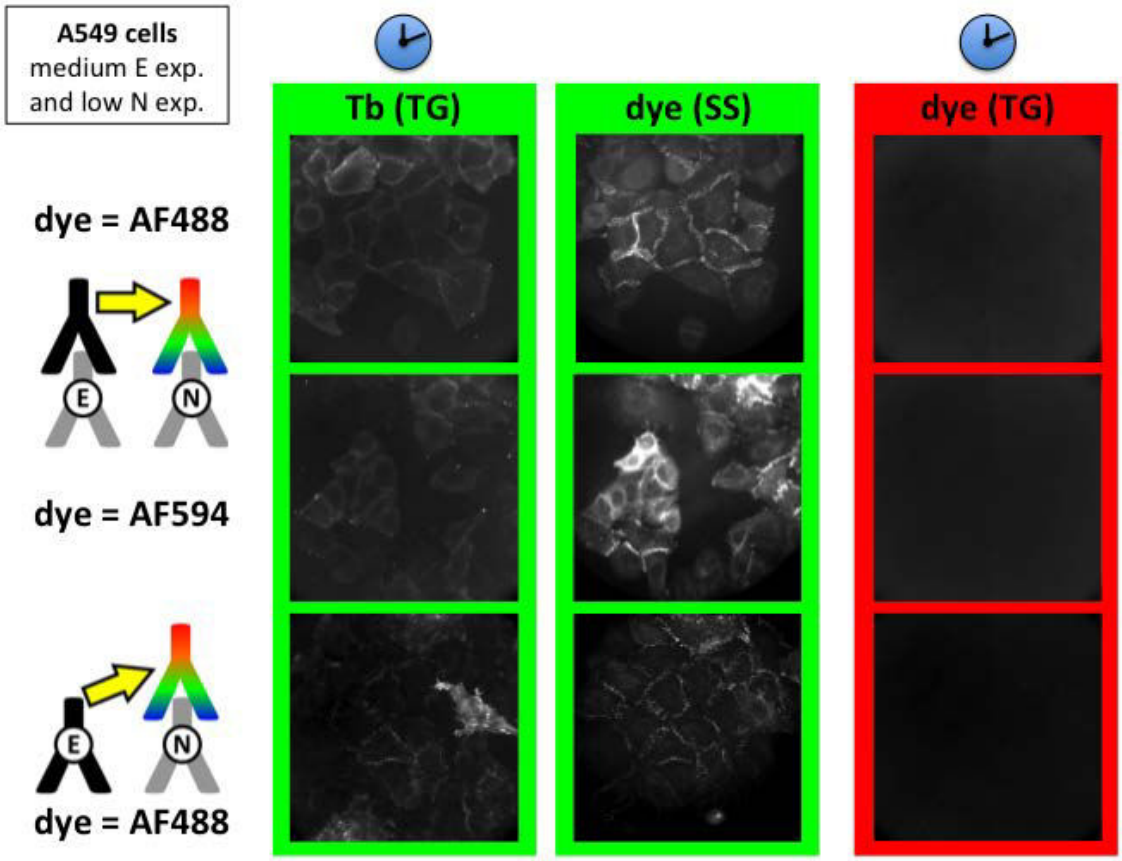

Figure S10: Time-gated and steady-state microscopy images of control experiments for E/N cadherin co-expression on A549 cells, using Tb- and AF488-labelled (or AF594-labelled) secondary antibodies against E- and N-cadherin primaries, respectively (two top lines). Bottom line: similar experiments but with Tb-labelled primary antibodies against E-cadherin and AF488-labelled secondaries against N-cadherin primaries. AF594 was measured with the AF568 transmission filter (607±4 nm) to suppress spectral crosstalk from Tb.

Additional images concerning photobleaching (Figure S11) and the order of image acquisition and successful co-labelling of N-cadherin with AF488 and AF568-labelled antibodies (Figure S12). In these Figures the identification of central transmission or reflection wavelengths of the filters and dichroic mirrors used is given by X/Y/Z, where X is the central transmission wavelength of the excitation filter, Y is the central wavelength between reflection and transmission of the dichroic mirror, and Z is the central transmission wavelength of the emission filter.

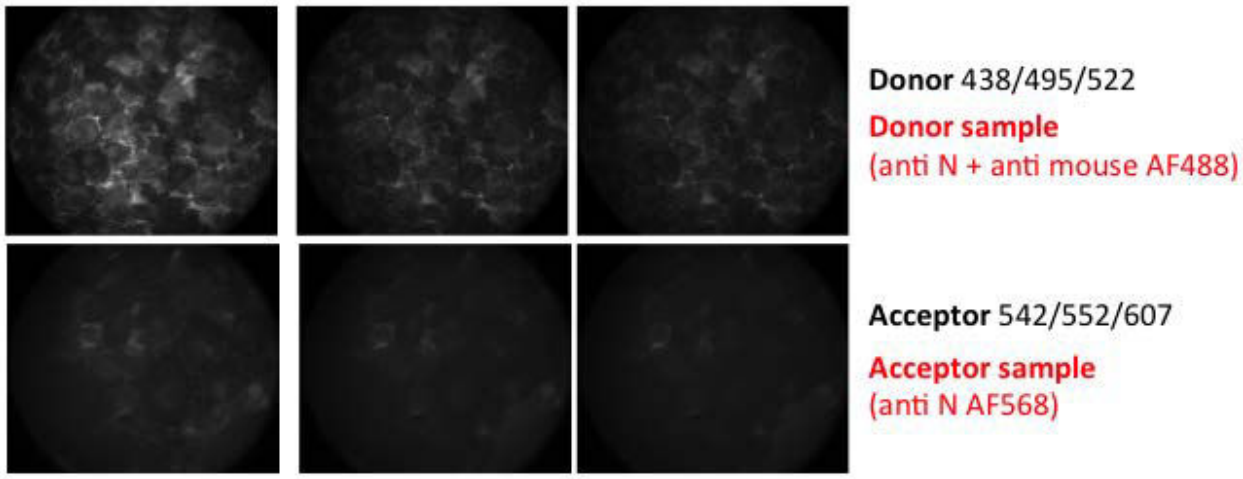

Figure S11: Photobleaching of acceptor and donor dyes using N-cadherin targeting in M4-T cells.

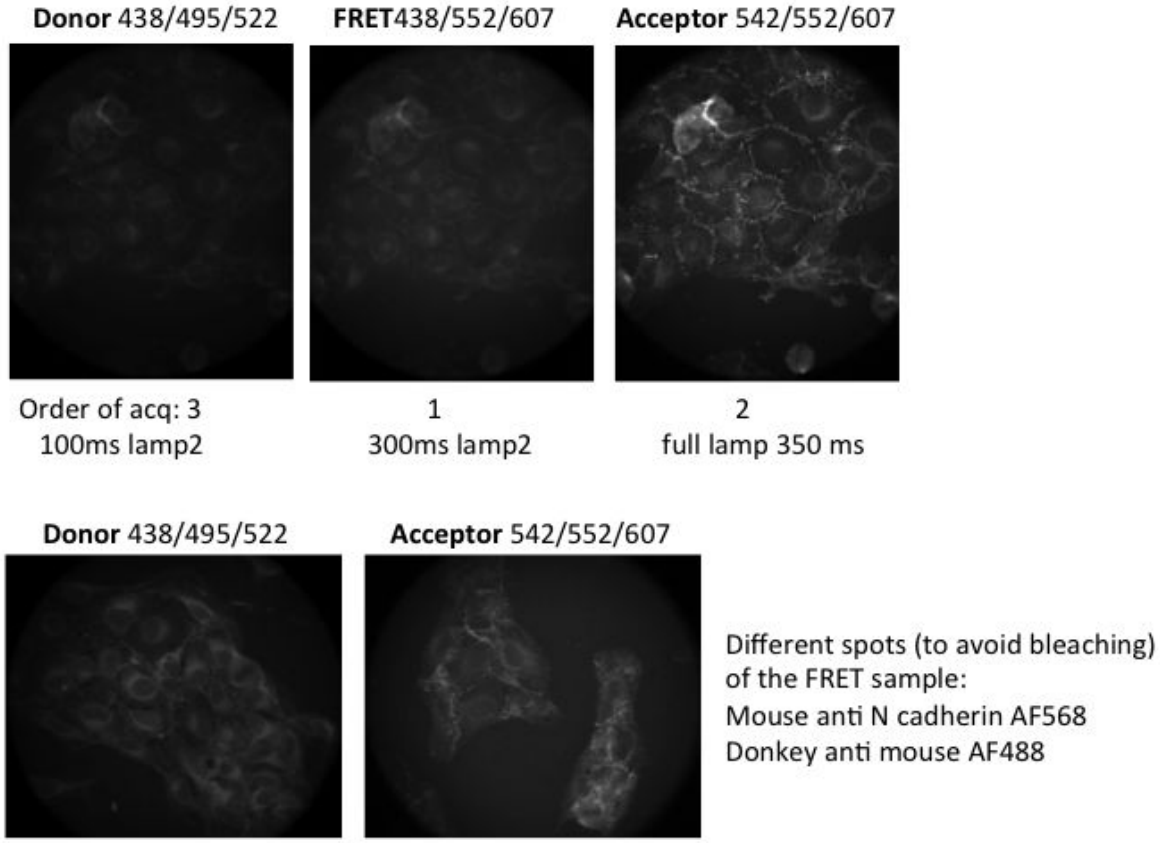

Figure S12: Top: The order of acquisition of the same imaging spot may change FRET interpretation because photobleaching is convoluted with donor quenching and acceptor sensitization. Bottom: Two images taken from the same sample at different cells to avoid photobleaching but to show co-staining of N-cadherins on the M4-T cells with AF488-labelled and AF568-labelled antibodies.

B Protocols

B.1 Cell culture and cell splitting

Cells were cultured in Dulbecco's Modified Eagle Medium (DMEM) or RPMI Media 1640 (Life Technologies, NY, USA), supplemented with 10% FBS (Fetal Bovine Serum and 1% Penicilin/Streptomycin). Cells from liquid nitrogen storage were thawed in a 37°C water bath and then washed in the complete media at 37°C and seeded in the culture flask. Cells were cultured at 37°C in incubator which constantly kept at 5% of CO_2 level.

Cells were maintained at confluency around 50-60%. When confluence reached 75%, cell were split and re-seeded. The procedure of cell passing is as follows: the flask is washed with PBS (1×), detached using 0.05% or 0.25% (depending on cell line) trypsin at 37°C for 1 min. Detached cell are washed with culture medium and centrifuged at 1200 rpm at 4°C for 3 min. Cell pellet are suspended in 10 mL of culture medium and seeded in appropriate number according to the size of the flask.

B.2 Immunofluorescence

1. Approximately 100,000 cells are seeded and grown until confluency onto glass coverslips (12 mm diameter) deposited on the bottom of 12-well cell culture plates. Cells are then left in culture for approximately 48 hours.

2. At confluency, medium was removed and coverslips was rinsed once with supplemented (whole) cell medium.

3. Thereafter, coverslips was exposed for 15 min at 37°C to a 3% formaldehyde(FA) solution in whole medium. Afterwards was removed and coverslips was rinsed once with 1 M glycine and twice with PBS modified with 2% FBS.

4. Fixed coverslips are then exposed for 30 min at 37°C to a blocking solution: PBS and 2 vol % FBS.

5. After removal of the blocking solution and without any further rinsing, coverslips are treated with 60 μL of a 1/100 (E-cadherin) or 1/200 (N-cadherin) dilution of the primary antibodies in blocking solution.

6. Coverslips are then rinsed 3× with blocking buffer and exposed for 1 h at 37°C to 60 μL of the fluorescently-labeled secondary antibodies.

7. Finally, coverslips are rinsed once with DAPI in PBS followed by 3× rinsing with PBS. Slides are mounted with Fluoromount-G to be observed in the confocal microscope.

B.3 Flow cytometry

1. Culture flasks are washed once with PBS. Versene solution (ref. 15040-066, life technologies, USA) was then used to dissociate cells at 4°C. Aliquots of 5-6×10^5 dissociated cells are prepared and washed twice with PBS + 2% FBS (washing buffer).

2. Cells are then incubated with the washing buffer for 30 minutes at 4°C as a protein blocking step.

3. After removing the washing buffer, the fluorophore-labeled primary antibodies APC anti-human CD324 E-Cadherin (ref. 324108, BioLegend, San Diego, USA) and PE anti-human CD325 N-Cadherin (ref. 350805, BioLegend) are added. For the control, we used the corresponding fluorophore conjugated isotype APC Mouse IgG1, κ Isotype Ctrl (ref. 400122, BioLegend) and antibody PE Mouse IgG1, κ Isotype Ctrl (ref. 400114, BioLegend) diluted in the washing buffer. Aliquots are then kept at 4°C for 1 hour.

4. The samples are washed 3 times with the washing buffer before measurements. The flow cytometer used is a guava easyCyte model (EMD Millipore, Massachusetts).

B.4 Spectrum of QDots used in this study

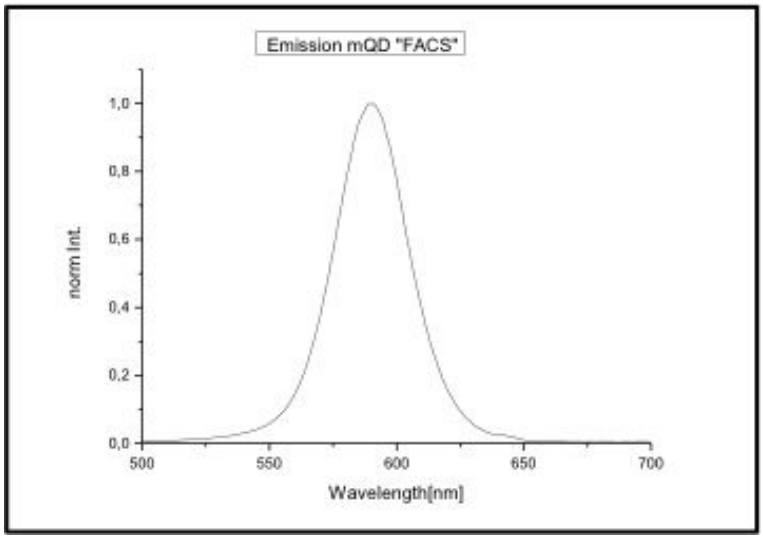

Figure B.1 : ***Emission spectrum of QD580 used to conjugate QDots to antibodies through protein A/G in chapter 5*** *. The peak absorption was at 360 nm and maximum emission observed at 580 nm .*

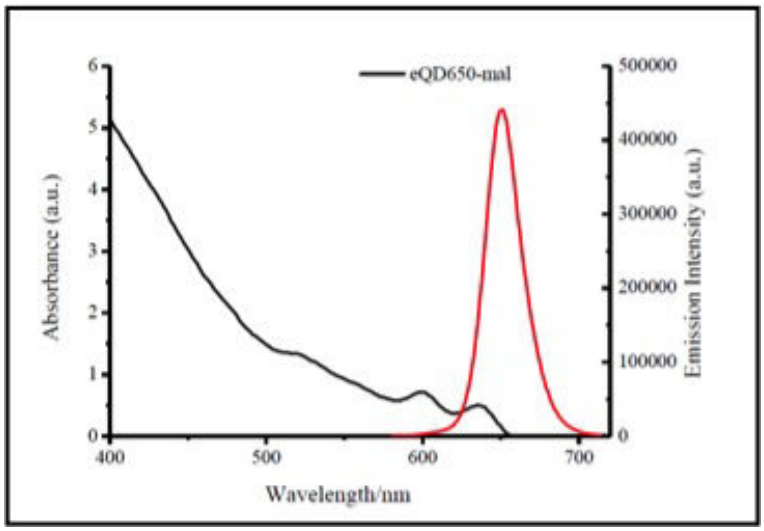

Figure B.2 : ***Spectrum of commercial QD650 used to conjugate QDots to secondary antibody with free sulfhydryl (thiol) group in chapter 5*** *. The maximum absorption was at 350 nm and maximum emission observed at 650 nm.*

Bibliography

[1] B. Vogelstein, N. Papadopoulos, V. E. Velculescu, S. Zhou, L. A. Diaz, et K. W. Kinzler. "Cancer genome landscapes." *science*, **339**, 1546 (2013).

[2] C. Kandoth, *et al.* "Mutational landscape and significance across 12 major cancer types." *Nature*, **502**, 333 (2013).

[3] D. Hanahan et R. A. Weinberg. "Hallmarks of cancer: the next generation." *Cell*, **144**, 646 (2011).

[4] C. J. Gottardi, E. Wong, et B. M. Gumbiner. "E-cadherin suppresses cellular transformation by inhibiting β-catenin signaling in an adhesion-independent manner." *The Journal of cell biology*, **153**, 1049 (2001).

[5] G. Mbalaviele, C. R. Dunstan, A. Sasaki, P. J. Williams, G. R. Mundy, et T. Yoneda. "E-cadherin expression in human breast cancer cells suppresses the development of osteolytic bone metastases in an experimental metastasis model." *Cancer research*, **56**, 4063 (1996).

[6] M. Mareel, T. Boterberg, V. Noe, L. Van Hoorde, S. Vermeulen, E. Bruyneel, et M. Bracke. "E-cadherin/catenin/cytoskeleton complex: A regulator of cancer invasion." *Journal of cellular physiology*, **173**, 271 (1997).

[7] A. S. Wong et B. M. Gumbiner. "Adhesion-independent mechanism for suppression of tumor cell invasion by e-cadherin." *The Journal of cell biology*, **161**, 1191 (2003).

[8] M. Herzig, F. Savarese, M. Novatchkova, H. Semb, et G. Christofori. "Tumor progression induced by the loss of e-cadherin independent of β-catenin/tcf-mediated wnt signaling." *Oncogene*, **26**, 2290 (2006).

[9] G. Berx et F. van Roy. "**Involvement of Members of the Cadherin Superfamily in Cancer**." *Cold Spring Harbor Perspectives in Biology*, **1**, a003129 (2009).

[10] K. Pantel et R. H. Brakenhoff. "Dissecting the metastatic cascade." *Nature Reviews Cancer*, **4**, 448 (2004).

[11] K. Kessenbrock, V. Plaks, et Z. Werb. "Matrix metalloproteinases: regulators of the tumor microenvironment." *Cell*, **141**, 52 (2010).

[12] J. A. Joyce et J. W. Pollard. "Microenvironmental regulation of metastasis." *Nature Reviews Cancer*, **9**, 239 (2008).

[13] J. S. Desgrosellier et D. A. Cheresh. "Integrins in cancer: biological implications and therapeutic opportunities." *Nature Reviews Cancer*, **10**, 9 (2010).

[14] J. P. Thiery. "Epithelial–mesenchymal transitions in tumour progression." *Nature Reviews Cancer*, **2**, 442 (2002).

[15] P. Carmeliet et R. K. Jain. "Molecular mechanisms and clinical applications of angiogenesis." *Nature*, **473**, 298 (2011).

[16] W. Guo et F. G. Giancotti. "Integrin signalling during tumour progression." *Nature reviews Molecular cell biology*, **5**, 816 (2004).

[17] A. F. Chambers, A. C. Groom, et I. C. MacDonald. "Metastasis: dissemination and growth of cancer cells in metastatic sites." *Nature Reviews Cancer*, **2**, 563 (2002).

[18] R. Kalluri, R. A. Weinberg, *et al.* "The basics of epithelial-mesenchymal transition." *The Journal of clinical investigation*, **119**, 1420 (2009).

[19] J. Yang, *et al.* "Twist, a master regulator of morphogenesis, plays an essential role in tumor metastasis." *Cell*, **117**, 927 (2004).

[20] M. T. Nieman, R. S. Prudoff, K. R. Johnson, et M. J. Wheelock. "N-cadherin promotes motility in human breast cancer cells regardless of their e-cadherin expression." *The Journal of cell biology*, **147**, 631 (1999).

[21] R. B. Hazan, G. R. Phillips, R. F. Qiao, L. Norton, et S. A. Aaronson. "Exogenous expression of n-cadherin in breast cancer cells induces cell migration, invasion, and metastasis." *The Journal of cell biology*, **148**, 779 (2000).

[22] B. Seidel, S. Braeg, G. Adler, D. Wedlich, et A. Menke. "E-and n-cadherin differ with respect to their associated p120ctn isoforms and their ability to suppress invasive growth in pancreatic cancer cells." *Oncogene*, **23**, 5532 (2004).

[23] S. Nakajima, *et al.* "N-cadherin expression and epithelial-mesenchymal transition in pancreatic carcinoma." *Clinical Cancer Research*, **10**, 4125 (2004).

[24] N. L. Tran, R. B. Nagle, A. E. Cress, et R. L. Heimark. "N-cadherin expression in human prostate carcinoma cell lines: an epithelial-mesenchymal transformation mediating adhesion with stromal cells." *The American journal of pathology*, **155**, 787 (1999).

[25] T. Z. Tan, Q. H. Miow, Y. Miki, T. Noda, S. Mori, R. Y.-J. Huang, et J. P. Thiery. "Epithelial-mesenchymal transition spectrum quantification and its efficacy in deciphering survival and drug responses of cancer patients." *EMBO molecular medicine*, page e201404208 (2014).

[26] S. Yachida, *et al.* "Distant metastasis occurs late during the genetic evolution of pancreatic cancer." *Nature*, **467**, 1114 (2010).

[27] C. Swanton. "Intratumor heterogeneity: evolution through space and time." *Cancer research*, **72**, 4875 (2012).

[28] X. Wu, *et al.* "Clonal selection drives genetic divergence of metastatic medulloblastoma." *Nature*, **482**, 529 (2012).

[29] T. Reya, S. J. Morrison, M. F. Clarke, et I. L. Weissman. "Stem cells, cancer, and cancer stem cells." *nature*, **414**, 105 (2001).

[30] A. Kreso et J. E. Dick. "Evolution of the cancer stem cell model." *Cell stem cell*, **14**, 275 (2014).

[31] H. Clevers. "The intestinal crypt, a prototype stem cell compartment." *Cell*, **154**, 274 (2013).

[32] F. Yu, *et al.* "Regulates self renewal and tumorigenicity of breast cancer cells." *Cell*, **131**, 1109 (2007).

[33] D. Friedmann-Morvinski et I. M. Verma. "Dedifferentiation and reprogramming: origins of cancer stem cells." *EMBO reports*, **15**, 244 (2014).

[34] C. L. Chaffer, *et al.* "Normal and neoplastic nonstem cells can spontaneously convert to a stem-like state." *Proceedings of the National Academy of Sciences*, **108**, 7950 (2011).

[35] P. B. Gupta, C. M. Fillmore, G. Jiang, S. D. Shapira, K. Tao, C. Kuperwasser, et E. S. Lander. "Stochastic state transitions give rise to phenotypic equilibrium in populations of cancer cells." *Cell*, **146**, 633 (2011).

[36] T. Ashworth. "A case of cancer in which cells similar to those in the tumours were seen in the blood after death." *Aust Med J*, **14**, 146 (1869).

[37] M. Cristofanilli, *et al.* "Circulating tumor cells, disease progression, and survival in metastatic breast cancer." *New England Journal of Medicine*, **351**, 781 (2004).

[38] M. Balic, A. Williams, H. Lin, R. Datar, et R. J. Cote. "Circulating tumor cells: from bench to bedside." *Annual review of medicine*, **64** (2013).

[39] M. C. Miller, G. V. Doyle, et L. W. Terstappen. "Significance of circulating tumor cells detected by the cellsearch system in patients with metastatic breast colorectal and prostate cancer." *Journal of oncology*, **2010**, 617421 (2009).

[40] M. G. Krebs, *et al.* "Evaluation and prognostic significance of circulating tumor cells in patients with non–small-cell lung cancer." *Journal of clinical oncology*, **29**, 1556 (2011).

[41] J.-M. Hou, *et al.* "Clinical significance and molecular characteristics of circulating tumor cells and circulating tumor microemboli in patients with small-cell lung cancer." *Journal of Clinical Oncology*, **30**, 525 (2012).

[42] M. G. Krebs, R. L. Metcalf, L. Carter, G. Brady, F. H. Blackhall, et C. Dive. "Molecular analysis of circulating tumour cells [mdash] biology and biomarkers." *Nature Reviews Clinical Oncology*, **11**, 129 (2014).

[43] C. Alix-Panabieres et K. Pantel. "Challenges in circulating tumour cell research." *Nature Reviews Cancer*, **14**, 623 (2014).

[44] M. Ilie, *et al.* "Sentinel circulating tumor cells allow early diagnosis of lung cancer in patients with chronic obstructive pulmonary disease." *PloS one*, **9**, e111597 (2014).

[45] T. P. Butler et P. M. Gullino. "Quantitation of cell shedding into efferent blood of mammary adenocarcinoma." *Cancer Research*, **35**, 512 (1975).

[46] L. Flores, *et al.* "Improving the yield of circulating tumour cells facilitates molecular characterisation and recognition of discordant her2 amplification in breast cancer." *British journal of cancer*, **102**, 1495 (2010).

[47] W. W. Yu et X. Peng. "Formation of high-quality cds and other ii–vi semiconductor nanocrystals in noncoordinating solvents: Tunable reactivity of monomers." *Angewandte Chemie International Edition*, **41**, 2368 (2002).

[48] M. Yu, *et al.* "Circulating breast tumor cells exhibit dynamic changes in epithelial and mesenchymal composition." *science*, **339**, 580 (2013).

[49] L. E. Lowes et A. L. Allan. "Recent advances in the molecular characterization of circulating tumor cells." *Cancers*, **6**, 595 (2014).

[50] A. Truini, *et al.* "Clinical applications of circulating tumor cells in lung cancer patients by cellsearch system." *Frontiers in oncology*, **4** (2014).

[51] W. J. Allard, *et al.* "Tumor cells circulate in the peripheral blood of all major carcinomas but not in healthy subjects or patients with nonmalignant diseases." *Clinical Cancer Research*, **10**, 6897 (2004).

[52] M. Naoe, *et al.* "Detection of circulating urothelial cancer cells in the blood using the cellsearch system." *Cancer*, **109**, 1439 (2007).

[53] E. Racila, D. Euhus, A. J. Weiss, C. Rao, J. McConnell, L. W. Terstappen, et J. W. Uhr. "Detection and characterization of carcinoma cells in the blood." *Proceedings of the National Academy of Sciences*, **95**, 4589 (1998).

[54] S. Pece, *et al.* "Biological and molecular heterogeneity of breast cancers correlates with their cancer stem cell content." *Cell*, **140**, 62 (2010).

[55] S. Nagrath, *et al.* "Isolation of rare circulating tumour cells in cancer patients by microchip technology." *Nature*, **450**, 1235 (2007).

[56] Z. Svobodova, J. Kucerova, J. Autebert, D. Horak, L. Bruckova, J.-L. Viovy, et Z. Bilkova. "Application of an improved magnetic immunosorbent in an ephesia chip designed for circulating tumor cell capture." *Electrophoresis*, **35**, 323 (2014).

[57] M. G. Krebs, *et al.* "Analysis of circulating tumor cells in patients with non-small cell lung cancer using epithelial marker-dependent and-independent approaches." *Journal of Thoracic Oncology*, **7**, 306 (2012).

[58] B. Mostert, S. Sleijfer, J. A. Foekens, et J. W. Gratama. "Circulating tumor cells (ctcs): detection methods and their clinical relevance in breast cancer." *Cancer treatment reviews*, **35**, 463 (2009).

[59] M. Alunni-Fabbroni et M. T. Sandri. "Circulating tumour cells in clinical practice: Methods of detection and possible characterization." *Methods*, **50**, 289 (2010).

[60] C. Alix-Panabieres, *et al.* "Full-length cytokeratin-19 is released by human tumor cells: a potential role in metastatic progression of breast cancer." *Breast Cancer Res*, **11**, R39 (2009).

[61] K. Pantel, C. Alix-Panabières, et S. Riethdorf. "Cancer micrometastases." *Nature reviews Clinical oncology*, **6**, 339 (2009).

[62] P. De Cremoux, *et al.* "Detection of muc1-expressing mammary carcinoma cells in the peripheral blood of breast cancer patients by real-time polymerase chain reaction." *Clinical cancer research*, **6**, 3117 (2000).

[63] J. E. Hardingham, P. J. Hewett, R. E. Sage, J. L. Finch, J. D. Nuttall, D. Kotasek, et A. Dobrovic. "Molecular detection of blood-borne epithelial cells in colorectal cancer patients and in patients with benign bowel disease." *International journal of cancer*, **89**, 8 (2000).

[64] L. Xi, D. G. Nicastri, T. El-Hefnawy, S. J. Hughes, J. D. Luketich, et T. E. Godfrey. "Optimal markers for real-time quantitative reverse transcription pcr detection of circulating tumor cells from melanoma, breast, colon, esophageal, head and neck, and lung cancers." *Clinical chemistry*, **53**, 1206 (2007).

[65] K.-A. Yoon, S. Park, S. H. Lee, J. H. Kim, et J. S. Lee. "Comparison of circulating plasma dna levels between lung cancer patients and healthy controls." *The Journal of Molecular Diagnostics*, **11**, 182 (2009).

[66] E. Papadopoulou, *et al.* "Cell-free dna and rna in plasma as a new molecular marker for prostate and breast cancer." *Annals of the New York Academy of Sciences*, **1075**, 235 (2006).

[67] H. Schwarzenbach, D. S. Hoon, et K. Pantel. "Cell-free nucleic acids as biomarkers in cancer patients." *Nature Reviews Cancer*, **11**, 426 (2011).

[68] P. Mandel. "Les acides nucleiques du plasma sanguin chez l'homme." *CR Acad Sci Paris*, **142**, 241 (1948).

[69] S. Leon, B. Shapiro, D. Sklaroff, et M. Yaros. "Free dna in the serum of cancer patients and the effect of therapy." *Cancer research*, **37**, 646 (1977).

[70] E. Gormally, E. Caboux, P. Vineis, et P. Hainaut. "Circulating free dna in plasma or serum as biomarker of carcinogenesis: practical aspects and biological significance." *Mutation Research/Reviews in Mutation Research*, **635**, 105 (2007).

[71] H. Esmaeilsabzali, T. V. Beischlag, M. E. Cox, A. M. Parameswaran, et E. J. Park. "Detection and isolation of circulating tumor cells: Principles and methods." *Biotechnology advances*, **31**, 1063 (2013).

[72] T.-L. Wu, D. Zhang, J.-H. Chia, K.-C. Tsao, C.-F. Sun, et J. T. Wu. "Cell-free dna: measurement in various carcinomas and establishment of normal reference range." *Clinica Chimica Acta*, **321**, 77 (2002).

[73] F. Diehl, *et al.* "Circulating mutant dna to assess tumor dynamics." *Nature medicine*, **14**, 985 (2007).

[74] A. J. Armstrong, *et al.* "Circulating tumor cells from patients with advanced prostate and breast cancer display both epithelial and mesenchymal markers." *Molecular Cancer Research*, **9**, 997 (2011).

[75] A. Lecharpentier, P. Vielh, P. Perez-Moreno, D. Planchard, J. Soria, et F. Farace. "Detection of circulating tumour cells with a hybrid (epithelial/mesenchymal) phenotype in patients with metastatic non-small cell lung cancer." *British journal of cancer*, **105**, 1338 (2011).

[76] B. Valeur et M. N. Berberan-Santos. *Molecular fluorescence: principles and applications*. John Wiley & Sons (2012).

[77] A. PIETRASZEWSKA-BOGIEL et T. Gadella. "Fret microscopy: from principle to routine technology in cell biology." *Journal of microscopy*, **241**, 111 (2011).

[78] A. Hillisch, M. Lorenz, et S. Diekmann. "Recent advances in fret: distance determination in protein–dna complexes." *Current opinion in structural biology*, **11**, 201 (2001).

[79] E. A. Jares-Erijman et T. M. Jovin. "Fret imaging." *Nature biotechnology*, **21**, 1387 (2003).

[80] A. Periasamy et R. Day. *Molecular imaging: FRET microscopy and spectroscopy.* Elsevier (2011).

[81] J. R. Lakowicz et C. D. Geddes. *Topics in fluorescence spectroscopy*, volume 1. Springer (1991).

[82] T. Forster. "10th spiers memorial lecture. transfer mechanisms of electronic excitation." *Discuss. Faraday Soc.*, **27**, 7 (1959).

[83] W.-C. Law, *et al.* "Optically and magnetically doped organically modified silica nanoparticles as efficient magnetically guided biomarkers for two-photon imaging of live cancer cells." *The Journal of Physical Chemistry C*, **112**, 7972 (2008).

[84] N. Sounderya et Y. Zhang. "Use of core/shell structured nanoparticles for biomedical applications." *Recent Patents on Biomedical Engineering*, **1**, 34 (2008).

[85] D. Bera, L. Qian, T.-K. Tseng, et P. H. Holloway. "Quantum dots and their multimodal applications: a review." *Materials*, **3**, 2260 (2010).

[86] B. A. Kairdolf, A. M. Smith, T. H. Stokes, M. D. Wang, A. N. Young, et S. Nie. "Semiconductor quantum dots for bioimaging and biodiagnostic applications." *Annual review of analytical chemistry (Palo Alto, Calif.)*, **6**, 143 (2013).

[87] L. Paavilainen, Å. Edvinsson, A. Asplund, S. Hober, C. Kampf, F. Pontén, et K. Wester. "The impact of tissue fixatives on morphology and antibody-based protein profiling in tissues and cells." *Journal of Histochemistry & Cytochemistry*, **58**, 237 (2010).

[88] T. E. Morgan et G. L. Huber. "Loss of lipid during fixation for electron microscopy." *The Journal of cell biology*, **32**, 757 (1967).

[89] E. Batlle, E. Sancho, C. Franci, D. Dominguez, M. Monfar, J. Baulida, et A. G. de Herreros. "The transcription factor snail is a repressor of e-cadherin gene expression in epithelial tumour cells." *Nature cell biology*, **2**, 84 (2000).

[90] Y. Shintani, M. Maeda, N. Chaika, K. R. Johnson, et M. J. Wheelock. "Collagen i promotes epithelial-to-mesenchymal transition in lung cancer cells via transforming growth factor–β signaling." *American journal of respiratory cell and molecular biology*, **38**, 95 (2008).

[91] J. M. Halbleib et W. J. Nelson. "Cadherins in development: cell adhesion, sorting, and tissue morphogenesis." *Genes & development*, **20**, 3199 (2006).

[92] J. Behrens, M. M. Mareel, F. M. Van Roy, et W. Birchmeier. "Dissecting tumor cell invasion: epithelial cells acquire invasive properties after the loss of uvomorulin-mediated cell-cell adhesion." *The Journal of Cell Biology*, **108**, 2435 (1989).

[93] U. H. Frixen, *et al.* "E-cadherin-mediated cell-cell adhesion prevents invasiveness of human carcinoma cells." *The Journal of cell biology*, **113**, 173 (1991).

[94] B. K. Straub, *et al.* "E–n-cadherin heterodimers define novel adherens junctions connecting endoderm-derived cells." *The Journal of cell biology*, **195**, 873 (2011).

[95] V. Sundram, S. C. Chauhan, et M. Jaggi. "Emerging roles of protein kinase d1 in cancer." *Molecular Cancer Research*, **9**, 985 (2011).

[96] H. Zheng, *et al.* "Pkd1 phosphorylation-dependent degradation of snail by scf-fbxo11 regulates epithelial-mesenchymal transition and metastasis." *Cancer cell*, **26**, 358 (2014).

[97] M. Gschwendt, S. Dieterich, J. Rennecke, W. Kittstein, H.-J. Mueller, et F.-J. Johannes. "Inhibition of protein kinase c mu by various inhibitors. inhibition from protein kinase c isoenzymes." *FEBS letters*, **392**, 77 (1996).

[98] S. Bolte et F. P. Cordelieres. "A guided tour into subcellular colocalization analysis in light microscopy." *Journal of microscopy*, **224**, 213 (2006).

[99] N. Gahlaut et L. W. Miller. "Time-resolved microscopy for imaging lanthanide luminescence in living cells." *Cytometry Part A*, **77**, 1113 (2010).

[100] O. J. Harrison, *et al.* "The extracellular architecture of adherens junctions revealed by crystal structures of type i cadherins." *Structure*, **19**, 244 (2011).

[101] S. A. Kim, C.-Y. Tai, L.-P. Mok, E. A. Mosser, et E. M. Schuman. "Calcium-dependent dynamics of cadherin interactions at cell–cell junctions." *Proceedings of the National Academy of Sciences*, **108**, 9857 (2011).

[102] M. J. Rust, M. Bates, et X. Zhuang. "Sub-diffraction-limit imaging by stochastic optical reconstruction microscopy (storm)." *Nature methods*, **3**, 793 (2006).

[103] B.-A. Truong Quang, M. Mani, O. Markova, T. Lecuit, et P.-F. Lenne. "Principles of e-cadherin supramolecular organization in vivo." *Current Biology*, **23**, 2197 (2013).

[104] H. Liu, P. Hou, W. Zhang, et J. Wu. "The synthesis and characterization of polymer-coated feau multifunctional nanoparticles." *Colloids and Surfaces A: Physicochemical and Engineering Aspects*, **356**, 21 (2010).

[105] G. Liu, M. Swierczewska, S. Lee, et X. Chen. "Functional nanoparticles for molecular imaging guided gene delivery." *Nano Today*, **5**, 524 (2010).

[106] E. Giovanelli, E. Muro, G. Sitbon, M. Hanafi, T. Pons, B. Dubertret, et N. Lequeux. "Highly enhanced affinity of multidentate versus bidentate zwitterionic ligands for long-term quantum dot bioimaging." *Langmuir*, **28**, 15177 (2012).

[107] J. K. Jaiswal, H. Mattoussi, J. M. Mauro, et S. M. Simon. "Long-term multiple color imaging of live cells using quantum dot bioconjugates." *Nature biotechnology*, **21**, 47 (2002).

[108] J. J. Li, Y. A. Wang, W. Guo, J. C. Keay, T. D. Mishima, M. B. Johnson, et X. Peng. "Large-scale synthesis of nearly monodisperse cdse/cds core/shell nanocrystals using air-stable reagents via successive ion layer adsorption and reaction." *Journal of the American Chemical Society*, **125**, 12567 (2003).

[109] F. Morgner, D. Geißler, S. Stufler, N. G. Butlin, H.-G. Löhmannsröben, et N. Hildebrandt. "A quantum-dot-based molecular ruler for multiplexed optical analysis." *Angewandte Chemie International Edition*, **49**, 7570 (2010).

[110] K. D. Wegner, Z. Jin, S. Linden, T. L. Jennings, et N. Hildebrandt. "Quantum-dot-based fo?rster resonance energy transfer immunoassay for sensitive clinical diagnostics of low-volume serum samples." *ACS nano*, **7**, 7411 (2013).

[111] A. R. Clapp, I. L. Medintz, et H. Mattoussi. "Forster resonance energy transfer investigations using quantum-dot fluorophores." *ChemPhysChem*, **7**, 47 (2006).

Abstract

Les cellules tumorales circulantes (CTC) sont des cellules prèsentes en très faible proportion (une cellule pour un million de cellules normales) dans la circulation sanguine, et qui jouent un rôle important dans le processus de mètastase responsable de la majoritè des décès de patients atteints de cancer. La détection du cancer à un stade prècoce augmente les chances de survie des patients. Le but de ce travail a été de développer un ensemble de technologies permettant de mieux caractériser et détecter les CTC.

Nous avons concentré notre étude sur les cellules ayant un phénotype hybride, entre épithélial et mésenchymal, qui pourraient correspondre à des CTC de plus fort potentiel métastatique compte tenu du rôle joué par la transition épithelio-mésenchymateuse dans ce processus. Nous avons tout d'abord isolé, par immunofluorescence et cytométrie en flux, une lignée cellulaire de cancer (A549, le carcinome de poumon humain) co-exprimant la E- et la N-cadhérine, de sorte qu'elle puisse être utilisée comme modèle de CTC dans le développement de nouvelles techniques de détection. Nous avons en particulier adapté le système de microscopie de fluorescence et d'analyse d'images Pathfinder^{TM} à haut-débit de la société Imstar S.A. pour identifier efficacement quelques milliers de cellules A549 mélangées à du sang de patient, après une étape de filtration par la taille. Afin d'amèliorer l'identification des cellules hybrides, nous avons évalué la technique de transfert de Förster résolue en temps qui pourrait révéler avec un excellent rapport signal/bruit la présence á la membrane cellulaire d'agrégats compacts de N- et E-cadhérines. Enfin, afin d'augmenter le nombre de biomarqueurs simultanément détectés par immunofluorescence nous avons contribué à la mise au point de nanocristaux semi-conducteurs fluorescents conjugués avec un anticorps dirigé contre une protéine d'intérêt. Au final, nos résultats fournissent un ensemble de technologies qui pourront être utilisées pour améliorer la détection et la caractérisation des CTC.

Mots clés: Cellules tumorales circulantes, FRET, EMT, quantum dots, CTC detection, haut débit du système microscopique.

Abstract

Circulating tumor cells (CTCs) are rare cells (one in millions of normal cells) in blood circulatory system playing a key role in the process of metastasis, which is responsible for the majority of death of patients with cancer. Detecting cancer at early stage can give patients higher chances of survival. The aim of this work is to develop a set of technologies capable of characterizing and detecting the CTCs. We restricted our study to CTCs with hybrid phenotype, between epithelial and mesenchymal, that could correspond to circulating cells with the highest metastatic potential, considering the relation of the Epithelial to Mesenchymal Transition to cancer. Using immunofluorescence and flow cytometry, we first isolated a cancer cell line (A549, human lung carcinoma) co-expressing E- and N-cadherin, which is further used as a CTC model in the development of new detection techniques. In particular, we showed that the high throughput automated fluorescence microscope and image processing Imstar S.A. Pathfinder^{TM} system can recover efficiently a few thousands of A549 cells spiked in a blood sample, after an initial size-filtering step. We also used time-gated Fluorescence Resonant Energy Transfer to investigate the presence of E- and N-cadherin clusters at the cell membrane that could enhance the detection sensitivity of hybrid phenotype. Finally, in view of increasing the number of simultaneous biomarkers detection by immunofluorescence we contributed to the development of fluorescent semiconductor nanocrystals conjugated with antibody directed against the protein of interest. Altogether, our results provide a set of technologies that can be used to improve the detection and characterization of CTCs.

Keywords: Circulating tumor cells, FRET, EMT, quantum dots, CTC detection, high throughput microscopic system.